Study of a Micro Force Sensor for Colloidal Engines Applications

Engineering Final Thesis.

Author: Rafael Gómez Consarnau

Director: Jasmina Casals Terré

Co-director: Miquel Sureda Anfrés

Escola Tècnica Superior d'Enginyeries Industrial i Aeronàutica de Terrassa

Terrassa, September 17, 2011

Contents

List of Figures

8

11

List of Tables

Chapter 1

Introduction

In this chapter it is defined the introduction of the presented project, where it is made the study of a force sensor for colloidal engines applications, in the aerospace field.

1.1 Objective

The goal of this study is the design, manufacturing and test of micro-force sensors based on MEMS technology. With a wide range of application it focuses on the characterization of the propulsive properties of the colloidal engines in the aerospace field.

There is a wide range of applications for microforce sensors but in this project we have focused on the characteristics of colloidal engines for aerospace field in order to determine the resolution and the ranges of forces that the sensor should measure.

1.2 Scope

- Determination and analysis of force range requirements.

- The structural theory of a pre-buckled beam are analyzed.

- Analysis of the amplification mechanism for initially straight beams and initially pre-buckled beams.

- Validation of the analytical solutions using Finite Elements Analysis (FEA).

- Different designs are studied two of 1DOF and three of 2DOF.

- The DAS is chosen in order to fulfill the force range requirements.

- The characterization of the performance of each device is achieved using the Data Acquisition System (DAS) resolution parameters.

15

Terminology	Mass [kg]
Mini	100-500
Micro	10-100
Nano	1-10
Pico	0.1-1

Table 1.1: Differentiation between different satellite sizes.

- A FEA harmonic analysis has been done to avoid the interaction between the driving forces of the characterization circuit and the device.

- The devices are fabricated using a Silicon-On-Insulator (SOI) wafer and typical in-vivo fabrication techniques.

- The experimental setup for the calibration devices is designed and a validation of the performance device is done.

- A partial validation process is performed.

- The economic feasibility of the project is made.

1.3 Background

Nowadays the most common way to measure the thrust and specific impulse in colloidal engines use the measurement of the flux of the charged droplets added on a conductor. This conductive surface receive the flux of charged droplets that will flux through a circuit that measures the current due to this flux see [4] and [5].

Because of the well known current and the liquid density of charge ratio $\frac{q}{m}$, it is possible to measure the mass rate, thrust and therefore the specific impulse.

Nowadays days there is no mention in the bibliography about the implementation of a capacitive force sensor based on MEMS technology, to do such tests is where lies the challenge of the presented work.

1.4 Justification

During the beginning of the twenty-first century there is a boom in the development of small satellites from mini to pico satellites, widely explained in [19].

The uniqueness of these devices is that they have to have a reduced size and weight, Table 1.4 describes the mass range of the small satellite models.

Due to the small size, mass and inertia of these novel satellites, the requirements for pointing, attitude control and position in orbit are higher than the conventional ones. An
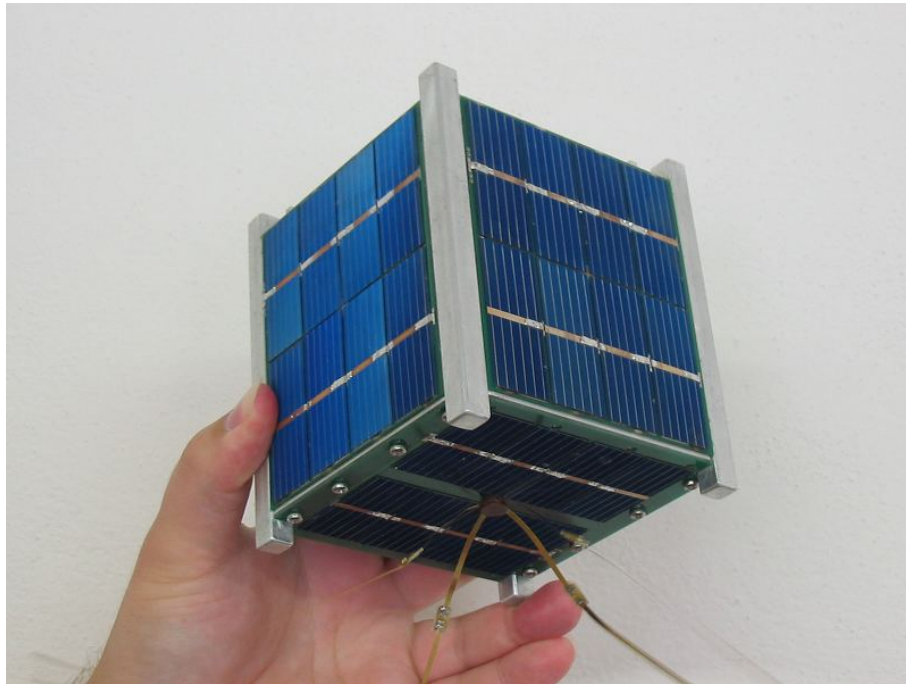
Figure 1.1: Image of the EADS Astrium Nanosatellite X-ray Spectrometer (NXS), font [18]

example of nanosatellite can be seen in Fig.1.1 designed by astrium [18]. Other applications include orbital maneuvers that require a high momentum and thus the requirement of a high specific impulse. These can be changes in periapsis, apoapsis, argument of perigee, line of nodes, changes in the eccentricity of the orbit, depending on the mission requirements of the vehicle.

The propulsive control mechanisms require both: very high precision and very low thrust.

Therefore colloidal engines are characterized by a high specific impulse with a thrust range generally low, as shown in Figure 1.2, in more detail in the thesis found in [3], where it can be seen that the colloidal thrusters applications lay on the ranges from mN to below.

Due to this narrow range of forces to be measured and the feasibility of the fabrication process the chosen technology for the fabrication of the force sensor is based on the MEMS technology. This is characterized by small size of denis and manufacturing process of relatively low cost. This new technology to manufacture force sensors can complement the present market of force sensor devices in this range and moreover represents a cheaper and simple alternative.

The sensing system will be based on the capacitance phenomena, the idea is to take advantage of the elasticity of movable parts of MEMS in order to modify the capacitance and therefore this can be measured via a capacitor based using a data acquisition system.

17
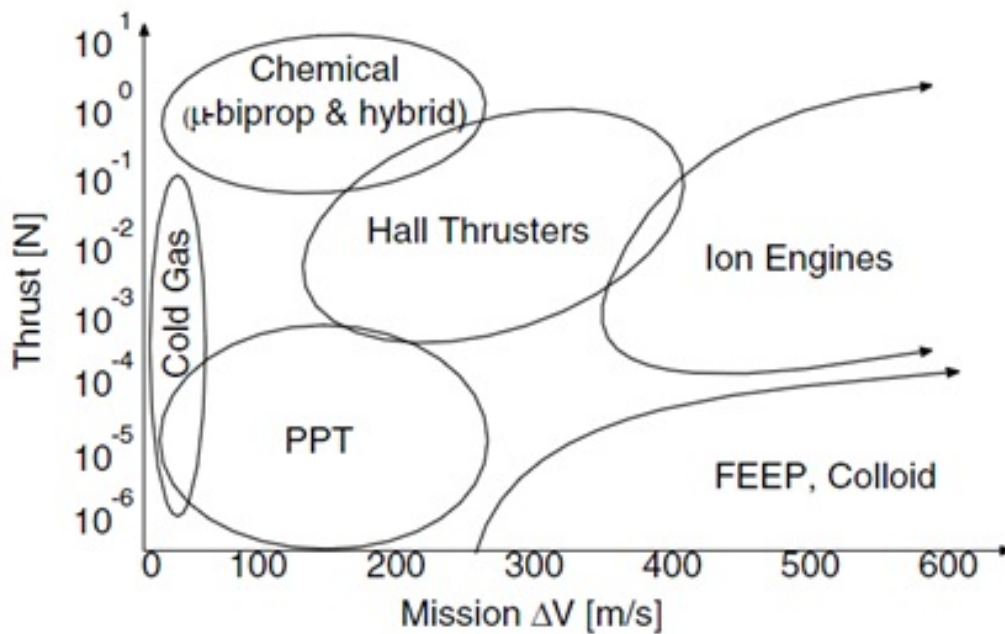
Figure 1.2: Thrust vs ISP for different propulsive technologies found in [3]

1.5 Brief description of a typical colloidal engine operating principle

The colloidal engines uses the principle of action and reaction to speed of ionic liquid droplets with net positive charge, through a cathode it is created a potential difference and thus a net electrostatic force on the liquid exposed surface, this is guided through small channels to reach the tip of the needle for its exit obtaining a net change in momentum.

These engines are being developed since the 1960's and becoming the first patent in 1978 by (Bartoli and Rhoden) see a brief history of FEEP in [20]. Thought as an alternative as the normal ion engines. Initially it was limited by technological difficulties to fulfill the high requirements of potential difference between cathode and anode. So until the 1990's have not begun to be more important given the technological improvements that allow miniaturization and the high potential difference to apply in a sustained and independent way.

This liquid must be broken down into small droplets to further increase in acceleration. This is achieved by applying a high electric field produced by the cathode on the outside, which must overcome the forces produced by the surface tension that prevents the fluid to disperse.

The application of a difference of electrical potential at the liquid interface ends up generating a high instability in the surface of the conductive fluid and thus the generation of a conoidal form on the surface shown in Fig.1.3 closest to the cathode, this phenomena is called "Taylor cone" in honor of its discoverer Sir Geoffrey Ingram Taylor in 1964.

18
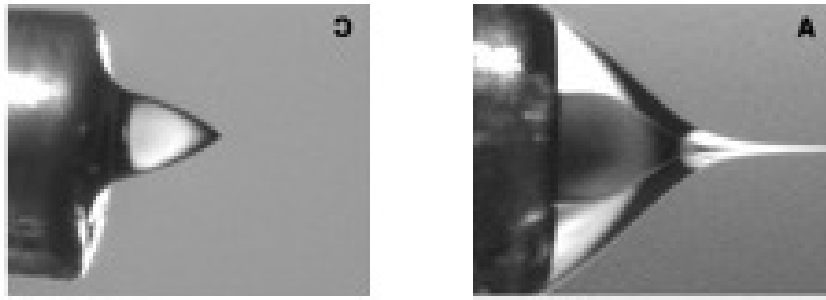
Figure 1.3: Taylor Cone perturbation detail evolution.
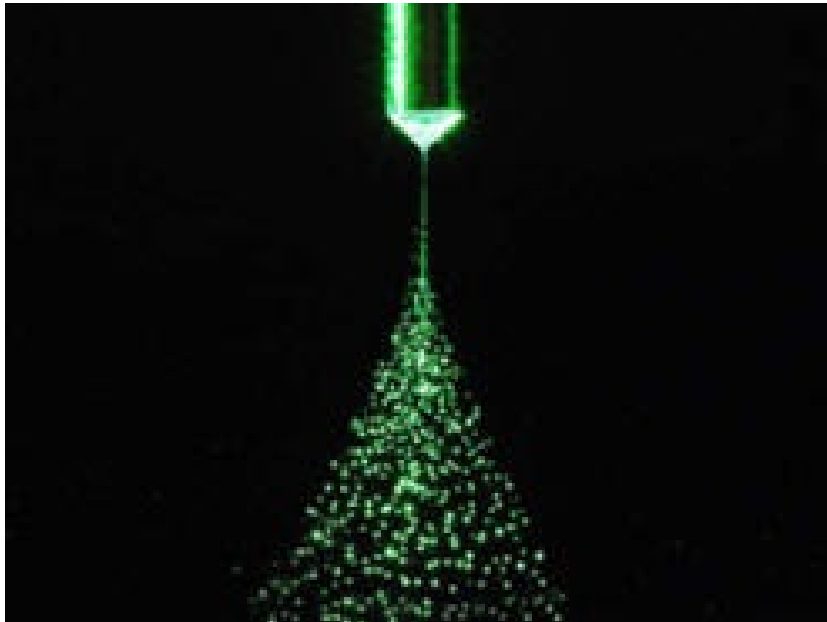
Figure 1.4: Colloidal regime emission font [21].

This instability process ends with the expulsion of the droplets by the protruding end of the cone which is smaller at higher applied electric field or potential difference.

The whole process represents a change in momentum due to droplets of fluid expelled. This reaction is transmitted by the engine creating thrust or force in the opposite direction. The results can be seen in Figure 1.4 in [21] where a electrospray it is shown using the same principle in colloid regime.

According to this an experimental montage has been thought to be used in order to measure the thrust and the mass rate of the Colloidal Engines. Therefore the idea is to measure in 2 independent components the magnitudes of thrust for reaction on the device, and mass rate as a variation in the device vertical weight or displacement. A concept of how can the measurements be successfully achieved are shown in Fig.1.5.
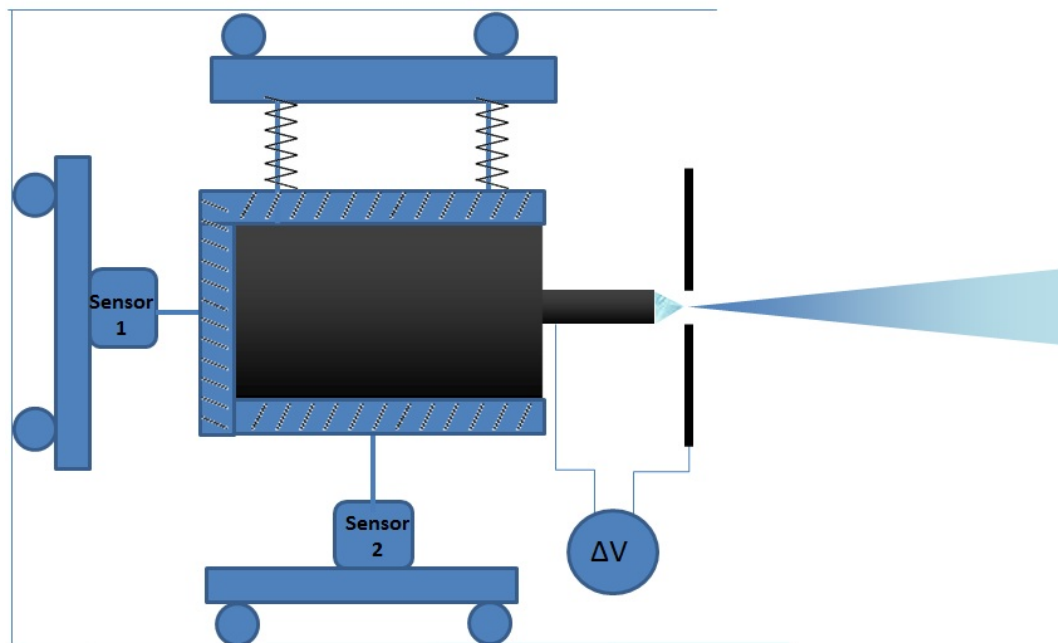
Figure 1.5: Scheme of the montage for the colloidal engine Thrust and ISP.

1.6 MEMS Introduction

MEMS is the acronym of Micro Electro Mechanical Systems, which is technology that uses mechanical and electrical properties of a concrete material to fabricate devices with an immense field of applications, using micro-fabrication techniques.

This technology is very useful in the miniaturization of structures, sensors, actuators and microelectronics. There is a relative broad range of fabrication sizes, depending on the application a common range of critical dimensions can vary from below a micron to fraction of millimeter. MEMS can be composed of fixed components and movable components, being the movable components actuators or sensors. They are composed of structures that can be designed to respond to an external force and measure a magnitude, sensors, or actuators that can apply different sort of forces such as electrical, thermal, etc...

In Fig1.6 and Fig.1.7 two examples of devices are shown, as explains MEMS world in [14].

Other important application is the use of transducers to transfer energy from one device to another, becoming a very unique way to get electrical energy from kinetic energy for example via undesired mechanical vibrations.

The wide application field can vary for example fr micro-sensors applications on the measurements of magnitudes such temperature, pressure, inertial forces, contaminants, magnetic fields, radiation to biomedical devices with a drug delivery systems. The most remarkable advantages regarding to the conventional sensors is that MEMS sensors

Figure 1.6: An image of how it can be obtained movable components using MEMS technology.
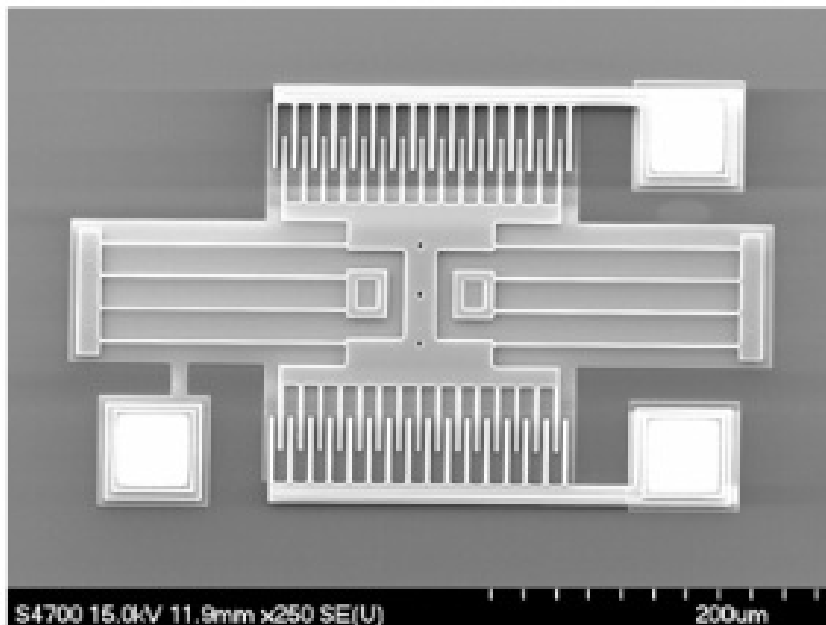
Figure 1.7: A surface micromachined resonator fabricated by the MNX. This device can be used as both a microsensor as well as a microactuator.
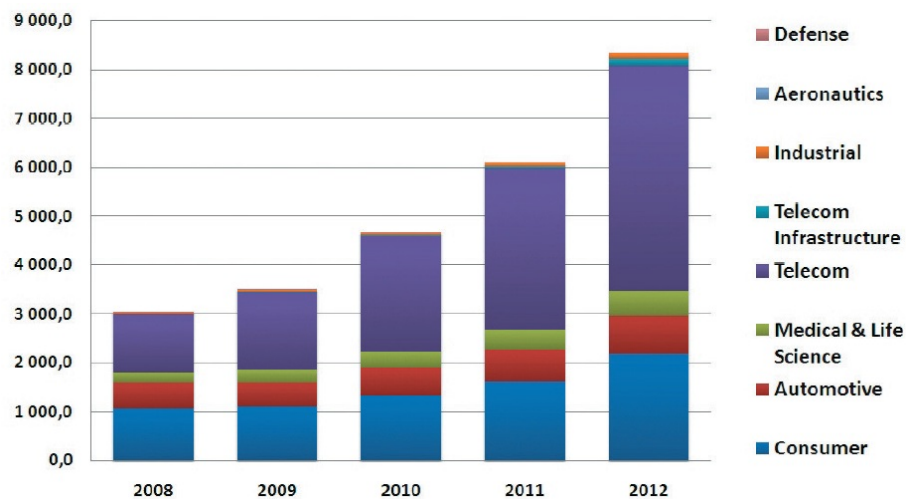
Figure 1.8: Actual tendency in the market of MEMS production reported in [15]

have demonstrated better performances in most of the cases in the sensitivity property, because in general the smaller the size of the internal structural parts the higher the mobility in regarding to an external stimulation.

A remarkable advantage of this technology rely on the relatively straight forward fabrication process and costs, because of the miniaturization a large number of repeatable structures leading to a low cost per unit compared to the conventional macrodevices.

Due to the amount of applications, MEMS industry has a successfully developed during the last decades. Nowadays MEMS market has become an important peace in the industry as it is reported in [15] the inversion in this technology is still growing up as it is found in Fig.1.8 for the next 2012 year the total productions unit is expected to be over 8 billion.

In the actual moment in aerospace applications there is a new tendency in the miniaturization of the space vehicles and probes this represents a huge opportunity for the MEMS technology to take advantage of its unique properties.

Chapter 2

Capacitive sensors introduction

In this chapter the principle of sensing is presented including definitions of the used configurations and a brief description of the electrical instability is presented. At the end it is defined the most important parameters that define the capacitor sensors in general.

2.1   Capacitive sensing principle

A capacitive sensor can be defined as a device that is capable of measuring the capacitance property. Experiments show that the amount of charge Q stored in a capacitor is linearly proportional to, the electric potential difference between the plates. Physically, capacitance is a measure of the capacity of storing electric charge for a given potential difference. In order to find the equation that represents the capacitance magnitude for different problems it is useful the Maxwell equation of the Gauss law in integral form Eq.2.1, this equation particularized in the case of two parallel plates like the shown in Fig.2.1 yields to the solution of Eq.2.1, where $\oint \vec{E}$ is the electrical field, $\vec{dA}$ is the differential of area, $Q(V)$ is the charge distribution as a function of the electric potential V and ϵ_o is the permittivity ; founding its particularization for a Parallel Plates configuration in Eq.2.3. Where the parameters ϵ is the permittivity of the medium within the plates, S is the common fronted area between plates and g is the gap between both plates.

$$\oint \vec{E} \cdot \vec{dA} = \frac{Q(V)}{\epsilon_o} \tag{2.1}$$

The capacitance then is directly proportional to the surface area of the objects and the dielectric constant of the material between them, and inversely proportional to the distance between them.

$$Q = C \cdot \mid \Delta V \mid \tag{2.2}$$
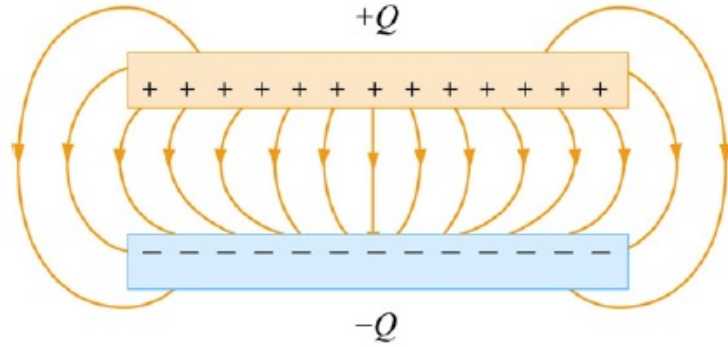
Figure 2.1: Electric field between two parallel plates due to the charge distribution, found in theory of capacitors and dielectrics [22].

$$C = \frac{\epsilon S}{g} \tag{2.3}$$

This devices proposed in the project will use an alternating voltage which will causes the charges to continually reverse their positions. The moving of the charges creates an alternating electric current which is detected by the sensor, see Fig.2.2.

The amount of current flow is determined by the capacitance, and the capacitance is determined by the area and proximity of the conductive objects. Larger and closer objects cause greater current than smaller and more distant objects. The capacitance is also affected by the type of nonconductive material in the gap between the objects.

Although its time dependence measurements, it is important to say that the sensing system is thought to be working as quasi static, because of the velocity of the movable forced parts to measure in the device are expected to be lower than the resonance frequency of the device itself. Thus the measurements can be performed by a quasi static capacitance variation taking advantage of the well known formulation for the static capacitance.

It is easy to see that the higher the exposed surface S the higher the capacitance and so with the medium permittivity, on the other and the smaller the gap g the higher the capacitance. In order to maximize the measurements i.e. the measured capacitance magnitude, it seems intuitively that it can be modified the gap g and the exposed surface S in a range to satisfy the requirements of force for the measurements.

Thus the designs are based solely on the study of microsensors of capacitive force.
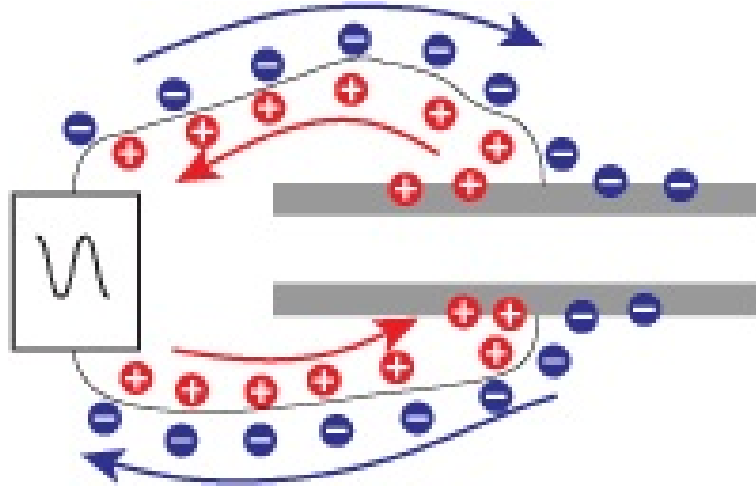
Figure 2.2: Charge flux due to the alternating electrical field applied, causing the alternating current, found in [16].

2.1.1 Pull in voltage instability definition

When using electrical forces between movable components, it is very important to define where is the limit in the equilibrium of the system that involves structural potential energy and electrical energy.

Therefore the equilibrium of forces in a system can be described by the use of a spring and a capacitor shown schematically in Fig.2.3, the first ten to oppose to the displacements whilst the second one acts as an attractive source of force.

The equilibrium equation found in Eq.2.4 is assumed to be for 1 Degree Of Freedom DOF, x, system.

Where the therm k is the equivalent spring i.e. internally structure stiffness, F_c corresponds to the electrical force due to the capacitance variation and voltage difference between both sides of the capacitors as shown Eq.2.5 and for a pair of parallel plates is found using Eq.2.3, becoming Eq.2.7.

$$F_c - k \cdot x = 0 \tag{2.4}$$

$$F_c = \frac{1}{2}\frac{dC}{dx} \cdot V^2 \tag{2.5}$$

$$F_{cpp} = \frac{\epsilon S V^2}{2(g - (x))^2} \tag{2.6}$$

After imposing the equilibrium in Eq.2.4 the way to find a variation o the system that yields to an instability is to take the derivative of this equation regarding to the displacement. Thus it is found the instability displacement in Eq.2.8 i.e. x_{pi} is the value
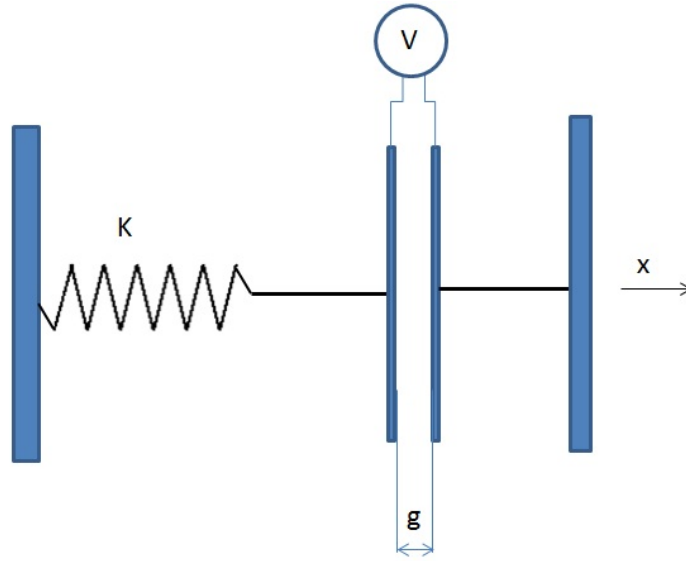
Figure 2.3: Representation of the system involving the stiffness of the internal structure and the attractive forces.

that minimize the equilibrium equation, now using this limit displacement the amount of voltage difference that is causing it is Eq.2.9, this is known as the pull-in voltage.

$$0 = -k + \frac{\epsilon S V^2}{(g - (x))^3} \tag{2.7}$$

$$x_{pi} = \frac{g}{3} \tag{2.8}$$

$$v_{pi} = (\frac{2k}{3\epsilon S} g^3)^{\frac{1}{2}} \tag{2.9}$$

Therefore the limitation in displacement is found as to be at $\frac{1}{3}$ of the initial gap g and also the limitation in voltage whether this parameter is also a DOF of the system.

2.2 Capacitor configuration

In this section two different kinds of capacitors are presented thought to be implemented in the design of the different capacitance based sensors.

2.2.1 Parallel plates

As it was mentioned in the previous chapters the formulation related to the measurement of the capacitance and also the instability are well described using this configuration
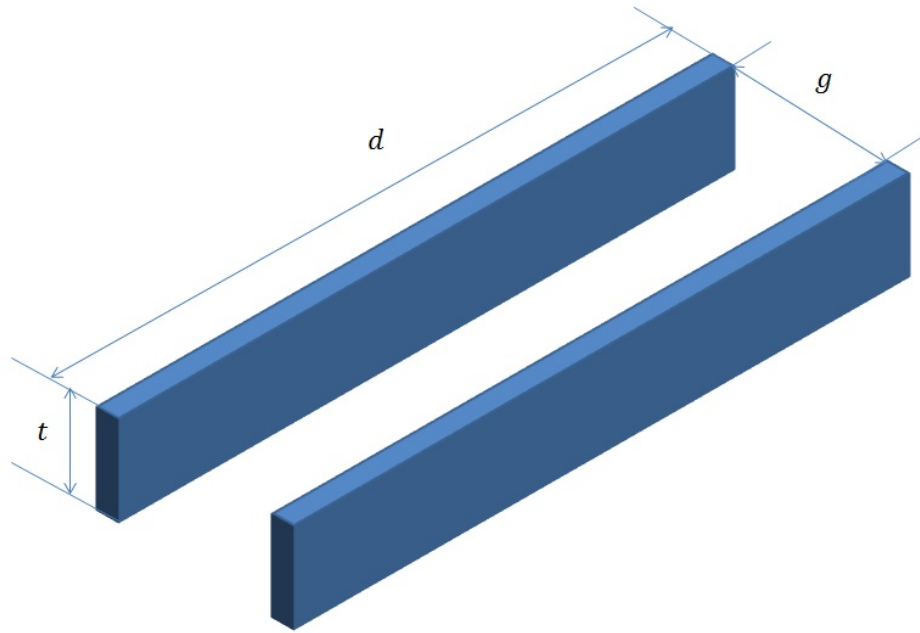
Figure 2.4: Representation of the Parallel Plates capacitor with the design parameters.

of capacitor see Fig.2.4.

As it has been explained the one important limitation is the pull-in voltage instability, when the gap is close to $\frac{2g}{3}$. In general for the measurement of the displacements, this should be generated by an external force and therefore the electrical force will not be the of big concern about the range of displacements.

It can be defined parameters of voltage needs for the capacitance measurements in order to be under the pull in voltage, as much as possible. This way the issue of the pull in limitation can be reduced letting the displacements easily to be further than the 33 percent of the initial gap.

Other limitation of this configuration is the one regarding to Eq.2.3 is the overlap surface area. Because the higher the area the higher the capacitance measured, this is a parameter to be maximized, the problem is that if there is a limitation in the plate thick i.e. out of plane, the area depends on the linear length of the capacitor. This involves a geometrical size limitation, moreover when in this case the size is thought to be a structural limitation.

Summarizing the parallel plates configuration yields a easy option if the instability is controlled via low voltages between capacitors. The high projected area towards the displacement makes it high sensitivity i.e. high capacitance variation, when the gaps are getting closer. Its projected area is very limited by the linear dimension so the capacitance must be optimized to work for a small gaps instead of big fronted areas.

27
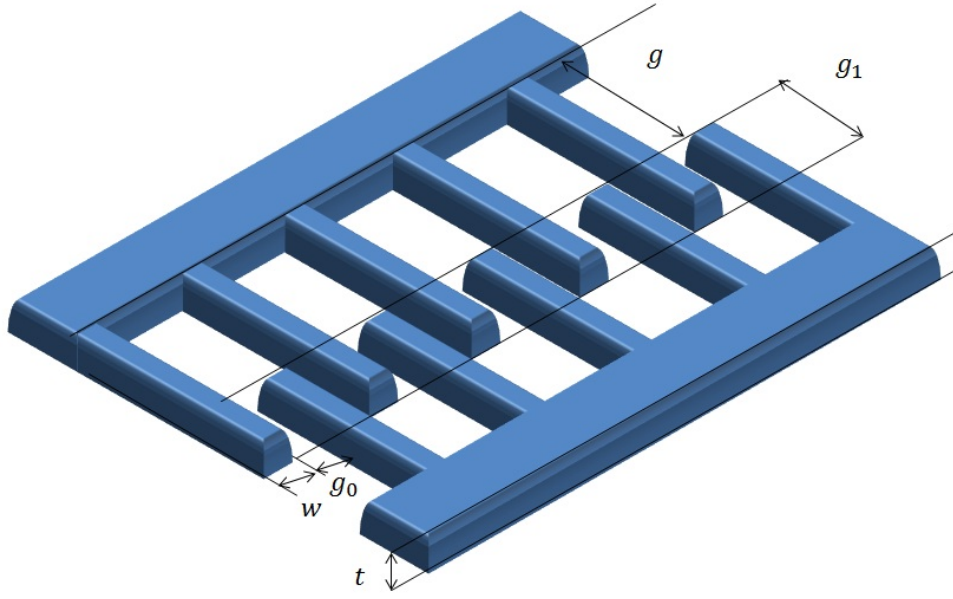
Figure 2.5: Representation of the Comb-Drive capacitor with the design parameters.

2.2.2 Comb-Drive

For this configuration it is presented the Comb-Drive capacitor configuration in Fig.2.5. The advantage of this configuration is that maximizes the fronted area between the capacitors, that represents a limitation in the parallel plate configuration.

This design maximizes the fronted area by the use of fingers, or small plates oriented in the displacement direction. The fingers configuration are distributed generally in the same amount for both sides of the capacitor as it can be seen in Fig.2.5. This way the fronted area using the principle of the parallel plates formula is modified as Eq.2.10. This equation not only shows that the higher the number of fingers the higher the measured capacitance but also the instability due to the fronted areas towards the displacements is almost neglected and the higher the gap between fingers the higher the capacitance.

Becoming a more stable and precise way of measure the capacitance, however it requires a more accurate design process in order to avoid imperfections that can cause irregularities in the geometry.

Even though the instability is almost neglected, it has to be taken in to account because of there is the same fronted area towards the displacement as the case of the parallel plates, but not by the same gap.

$$C = \frac{2n\epsilon t(g_1 + x)}{g_o} \tag{2.10}$$

Therefore the stability can be described using the again Eq.2.4 where now the electrical force F_e is decomposed in two terms because of the difference in the capacitance function, one due to comb-drive capacity found in Eq.2.10, where n is the finger number,

and t is the fingers depth, w is the finger with and g_0 is the overlap gap between fingers; and the one due to the the gap g between the fingers tips and its opposite finger roots acting as the parallel plate equation shows in 2.3, using S as the fronted area towards the displacement direction this is $S = 2nwt$. The instability point is found in Eq.2.11 as a function of the two mentioned gaps and the finger with.

$$x = \sqrt[3]{-gwg_0 + \sqrt{w^3{g_0}^3 + g^2 w^2 {g_0}^2}} - \frac{wg_0}{\sqrt[3]{-gwg_0 + \sqrt{w^3{g_0}^3 + g^2 w^2 {g_0}^2}}} + g \qquad (2.11)$$

Because of the Comb-Drive capacitance depends linearly on the overlap displacement the force contribution of this capacitance is considered a constant proportionally to the square of the applied voltage, this constant is the therm Eq.2.12. This amount means the higher the number of fingers n the higher the force, and the smaller the overlap gap g_0 the higher the force..

$$\frac{nt}{g_0} \qquad (2.12)$$

As a summary it can be said that Comb-Drive configuration is an interesting option for measure capacitance, its higher stability towards the displacements and the high surface area factor improves the parallel plates performance in this aspects. However the higher the number of fingers the higher the attractive force and inversely with the lateral gap. This can be a good solution if the system has a high stiffness and the measurements are focused more on small displacements rather than small forces, when the number of fingers is high. This represents itself a trade of because of high sensitivity in capacitance but higher structural stiffness to avoid large undesired deflections.

2.3   Important parameters that define a capacitance sensor in general

- **Sensitivity**

  Sensitivity indicates how much the output voltage changes as a result of a change in the gap between the target and the capacitive sensor.

- **Sensitivity error**

  A sensor's sensitivity is set during calibration. When sensitivity deviates from the ideal value this is called sensitivity error, gain error, or scaling error. Since sensitivity is the slope of a line, sensitivity error is usually presented as a percentage of slope; comparing the ideal slope with the actual slope.

- **Offset error**

  Offset error occurs when a constant value is added to the output voltage of the system. Capacitive sensor systems are usually "zeroed" during setup, eliminating any offset deviations from the original calibration. However, should the offset error

change after the system is zeroed, error will be introduced into the measurement. Temperature change is the primary factor in offset error.

- **Linearity Error**

  Sensitivity can vary slightly between any two points of data. This variation is called linearity error. The linearity specification is the measurement of how far the output varies from a straight line.

- **Error Band**

  Error band accounts for the combination of linearity and sensitivity errors. It is the measurement of the worst case absolute error in the calibrated range. The error band is calculated by comparing the output voltages at specific gaps to their expected value.

- **Bandwidth**

  Bandwidth is defined as the frequency at which the output falls to $-3dB$. This frequency is also called the cutoff frequency. A $-3dB$ drop in the signal level equates to approximately 70 percent drop in actual output voltage. With a $15kHz$ bandwidth, a change of $\pm1[V]$ at low frequency will only produce a $\pm0.7[V]$ change at $15kHz$. In addition to sensing high-frequency motion, fast responding outputs maximize phase margin when used in servo-control feedback systems.

- **Resolution**

  Resolution is defined as the smallest reliable measurement that a system can make. The resolution of a measurement system must be better than the final accuracy the measurement requires. If you need to know a measurement within $0.02[\mu m]$, then the resolution of the measurement system must be better than $0.02[\mu m]$.

  The primary determining factor of resolution is electrical noise. Electrical noise appears in the output voltage causing small instantaneous errors in the output. Even when the probe/target gap is perfectly constant, the output voltage of the driver has some small but measurable amount of noise that would seem to indicate that the gap is changing. This noise is inherent in electronic components and can only be minimized, but never eliminated.

  If a driver has an output noise of $0.002[V]$ with a sensitivity of $10[V/mm]$, then it has an output noise of $0.2[\mu m]$. This means that at any instant in time, the output could have an error of $0.2[\mu m]$.

  The amount of noise in the output is directly related to bandwidth. Generally speaking, noise is distributed uniformly over a wide range of frequencies. If the higher frequencies are filtered before the output, the result is less noise and better resolution see Fig.2.6 and Fig.2.7, see the capacitance sensing theory in more details in [16]. When examining resolution specifications, it is critical to know at what bandwidth the specifications apply.
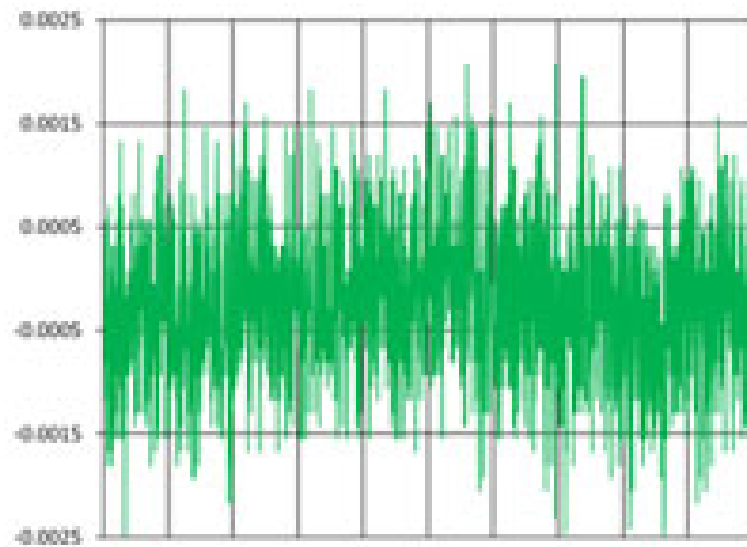
Figure 2.6: Noise from a 15kHz sensor, found in the theory introduction to capacitance sensing [16].
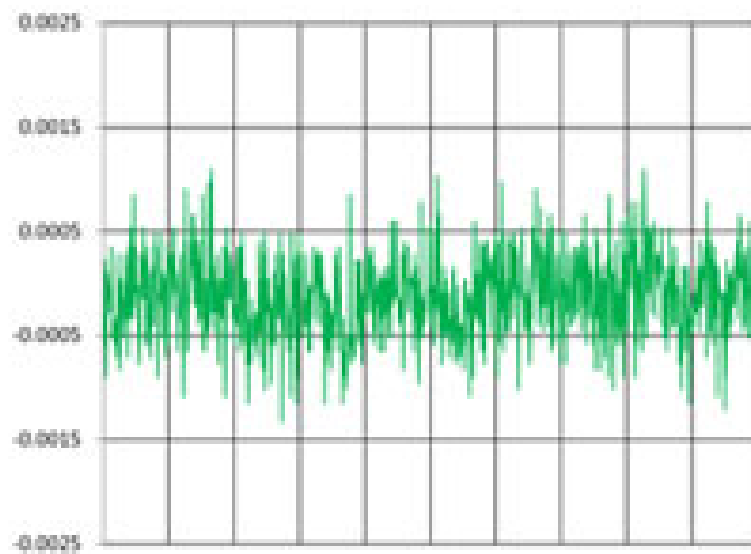
Figure 2.7: Noise from a 100Hz sensor, found in the theory introduction to capacitance sensing [16].

Chapter 3

Data Acquisition System and Calibration of the Sensors

In order to measure the change of capacitance generated by the external forces a Data Acquisition System (DAS) from Analog Devices is adopted.

The key parameters governing the selection of the DAS are the capacitance range and resolution. For the first one the issue arise in case of a very high capacitance off-set. If the capacitance grows up easily ,depending on the configuration design of the capacitors, the measured capacitance over the maximum will be cut and thus there will be no measurements. The other important factor, the resolution, it represent a limitation itself because of whether the measurements signal can vary between this amount, and therefore the signal cannot be distinguished.

In order to chose a few parameters within the affordable devices in the market, an estimation of the expected forces is carried out and so is the expected displacements in order to fix the requirements of capacitance range and resolution.

For colloidal engines applications the range of forces can be taken between $10[\mu N]$ and $1[nN]$. The straight beam design stiffness is generally higher than $0.5[\frac{N}{m}]$ for the Straight Beam Design. Consequently the maximum displacement will not exceed a few tens of micrometer roughly $20[\mu m]$ for the maximum force deflecting a structure.

For the resolution it is desirable to detect forces of the order of tenths of $[nN]$, to ensure a smooth measurement of the phenomena.

Therefore the minimum detectable force must be in the order of tens or cents of $[pN]$. Supposing it to be $\delta P = 500[pN]$. With the minimum stiffness mentioned above and this resolution of force the minimum detectable displacements must be of roughly of $1[nm]$ using Eq.3.3 which is a linearization around any point x see Fig.3.1, takin the derivation of the force as the mentioned stiffness and the resolution of force.

Because of the capacitance can be measured with a parallel plates configuration, the equation of the capacitance used is Eq.2.3. Taking the reference parameters of maximum displacement as to be the initial gap between the capacitors and a reference fronted area

33
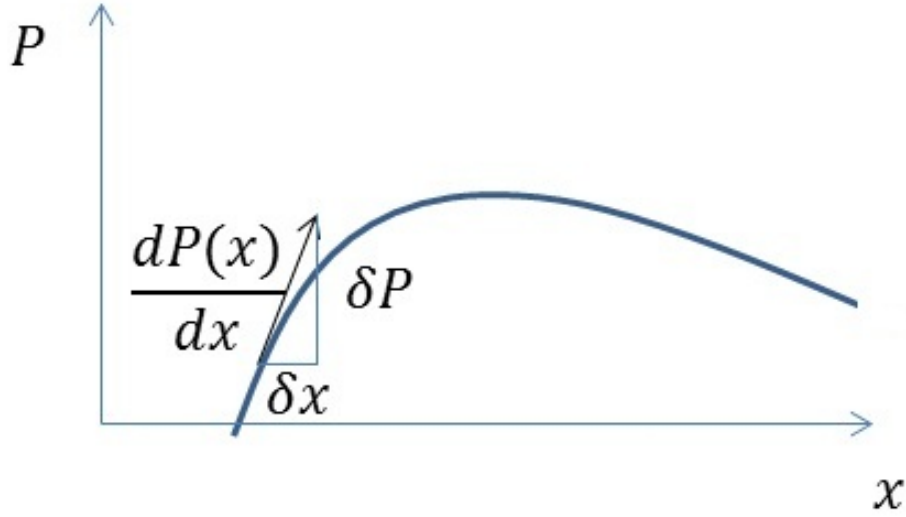
Figure 3.1: Linear approximation to the derivative of the applied force regarding to the displacement.

composed of the thickness taking $50[\mu m]$ and the fronted perimeter between capacitors of $8[mm]$, and the air permittivity. Then for a variation of the gap from $20[\mu m]$ to $2[\mu m]$ and using Eq.**??**cap] to obtain the capactance variation due to this gap displcement the obtained capacitance vary from $0.18[pF]$ to $1.8[pF]$ then the range is defined to be higher than this maximum value.

Regarding to the capacitance resolution, taking the derivative of Eq.2.3 and isolating dC assuming it as an increment of capacitance, $dC \approx \delta C$, using Eq.3.1 acting in the same way as in the force increments, thus can be obtained the minimum detectable increment of capacitance knowing the minimum displacement detectable shown above and using it for the initial gap, it is obtained the resolution in capacitance to be of $4.3 \cdot 10^{-18}[F]$.

$$\delta C \approx \frac{dC}{dx}\delta x \tag{3.1}$$

Also the increment in displacement it can be expressed as Eq.3.2 in case of δC is well known.

$$\delta x \approx \frac{dx}{dC}\delta C \tag{3.2}$$

$$\delta P \approx \frac{dP}{dx}\delta x \tag{3.3}$$

34

Figure 3.2: DAS chosen: Analog Devices AD7745/AD7746 Evaluation Board.

In summary the DAS requirements for capacitance range and resolution are:

$$C_{max} \geq 2[pF] \tag{3.4}$$

$$\Delta C \approx 4 \cdot 10^{-18}[F] \tag{3.5}$$

ANALOG Devices AD7745/AD7746 evaluation board accomplish these requirements, see the data sheet in [12], and will be used in all characteristic studies.

It has to be empathized that this parameters are chosen for parallel plate configuration, for the comb-drive design the resolution requirements are less restrictive because of the higher magnitude of $\frac{dC}{dx}$. Consequently the measured ranges for this designs must be controlled. This issue is not of big concern as the DAS can work in differential mode rather than absolute values of capacitance. As long as the differential mode will not exceed the device maximum range.

Chapter 4

Structural analysis and advantages of the prebuckled beams as a force sensors

In this chapter it is discussed how the buckling geometrical instability can be used to amplify relatively small displacements towards the the beam initial longitudinal axis. The deflection of the middle point of the beam are affected by small displacements on the beam causing an amplification phenomena useful for sensing small limited displacements.

4.1   Displacement amplification

The deflection of the central point of a straight beam axially loaded is almost negligible when the value of this force is smaller than its critical load. Once the critical load is overcome a small displacement due to an axial load will be amplified in the central midpoint of the beam. A pre-buckled beam has the advantage of the amplification phenomena on the displacements of its central point, without the need of overcoming the critical load. The displacement of the end where the force is applied can be orders of magnitude less that the displacement that will experience the central point of the beam. This relationship has to be fully understood in order to optimize the behavior of the sensor. The proposed force sensor will be based on a pre-buckled beam shape with an initial span a, see Figure 4.1 that after the input force is applied will be amplified till a value b.

The amplification phenomenon depends of the initial buckling and material properties. The relationship between the lateral displacements to the midpoint is obtained in order to optimize the magnitude of displacements needed in the midpoint of the beam to be sensed using variable capacitors.

According to the parameters described in Figure 4.2, the arc-length parameter s is
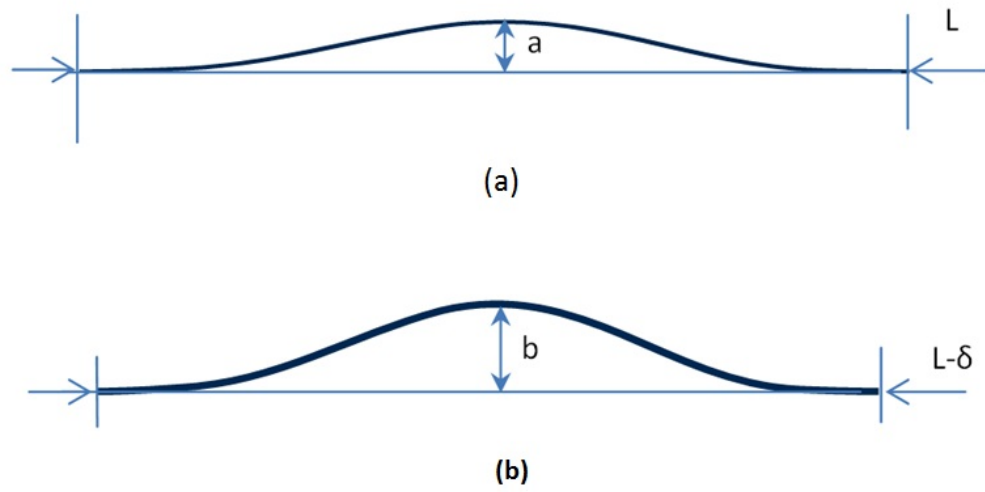
Figure 4.1: (a)Initially deformed beam shape (b) Deformed shape after the P applied axial force.
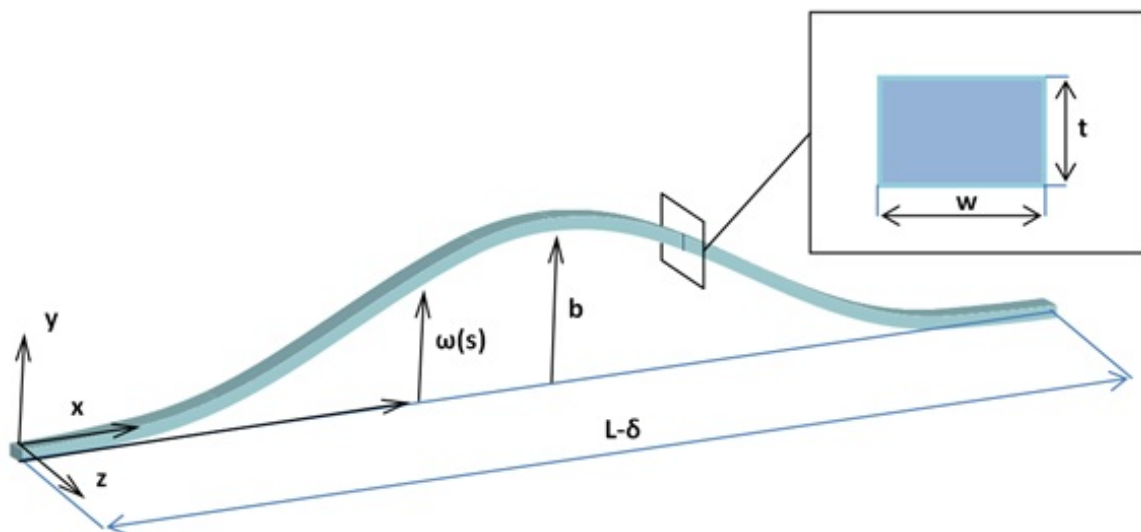
Figure 4.2: Representation of the beam geometry

related with the planar x component as:

$$x = \int_0^l \sqrt{1 - w'(s)^2} dx \tag{4.1}$$

Where $w'(s)$ is the first derivative of the lateral displacement as a function of the axial coordinate s. In order to solve this integral, an approximation of $w'(s) << 1$ is assumed. Then using the Mclaurin approximation the value of square root is approximated by

$$\sqrt{1 - w'(s)^2} \approx 1 - \frac{1}{2}w'(s)^2 - \frac{1}{8}w'(s)^4 \tag{4.2}$$

Moreover, the beam shape when deflecting is assumed to follow a cosine fuction. Finally the x axis projected arc length can be redefined as:

$$lx \approx l - \frac{1}{4}\frac{b^2\pi^2}{l} - \frac{3}{64}\frac{b^4\pi^4}{l^3} \tag{4.3}$$

Where l is the beam length, b the span of the beam at the midpoint. Then the axial tip displacement can be expressed as:

$$\varepsilon = lx - lxo \approx \frac{\pi^2}{4l}(a^2 - b^2) + \frac{3\pi^4}{64l^3}(a^4 - b^4) \tag{4.4}$$

Replacing b by $a + \delta$, and taking into account the first quadratic term of equation 4.4 as an approximation:

$$\varepsilon \approx \frac{\pi^2(\delta^2 + 2a\delta)}{4l} \tag{4.5}$$

Now for small displacements of both points it can be approximated as:

$$\frac{d\varepsilon}{d\delta} \approx \frac{(\delta + a)\pi^2}{2l} \tag{4.6}$$

If we call A the small displacement incremental ratio:

$$A = \frac{d\delta}{d\varepsilon} \tag{4.7}$$

$$A = \frac{2}{(\frac{\delta+a}{l})\pi^2} = \frac{2}{B\pi^2} \tag{4.8}$$

Analyzing equation 4.8, we notice that a high amplification factor $A(20 - 200)$ can be achieved for $B(10^{-2} - 10^{-3})$. In summary $A > 1$ is the region of interest. It is easy to see
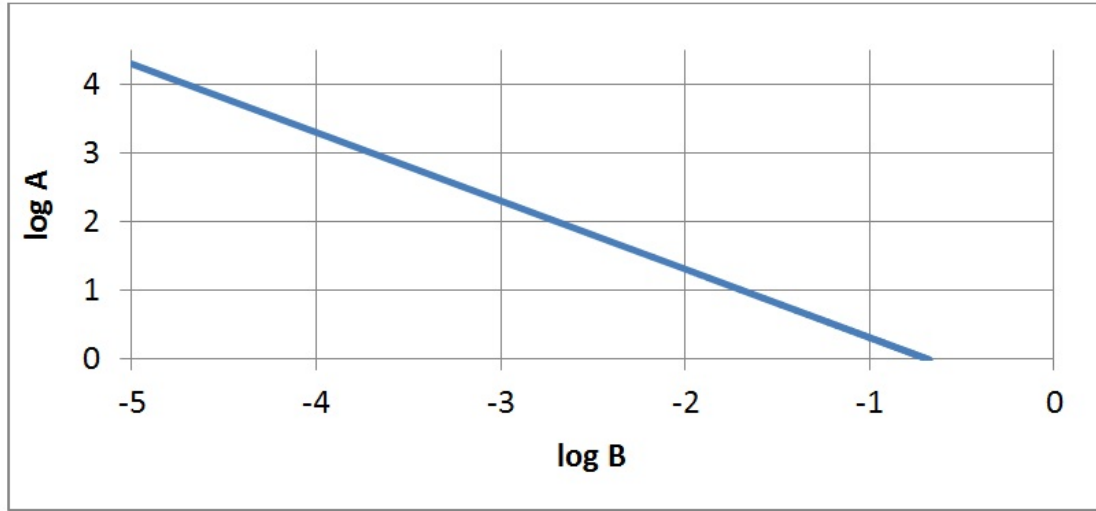
Figure 4.3: The amplification factor vs non-dimensional displacement

that this factor reaches its maximum when $\epsilon = 0$ i.e. the smaller the displacement the higher the A. Notice also that there is a limit in the amplification factor when $A = 1$ this being $B = 2/\pi^2 = 0.2$, this implies that the interest region can be found up a limit of delta as:

$$\delta_{lim} = \frac{2l}{\pi^2} - a \tag{4.9}$$

This amplification factor decreases as delta increases and for higher values of the initial amplitude a. This is easily seen in Figure 4.3 taking logarithm on both sides of equation 4.8:

$$\log(A) = -\log\left(\frac{B\pi^2}{2}\right) \tag{4.10}$$

If $log(A)$ is less than 0 a is less than 1 so there will be no further amplification increasing B, so the lateral displacement increments is smaller than the lateral one.

4.2 Structural analysis

In this chapter it is analyzed the theory behind the structural behavior of the buckling instability due to a axial force applied at the tip of the beam-structure, and how the addition of a capacitor placed at the middle point of the beam can affect to the displacement for censing interests. It is also validate the process using a FEA.
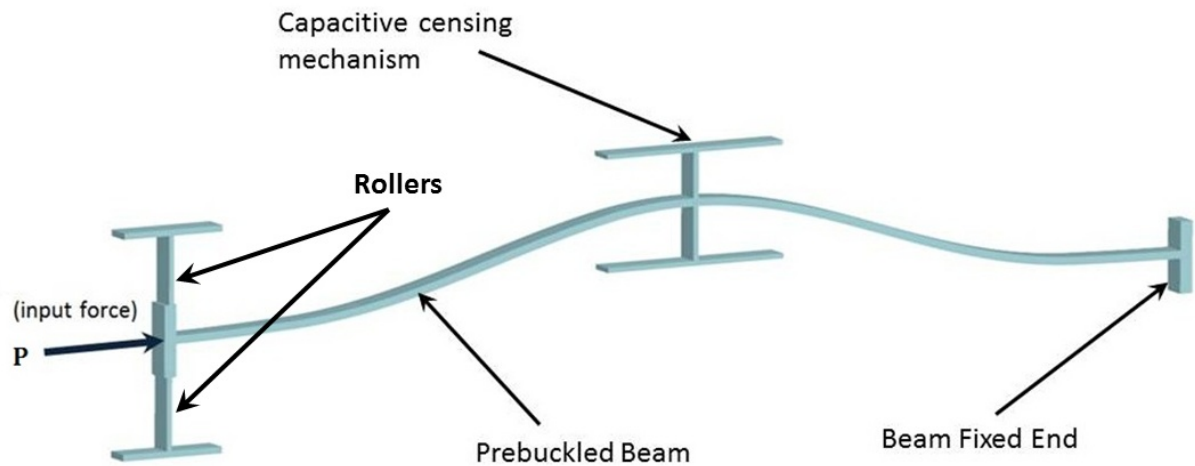
Figure 4.4: Pre-buckled beam with the actuation parallel plate capacitors.

4.3 Design of a force sensor using a pre-buckled beam

The amplification factor A justifies the use of a pre-buckled beam as a simple mechanism to measure axially loaded forces. The source of force to be measure i.e. colloidal engines in this application, applies a force F at the free end of the beam. This free end deflects insignificantly but the midpoint of the beam experience an amplified displacement that can be sensed using a capacitor, see Figure 4.4.

In order to sense the motion of the midpoint of the beam a pair of parallel plate capacitors will be attached to this point. The parallel plate capacitors will generate a force that is assumed to be a punctual load applied at the middle point of the beam.

To constrain the motion in the transverse direction, without affection in axial displacement the roller is placed on the tip based on slender cantilevers beams.

The relationship between the force applied and the midpoint deflection depends mainly on the geometry of the pre-buckled beam and the material properties. So, this relationship is analytically obtained to tune the design of the required force sensitivity with reasonable displacement at the midpoint.

The following assumptions are done to derive the analytical relationship between the axial force and the midpoint displacement:

- The mass forces are neglected.

- The length increase is neglected compared to the total length.

- The material is elastic and isotropic with a constant young modulus.

- The deformation in the transverse local direction is not considered.

- The initial length is well known.
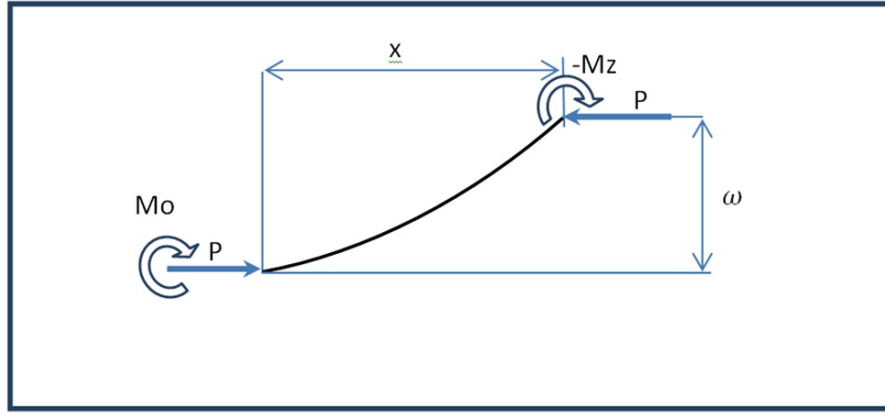
Figure 4.5: Description of the internal generalized forces on a beam segment

- The cross section of the beam keeps its high-width relationship constant.

- The initial beam shape is considered to be the same as its first mode i.e. cosine.

The bending moment equilibrium of a beam cross-section is shown in the Figure 4.5.

The moment is proportional to the curvature at each section of the beam, and assuming small deflections:

$$M_z = -EI\omega''$$
(4.11)

Where M_z refers to the internal flexural moment in z direction, E is the Young's modulus and I is the minimum moment of inertia from the neutral axis taken in z direction. Then replacing M_z as a function of s. The following differential equation is obtained

$$\omega''' + \frac{P}{EI}\omega' = 0$$
(4.12)

Solving the homogeneous equation, the general solution for w as function of s to equation 4.12 is:

$$\omega(s) = A\cos(\frac{2\pi}{l}s) + B\sin(\frac{2\pi}{l}s) + C$$
(4.13)

Equation 4.13 should verify the boundary conditions that are shown in Figure 4.6. One end is fixed and the other end is considered to be guided due to the presence of the roller of total length l_3 that will only allow the motion in $s \approx x$ direction.

Then the boundary conditions are:

$$\omega(0) = \omega'(0) = \omega(l) = \omega'(l) = 0$$
(4.14)
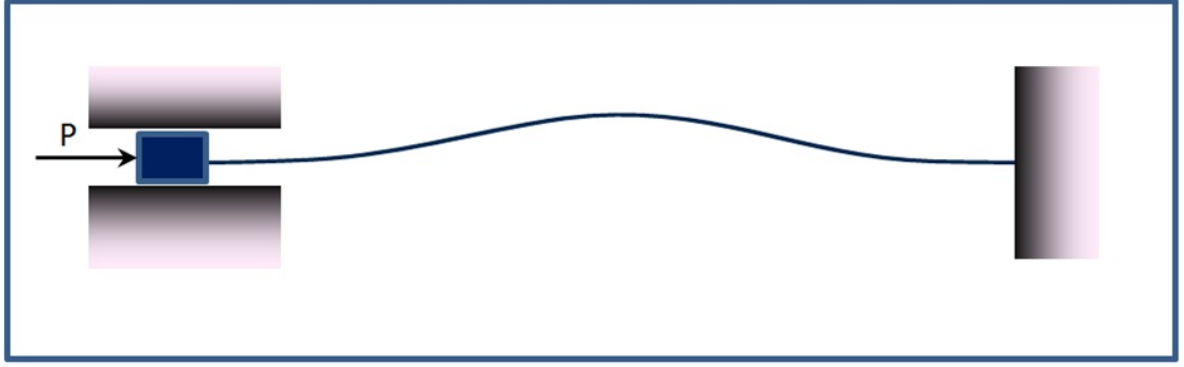
Figure 4.6: The boundary condition of the guide-fixed beam.

Because of the assumption of small tip displacements the function of x can be approximate by the function of s. When working with s the cosine pulsation can be considered constant so this parameter is independent from the arc-length parameter at any s point simplifying the solution treatment. Then the solution to equation 4.12 as function of s is:

$$\omega(s) = \frac{b}{2}(1 - \cos(\frac{2\pi}{l}s)) \tag{4.15}$$

Where b the amplitude at the middle point as seen in Fig.4.7. If equation 4.11 is written in term of the arc-length parameter, it can consider large displacements and becomes:

$$\frac{M_z(s)}{EI_z} = \frac{\omega_o''(s)}{\sqrt{1 - \omega_o'(s)^2}} - \frac{\omega''(s)}{\sqrt{1 - \omega'(s)^2}} \tag{4.16}$$

Where $\omega_o(s)$ is the initial beam shape.

The free body diagram of the pre-buckled beam is shown in Figure 4.7.

Where R is the resulting applied load applied to the free end. F_c is the resulting force of the two electrostatic forces generated by the capacitors. M_o, R_h, R_v are the flexural moment at the tip and the vertical and horizontal reactions.

Analyzing a general cross-section the resulting flexural moment is defined as:

$$M_z(s) = M_o + P\omega + \frac{F_c}{2}x = EI_z(\frac{\omega_0(s)''}{\sqrt{1 - \omega_0(s)'^2}} - \frac{\omega(s)''}{\sqrt{1 - \omega(s)'^2}}) \tag{4.17}$$

Being x and M_o:
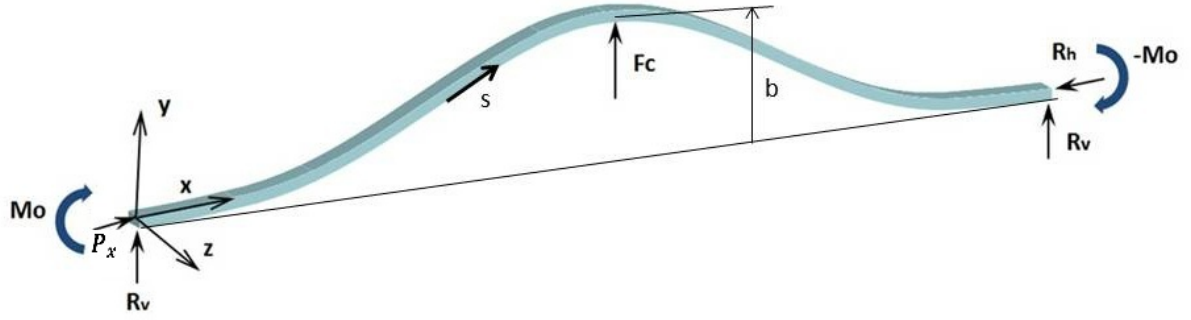
Figure 4.7: Representation of the externally generalized forces acting on the beam.

$$x = \int_0^l \sqrt{1 - w'(s)^2} dx \qquad (4.18)$$

$$M_o = -\frac{F_c l}{8} - \frac{bP}{2} \qquad (4.19)$$

To solve equation 4.18 an approximation to x up to 6 order McLaurin equation is used. It is assumed that $\omega(s)$ is a cosine function of arc-length and the rest of the parametric terms. Solving the equation 4.17 using the Galerkin method font [6]for the well-known solution shape and isolating the external load P_x as a function of the other parameters it is obtained:

$$P_x = \frac{192EI_z}{l_3{}^3} \frac{\pi^2(a^2 - b^2)}{l} + \frac{3\pi^4(a^4 - b^4)}{16l^3} + \alpha EI_z + \beta F_c \qquad (4.20)$$

Where the coefficients α and β are:

$$\alpha = \frac{\pi^2}{l}(4(1 - \frac{a}{b}) + (\frac{\pi^2}{l})\frac{b^2}{2}(1 - \frac{a^3}{b^3}) + (\frac{\pi}{l})^4\frac{b^4}{16}(1 - \frac{a}{b})) \qquad (4.21)$$

$$\beta = \frac{b^3}{l}(\frac{3\pi^4}{128} + \frac{\pi^2}{15}) + (\frac{b}{l})(\frac{\pi^2}{8}) - (\frac{1}{b})(\frac{2l}{\pi^2}) \qquad (4.22)$$

The constants a and b are the initially and the final amplitude of the middle point of the beam as shows Fig.4.1 respectively. E is the Young modulus of the material used for the structure, the parameter I_{z3} is the z moment of inertial the roller, l_3 is the mentioned roller length.

The force F_c is the electrical force due to the attraction between the parallel plates that composes the capacitor, that for this case is obtained in Eq.2.7. Becoming for this case a parallel plate configuration it is used Eq.4.23 because of the addiction of another capacitor on the opposite side of the beam adding a force term in opposite direction.
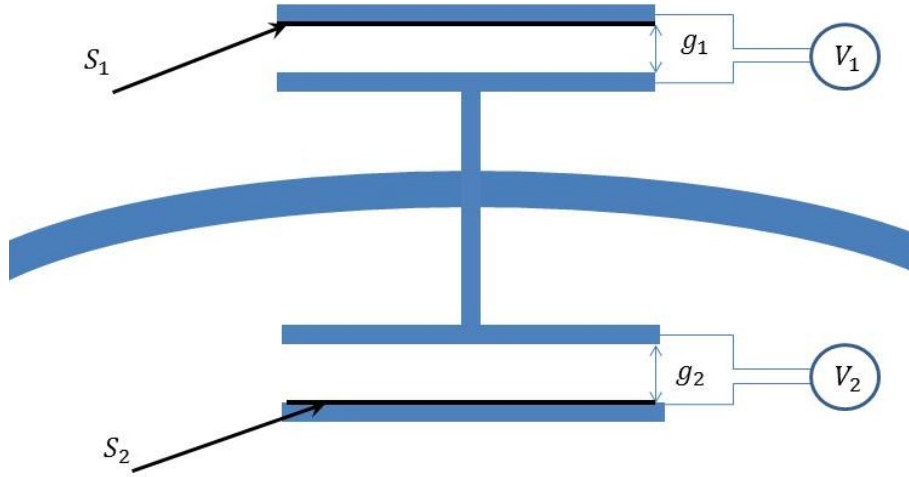
Figure 4.8: Detail of the parallel plate positioning and configuration parameters in the Prebuckled beam.

$$F_c = \frac{\varepsilon V_1^2 S_1}{2(g_1 - (b-a))^2} - \frac{\varepsilon V_2^2 S_2}{2(g_2 + (b-a))^2} \tag{4.23}$$

Where g_1 and g_2 are respectively the capacitor initial gap separation between the top and bottom plates respectively, ϵ is the permittivity of the medium between the capacitor, V_1 and V_2 are the electrical potential between the two pairs of plates respectively and S_1, S_2 are the capacitor faced plates areas respectively being shown in Fig.4.8.

Analytical Model Validation ANSYS FEM model of the pre-buckled beam has been created to validate the analytical model. The numerical simulation uses the next parameters: Geometrical parameters:

$$l = 5[mm]$$
$$a = 0.1[mm]$$
$$h = 20[\mu m]$$
$$t = 2[\mu m]$$
$$w = 10[\mu m]$$

The material property:

$$E = 170[GPa]$$

$$\tag{4.24}$$

Figure 4.9 shows the relationship between the axial load applied ant the displacement of the midpoint of the pre-buckled beam.
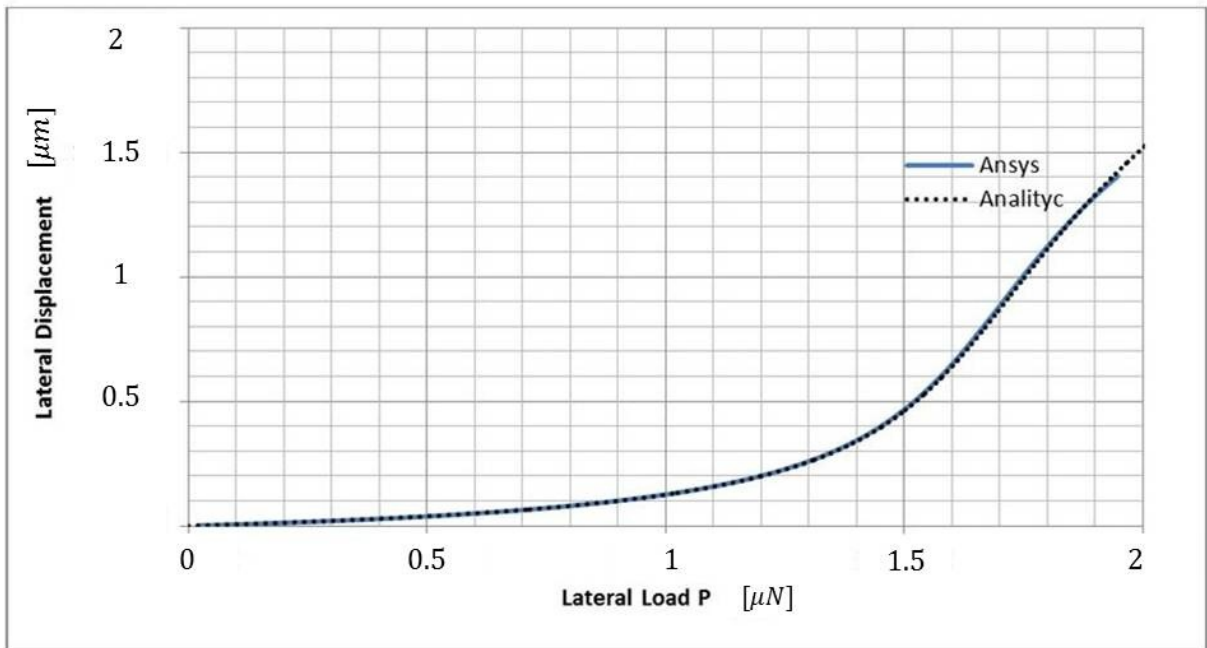
Figure 4.9: Lateral displacement vs axial force P.
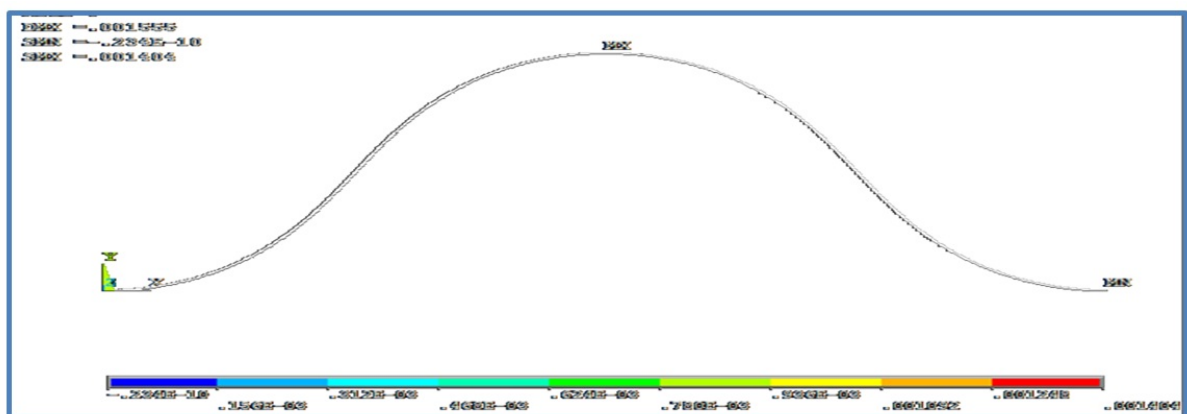
Figure 4.10: ANSYS plot of the final shape.
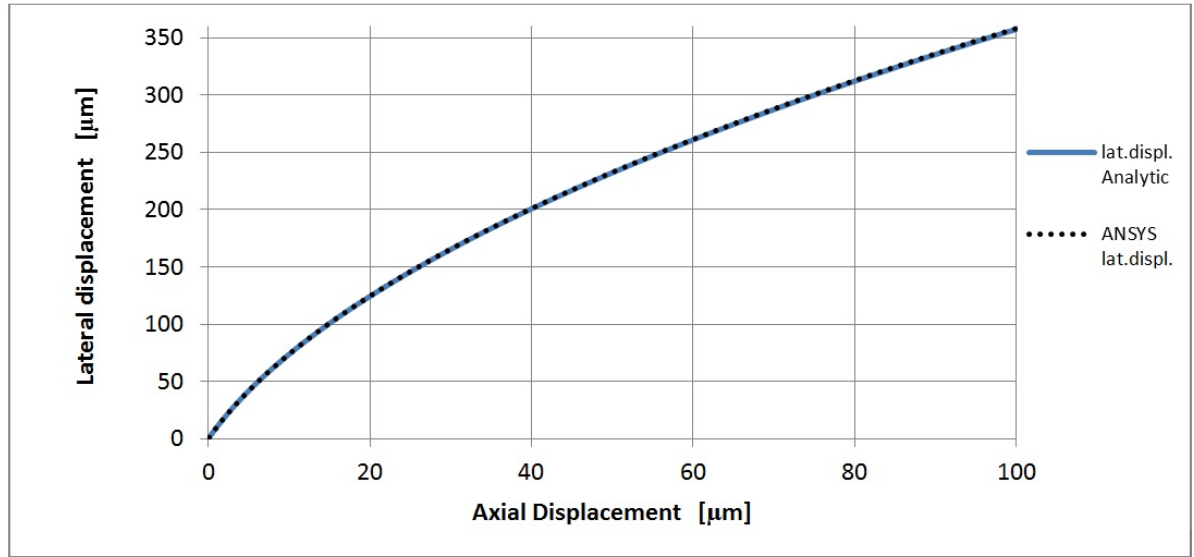
Figure 4.11: Lateral displacement vs axial displacement.

The relationship between axial- midpoint are also compared in the analytical solution and the FEA solution in Figure 4.11. The comparative of the two curves for the plotted range obtained validates the assumptions done to derive the analytical solution. However and in order to get a more accurate approximation more terms can be included in the analytical solution of the equation 4.2.

4.3.1   Preliminary design of a 1 DOF force sensor

In this chapter it is presented the study and design of a force sensor based in the Prebuckled beam design seen in Chapter 4.

This design presented schematically in Fig.4.12, it uses a prebuckled beam configuration with high ratio $\frac{a}{l}$ of initial deformation of its middle beam point. As it can be seen in Fig.4.12, the configuration of the capacitors is made by the use of two parallel plates capacitors placing each one at both sides of the middle point of the prebuckled beam, detailed in Fig.4.8.

In order to avoid the undesired vertical displacement of the beam exposed end, it has connected a two crossed beam configuration in order to overcome this issue this are called the roller. Even though this structural modification affects the stiffness in the undesired way the instability generated by the parallel plates reduce rigidity as it will be shown.

The geometry and material are the same as the previous example but in the complete force sensor the effect of the capacitors and the rollers is also included. The cantilever beams that act as roller has the following length and inertia:
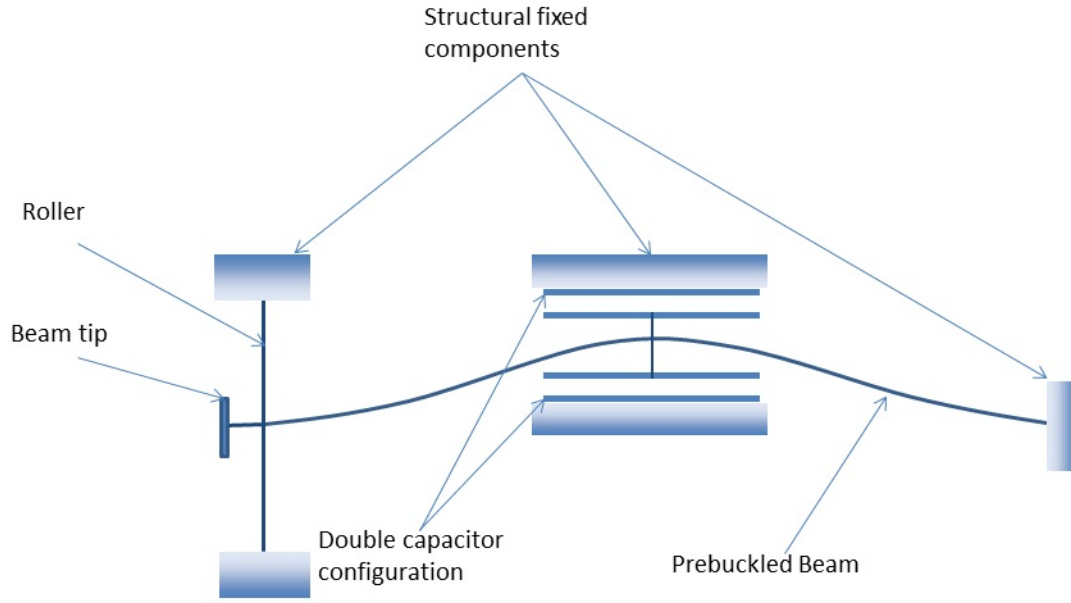
Figure 4.12: Scheme of the double capacitor parallel plate configuration components.

$$l_3 = 100[\mu m]$$
$$I_3 = 6.67 \cdot 10^{-24}[m^4]$$

Assuming an aqueous ambient which changes the vacuum permittivity to a higher value.

$$\varepsilon = 7.1 \cdot 10^{-9}[\frac{F}{m}]$$
$$S_1 = 0.4 \cdot lw = 2 \cdot 10^9[m2]$$

(4.25)

And an initial gap between both pair of plates of the capacitor:

$$g_1 = g_2 = 30[\mu m] \qquad (4.26)$$

Both are symmetrically separated from de middle point of the beam. With the voltage difference V as a free parameter to be changed in order to analyze the relationship. These values goes from 0 [V] to 2 [V].

Summarizing the results obtained in this preliminary design:

First of all it is studied the buckling instability behavior in order to seen its advantages and its limitations regarding to the external force stimulus. Figure 4.13 represents the
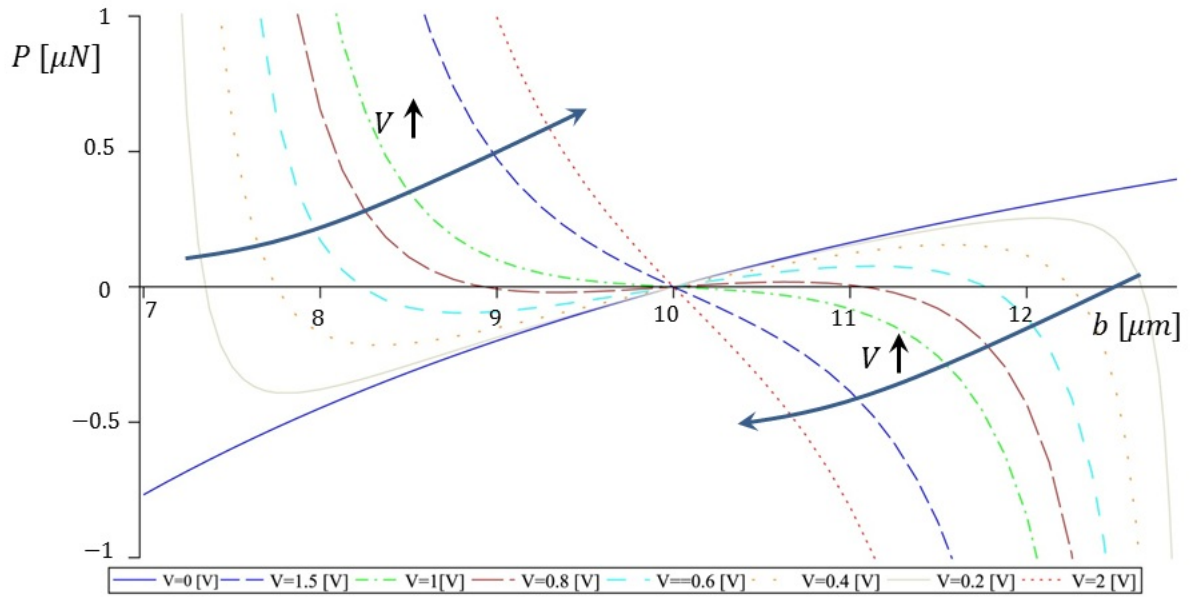
Figure 4.13: Axial force P vs lateral displacement y from the equilibrium point varying the applied voltage V.

axial force as a function of the lateral displacement around the initial deformed value. The behavior of the displacement changes when the voltage increases, therefore an almost flat slope can be achieved. This increases the sensitivity of the force sensor. Looking for a more sensitivity example, this is using the same parameters of the first example changing only the first amplitude a from 100 microns to 500 microns at voltage of 0.92 [V], the results are shown in the Figure 4.14.

Analyzing the Figure 4.14, it is clear that there are 3 equilibrium points. This determines the stability margin of the measurement process. The circular green point is the stability oscillating point (statically stable), the 2 symmetrical lateral equilibrium points (the black circles) are not stable. Any perturbation force would cause an increase of the displacement of the midpoint up to the pull in state, which of course is undesirable. However and continuing analyzing these curves the stability region can be redefined as the distance from the initial deflection up to the value at its relatives minimum and maximum. Intuitively it can be noticed that from P=0 to the mentioned value min.-max, if a small perturbation appears the behavior of the system will return the middle point i.e. to the initial position (green point). Between these two points (red points) it is defined the statically stability margin for the lateral displacement. This stability margin can be determined finding the minimum of the equation 20, this is also plotted in Figure 4.15, finding the value of the lateral displacement when the sensitivity is equal to 0.the sensitivity property is represented as a function on the lateral amplitude b.

Besides the stability range, the parameter that it has to be carefully studied is the displacement needed to sense capacitively (we need to know its order (microns or less)), because this defines the sensitivity of the device. In example 2 under study, seen Figure 4.14 and 4.15, a stability region of 1.5 microns is assumed. Then the maximum sensitivity, the worst value, is approximately 50[pN] measured at the equilibrium point, and falling
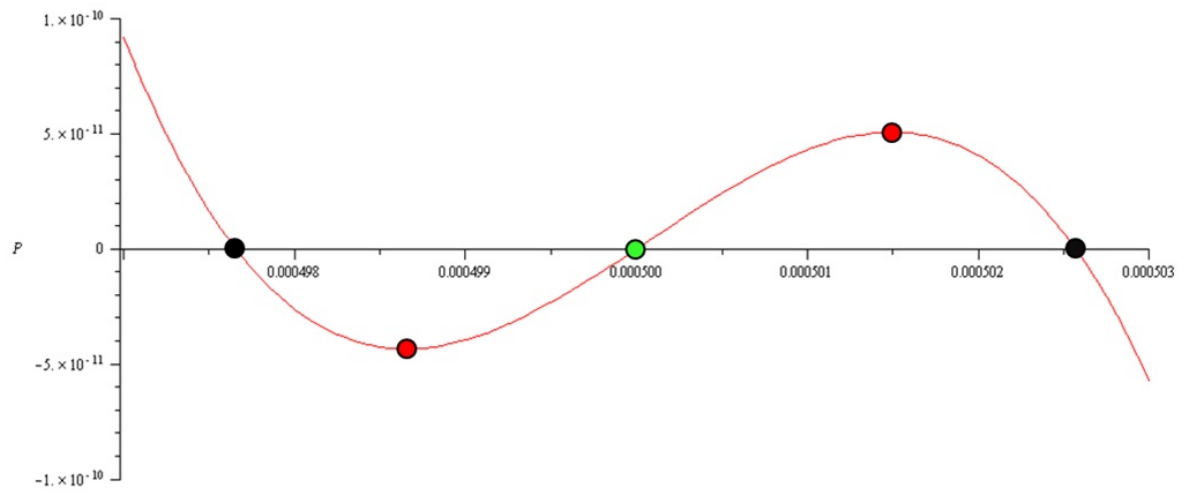
Figure 4.14: Plot of the external charge due to the lateral displacement for a=0.5[mm] V=0.92[V].
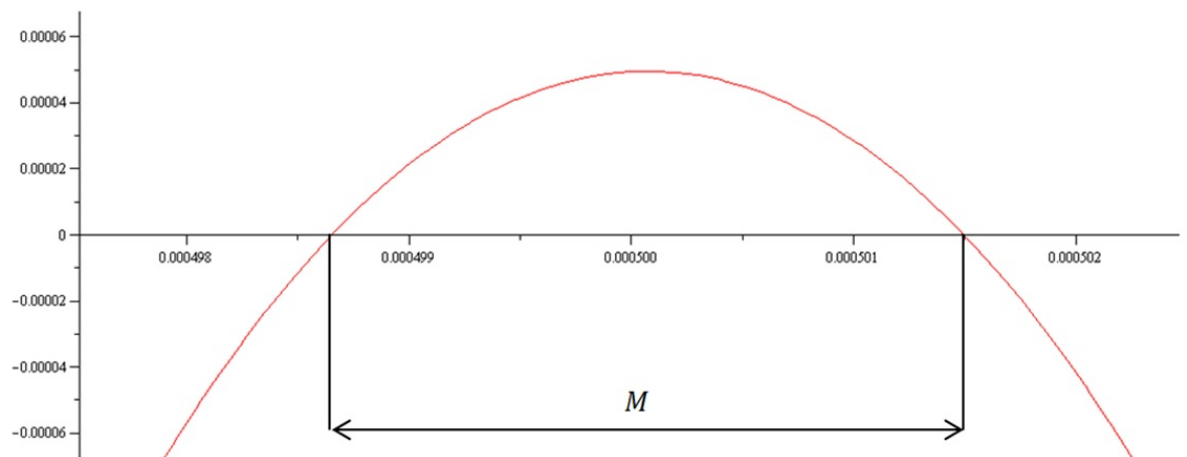
Figure 4.15: Representation of the sensitivity or the first derivate of the axial load P and the stability margin M.

down to 0 at the stability extremes. It is also interesting to see that the stability range is not symmetrical from the equilibrium middle point and shows a little smother fall in the increasing deflection direction. This have sense because the higher displacements the higher load P, as it shows the Figure 4.11.

Summarizing the instability based study:

The voltage can tune the sensitivity of the device, but the stability margin has to be considered. Other factors that improve the sensitivity are:

- The initial displacement a. If a increases the sensitivity is reduced and the stability margin increases un to a few [pN] per micron.

- The initial gap between the plates of the capacitor. The higher the gap the wider the stability region.

- The beam length. The longer the beam the smaller the critical charge and thus the sensitivity.

The inclusion of the rollers introduces more rigidity but it has very small influence on the sensitivity and the stability margin.

4.4   Design of a 1 DOF force sensor based on buckling instability

In this design the theory taken is from the prebuckled beam theory, the particularity as a difference with the preliminary design is that the beam is designed with a very small ratio $\frac{a}{l}$ of prebuckled geometrical parameter, this is because it is thought to use the higher amplification factor for a very small initial amplitudes of the middle point as it is described in Fig.4.3.

However there is an important issue regarding to reach this point of high gain in displacements this involves the critical load of the beam.

The definition of the critical load is defined in Eq.4.27, where is the function of the external non-dimensional applied load $\bar{P} = \frac{P}{P_c}$ versus the non-dimensional displacement of the beam middle point $\bar{y}$, r is the ratio of geometric parameters a/l being applied. In Fig.**??** it can be seen Eq.4.27 as a function of $\bar{y}$ for a different ratios r. It is notorious that because of the stiffness is considered to be the derivative of the external force regarding to the displacement, this is reaches its minimum at $P = 1$ and for $r = 0$ which means that the maximum sensitivity reachable is for a straight beam with an applied force of $P = P_c$ which is exactly the Euler critical load for this boundary conditions being $P_c = \frac{4\pi^2 EI}{l^2}$.

$$\bar{P} = \frac{\bar{y}\left(64 + (r + \bar{y})^4\,\pi^4 + \left(24\,r^2 + 24\,r\bar{y} + 8\,\bar{y}^2\right)\pi^2\right)}{64\,r + 64\,\bar{y}} \tag{4.27}$$
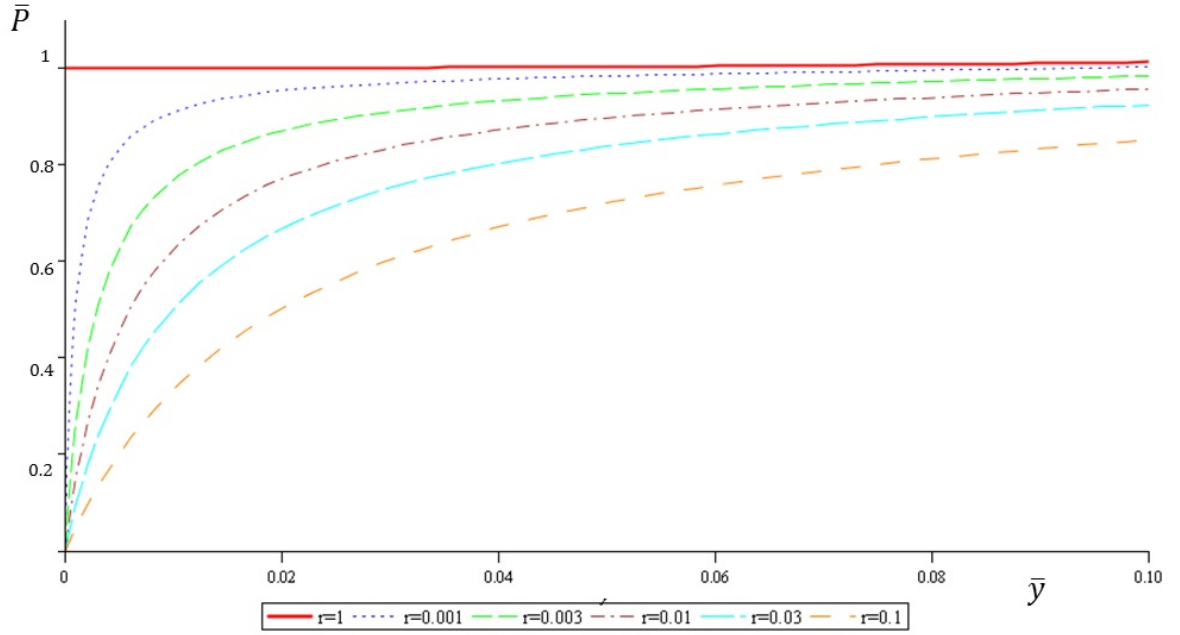
Figure 4.16: Non-dimensional external axial load versus the non-dimensional lateral displacement for different ratios $r = \frac{a}{l}$.

In order to take advantage of the mentioned sensitivity gain close to the straight beam configuration this device uses the critical load beam as an amplification factor for the lateral displacement. The concept idea is shown in a scheme in Fig.6.1.

This force will be applied at the end of the beam and on axial compressive direction, this is shown in Fig.6.1 being originated by the potential voltage difference ΔV_l applied on a capacitor placed close to the beam tip. This configuration also uses two folded beam suspension in series in order to avoid transverse displacements on the actuator as a roller.

The concept of a folded beam suspension is the same as to use a single beam as a roller with the advantage of less stiffness is added to the entire system because the length of the equivalent crossed roller beam is doubled, reducing the stiffness by a factor of 8 as is shows Eq.4.28 for a single crossed beam with a load applied at its middle point in shear direction.

$$K = \frac{192 \cdot EI}{l^3} \tag{4.28}$$

Taking advantage of the structural analysis for the prebuckled beam it can be obtained the model os the device by the way of an additional modification, this is by modifying equation 4.20 discomposing the external axial force P to be the sum of both the electrical induced and the external one on the tip, this is $P = P_{ext} + F_{c2}$.

Adding this new lateral electrical force generated by parallel plates Eq.2.7 separated
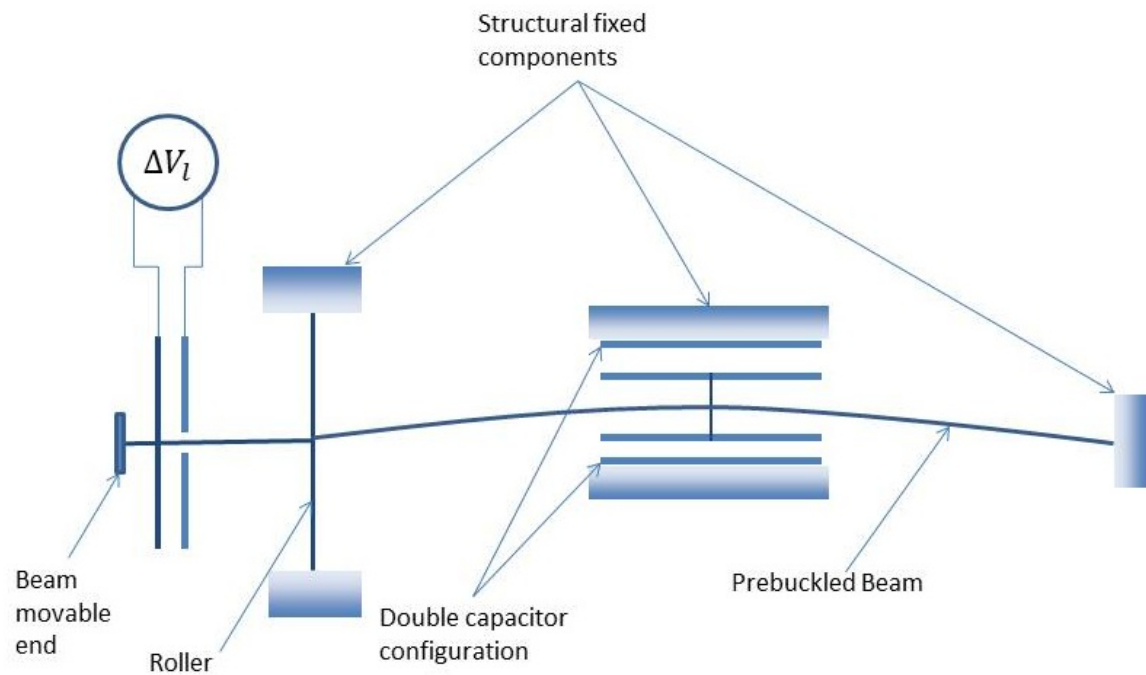
Figure 4.17: Scheme of the single prebuckled beam sensor based on the induced critical load device.

a gap g, other parameters that should be chosen to fulfil the stiffness requirements for a measuring desired range.

Due to the instability margin the initial voltage value has to be chosen both in order to reach an equilibrium point and to have an acceptable displacement margin.

Another important parameter to take into account for the design is the ratio r in this case it is taken a small ratio in order to guaranty deflection of the middle point of the beam and at the same time a high gain in sensitivity.

The capacitance configuration chosen for this example is a Comb-Drive using the next design parameters:

$$l = 6[mm]$$
$$a = 1[\mu m]$$
$$w = 5[\mu m]$$
$$t = 50[\mu m]$$
$$\Delta V_l = 35.4[V]$$
$$g_0 = 5[\mu m]$$
$$g = 20[\mu m]$$

$$n = 800$$
$$\epsilon = 8.8542[\frac{pF}{m}]$$
$$\Delta C = 12[aF] \tag{4.29}$$

Where the new parameters counted are n the number of fingers of the Comb-Drive capacitor configuration.

Now applying Eq.3.2 to solve for this case dy the minimum detectable displacement in y direction, obtaining Eq.4.30. Where the parameters of design are: g_0 the fingers lateral gap, and g is the gap between finger tips and the opposite finger roots as shown in Fig.2.5.

The results of this formula depends linearly on the resolution of the DAS, in this case this magnitude is at the value of the ratio $\frac{Carrier}{Noise}$ is greater than 1, taken the above magnitude of $4[aF] = 4 \cdot 10^{-18}[F]$ with a conservative augmentation value of 3 times, predicting a higher noise than the declared one.

$$\delta y \approx (\frac{\Delta C}{(2t \cdot \epsilon \cdot n)})(\frac{1}{(\frac{1}{g_0} + \frac{w}{(g-y)^2})}) \tag{4.30}$$

The externally force versus the lateral displacement is represented in Fig.4.20, the minimum detectable displacement using the minimum capacitance at the equilibrium point is obtained using Eq.4.30, being:

$$y_{min} = 82.472[pm]$$

Thus the minimum detectable force at the equilibrium point is:

$$P_{ymin} = 19.243[pN]$$

The maximum compressive force is limited due to the pull instability point this is:

$$P_{ymax} = 0.172[\mu N]$$
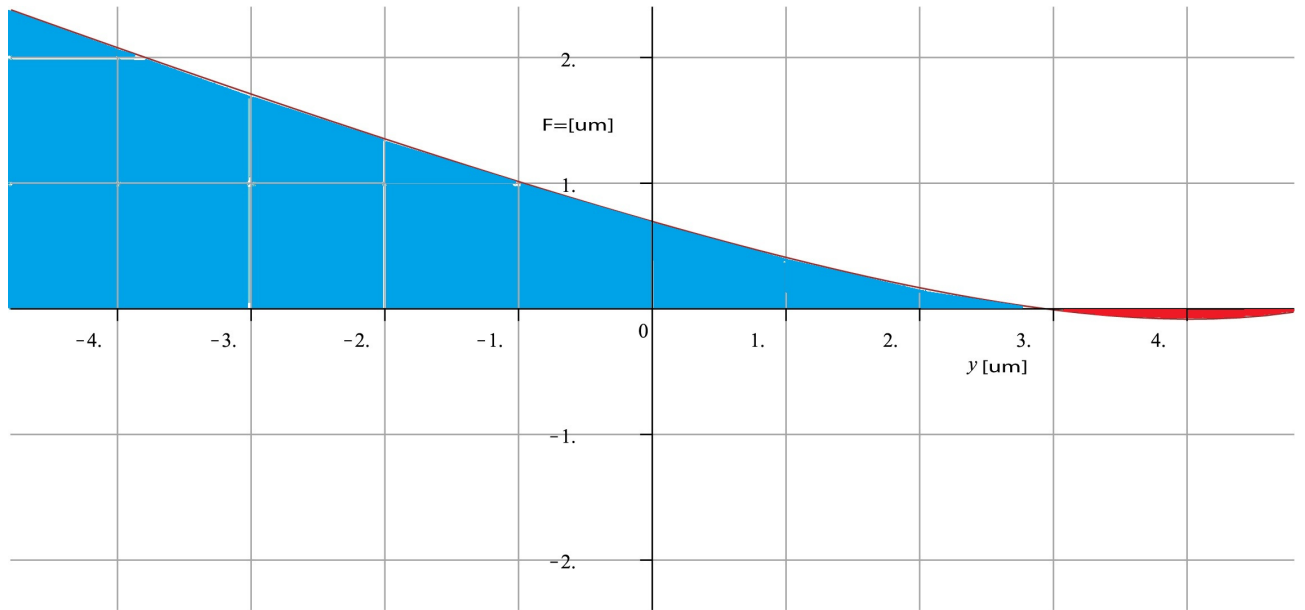
Figure 4.18: Externally force P versus the lateral displacement y for the critical load based design, blue is traction red compression.

In order to measure variations of external force δP it is also needed a derivative of the external force regarding to the displacement direction using Eq.3.3, for the solution for the device resolution.

As it can be seen in Fig.4.20 the values of the minimum detectable force changes with the displacement of the middle point. The close to the instability point the higher the sensitivity. Other important factor is that in one hand the higher the voltage applied the lower the initial force measurable from the equilibrium point in the other hand is that the smaller the compression margin of the forces, because of the proximity to the minimum in the force and therefore the low tend to 0 of the slope-stiffness. This is compression allowed zone is plotted in Fig.4.20 in red area, where also it can be seen the traction margin printed in blue area, which has avoid this margin issue.

Due to this fact this device is thought to work mostly in a very high range of traction forces plotted in blue in Fig.4.20, limited by the Yield strength of the Silicon; this range is from (0 to 158) $[mN]$. Because of the elasticity of the material up to $158[mN]$ will make the device to reach its internal contact between the capacitor gaps.

Describing the external force in front of the input voltage, shown in Fig.4.19 if the voltage is increased a different equilibrium point arises. This in fact reduces the range of displacements and the applications will depend on the offset or mean magnitude of the force. If this force is an oscillating depending on the amplitude the range has to be chosen to be fitten in the stable range of compressive forces. The higher the amplitude of the oscillation force the higher the of the range in compression must be set, this can be done by decreasing the applied voltage that forces the beam.

Nevertheless this represents a tradeoff because the higher the range of measurable forces the higher of the value of the minimum detectable force i.e. the lower the resolution,
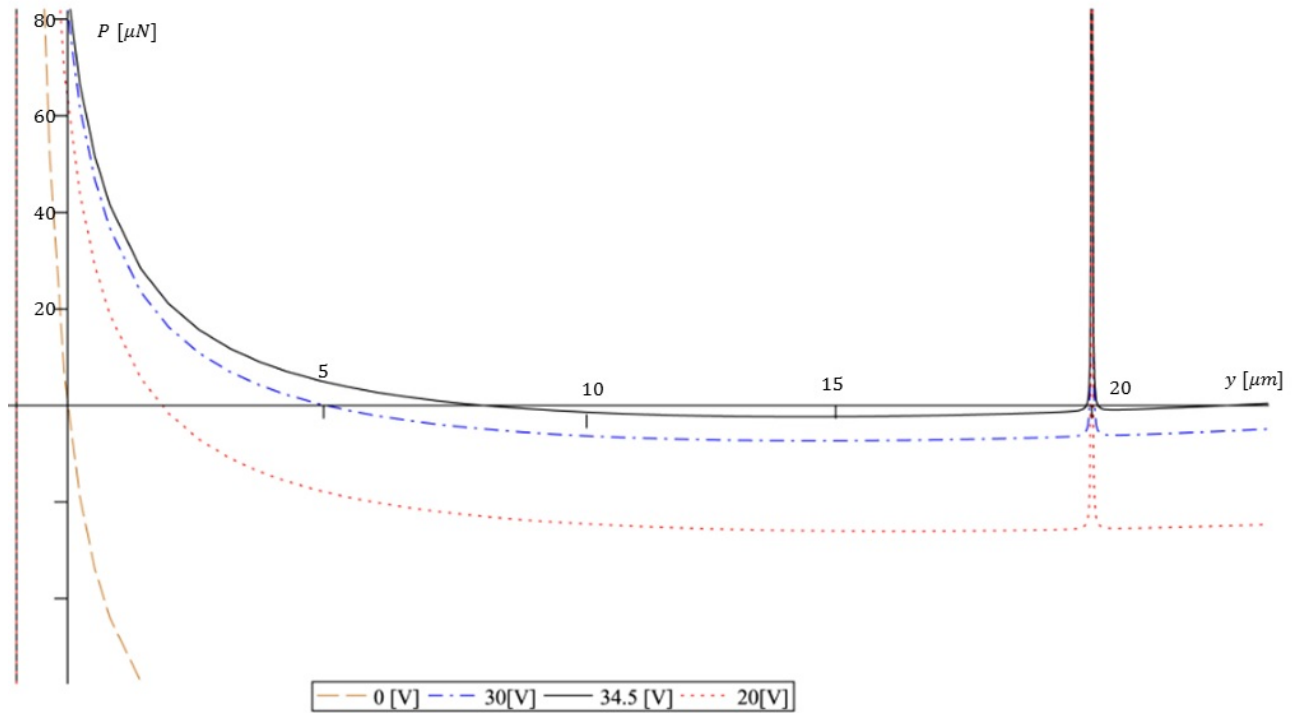
Figure 4.19: Externally force P versus the lateral displacement y of the critical load based design for different input voltages applied.

as it can be seen in Fig.4.20. Where it also shows that for higher applied voltage lower detectable force at the same measured displacement. Hence by modifying the input voltage it can be measured a wide range of forces and to get different resolutions.
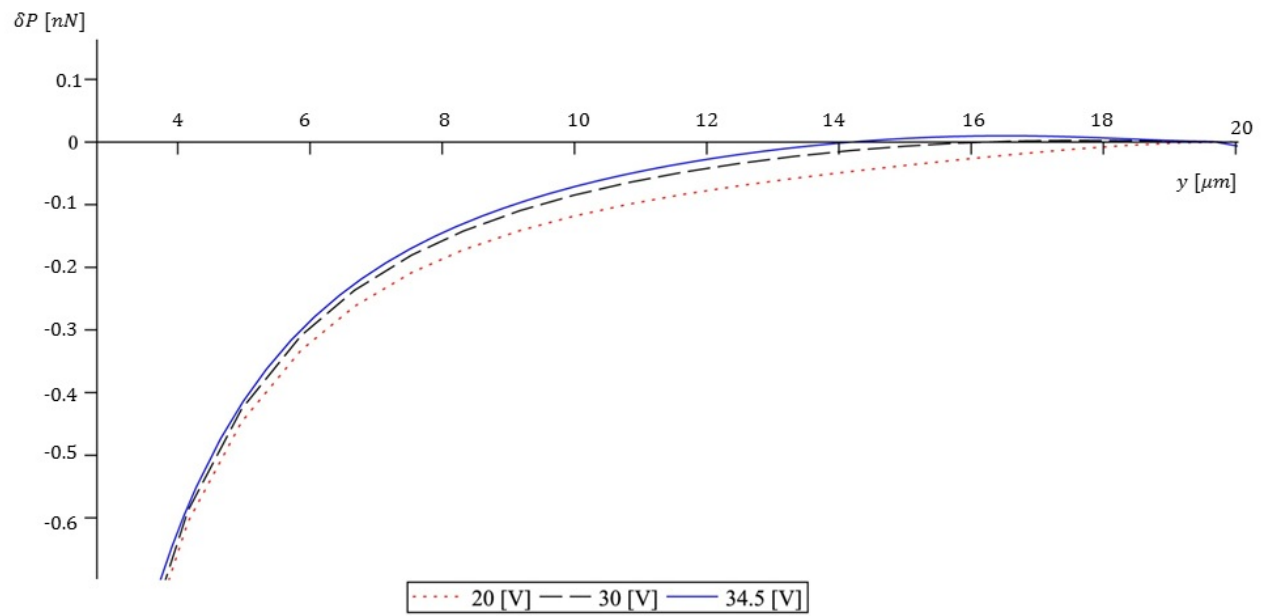
Figure 4.20: Force resolution δP versus the lateral displacement y of the critical load based design for different input voltages applied.

Chapter 5

Design of 2 DOF devices

In this chapter it is presented the study and design of two different designs for measure forces forces in two DOF, one is based on prebuckled beams and the other one is based on the straight beams.

5.1 Single prebuckled beam design

5.1.1 Standard Configuration Sensor

For this design, the two direction force sensor is based on the prebuckled geometry as shown schematically in Fig.5.1.

The geometrical parameters that define the device are shown in Fig.5.2.

Taking advantage of the first chapter theory the stiffness of the single prebuckled beam is well known, the rest of the stiffness is due to the restriction in the displacement to be of 1 dof. Therefore it has implemented two folded beam suspensions, one in order to avoid the undesired lateral displacement of the tip, shown in Fig.5.4 detail a. And the other one to permit the mobility of the specimen in 2 dof whilst the beam tip can not, this is shown in Fig.5.4 detail b.

Due to this design the force applied in one direction for example in x is affected no only by the x axis beam oriented device only, but also for the stiffness that forbid the displacement in x direction of the y oriented beam device i.e. the double folded beam suspension inside the triangular structure see Fig.5.3. Therefore there is always the addition of a second stiffness due to this interference, this is the equivalent series stiffness.

The grid structure in a triangle form observed in the final design Fig.5.3 is due to the relative to the movable structure folded beams roots, this structure is released from the substrate letting the decoupled displacement on plane 2DOF of the device end.

Because of the series spring equivalent system the complete stiffness model is the
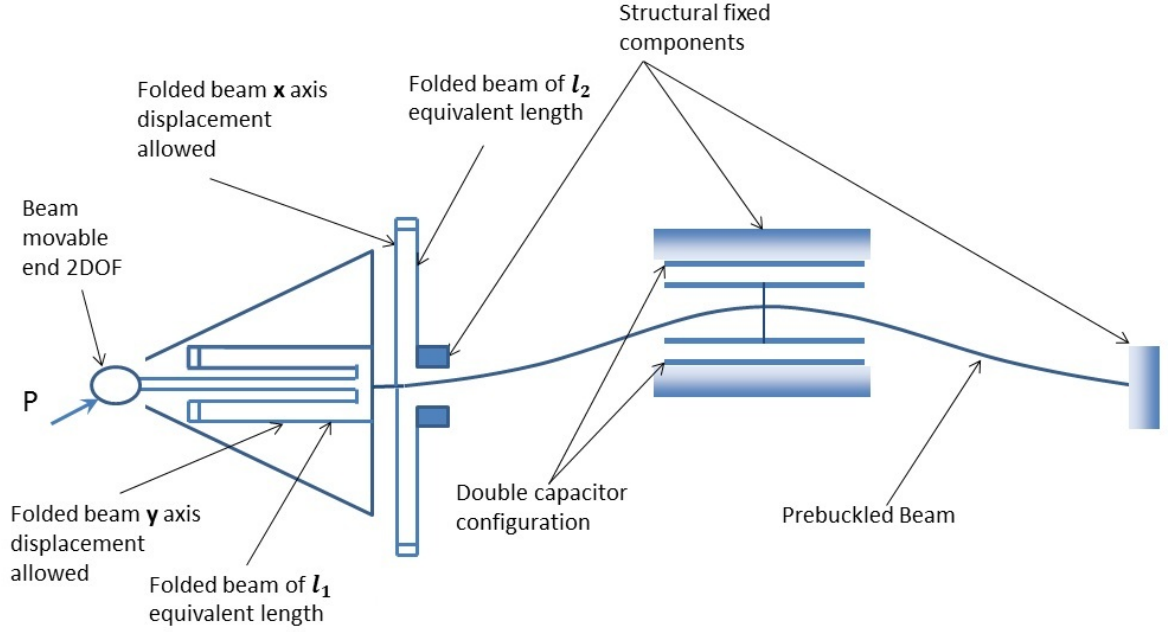
Figure 5.1: Scheme of the Single Prebuckled Design showing 1DOF branch characteristics components.

sum of two double folded beam suspension added to the x direction prebuckeld beam stiffness, thus the relationship between the axial force applied by the specimen and the lateral displacement of the middle point of the curved beam. The complete stiffness model is computed in Eq.5.1 generated by a x axis force-displacement P_x.

$$P_x = 192EI_z(\frac{1}{l_1{}^3} + \frac{1}{l_2{}^3})x + \alpha EI_z + \beta F_c \tag{5.1}$$

$$x = \frac{\pi^2(a^2 - b^2)}{l} + \frac{3\pi^4(a^4 - b^4)}{16l^3} \tag{5.2}$$

$$\alpha = \frac{\pi^2}{l}(4(1 - \frac{a}{b}) + (\frac{\pi^2}{l})\frac{b^2}{2}(1 - \frac{a^3}{b^3}) + (\frac{\pi}{l})^4\frac{b^4}{16}(1 - \frac{a}{b})) \tag{5.3}$$

$$\beta = \frac{b^3}{l}(\frac{3\pi^4}{128} + \frac{\pi^2}{15}) + (\frac{b}{l})(\frac{\pi 2}{8}) - (\frac{1}{b})(\frac{2l}{\pi^2}) \tag{5.4}$$

$$F_e = \frac{k_1}{(g_2 - (b - a))^2} - \frac{k_2}{(g_1 + (b - a))^2} \tag{5.5}$$

Where x and the coefficients alpha and beta are function of a, b, l and the length parameter l_1 and l_2 means each folded beam length respectively. The k constants are $k_1 = \frac{1}{2}V^2\epsilon tl_3$ and $k_2 = \frac{1}{2}V^2\epsilon tl_4$, where the parameters are shown in Fig.6.4.

The sensing scheme is based on parallel plates capacitors, connected in differential mode then the capacitance measure instantaneous gap variations.
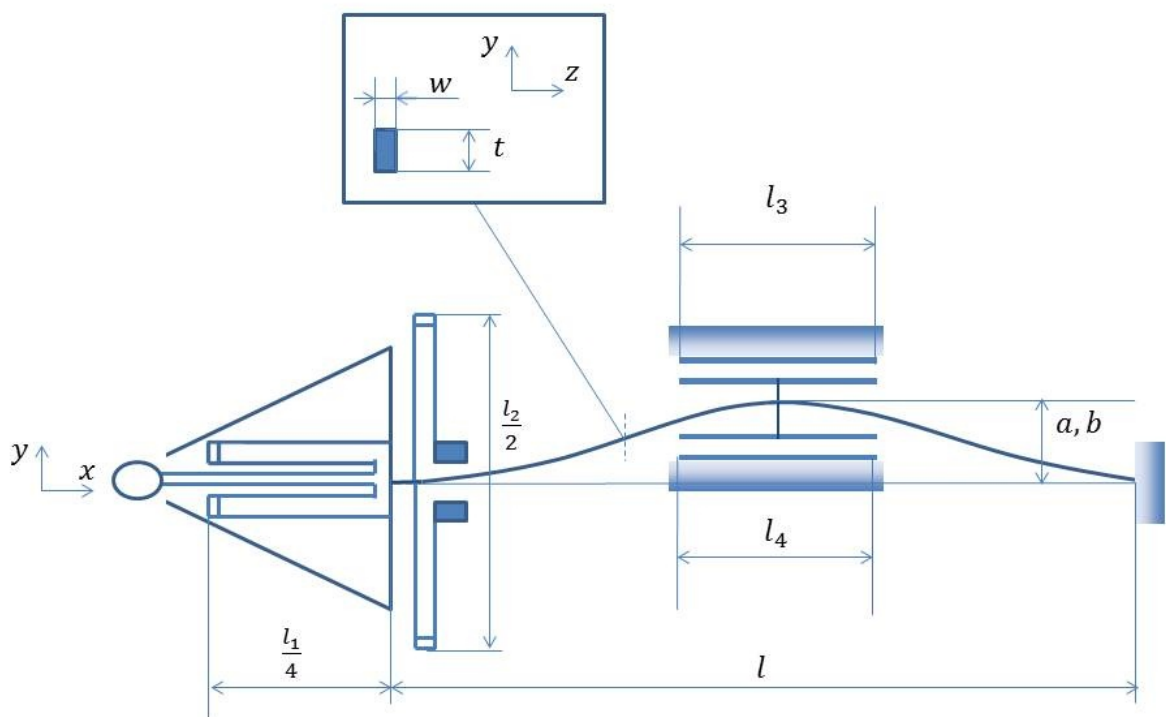
Figure 5.2: Scheme of the Single Prebuckled Design showing 1DOF branch detailed design parameters.
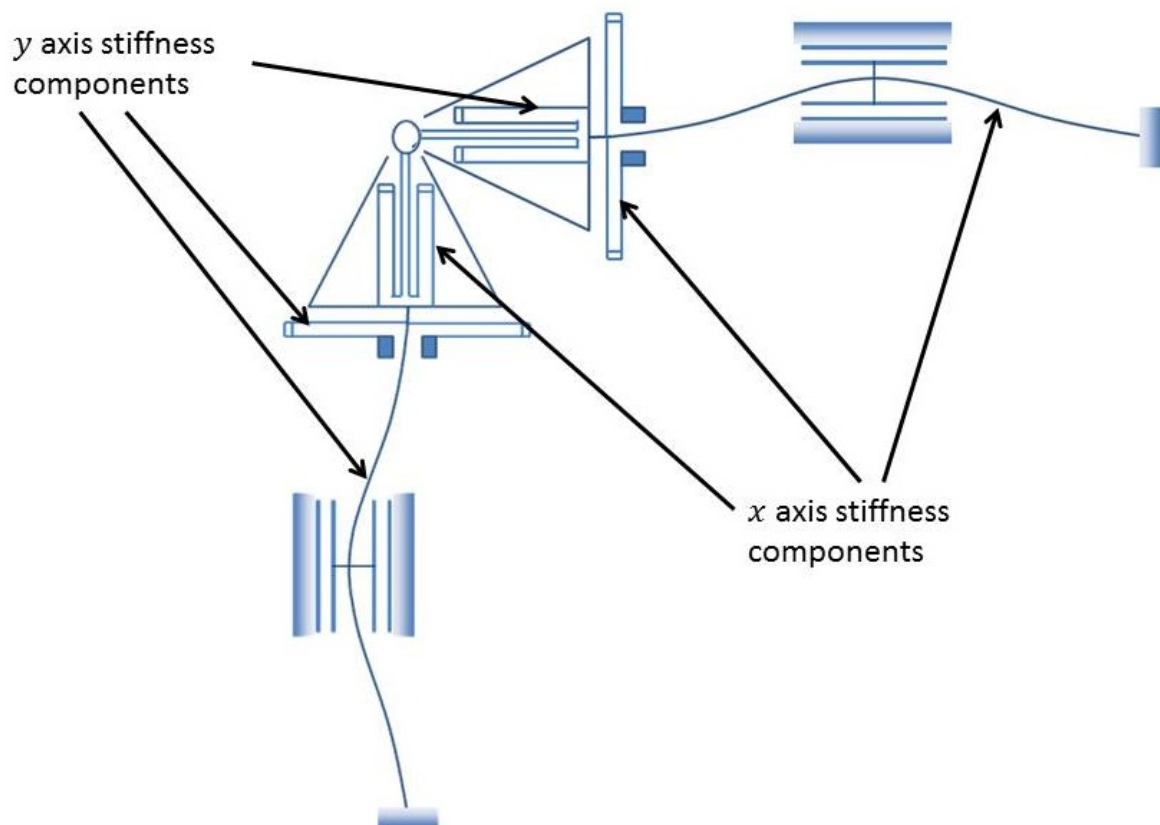
Figure 5.3: Scheme of the Single Prebuckled 2DOF Design equivalent stiffness due to the structural union.
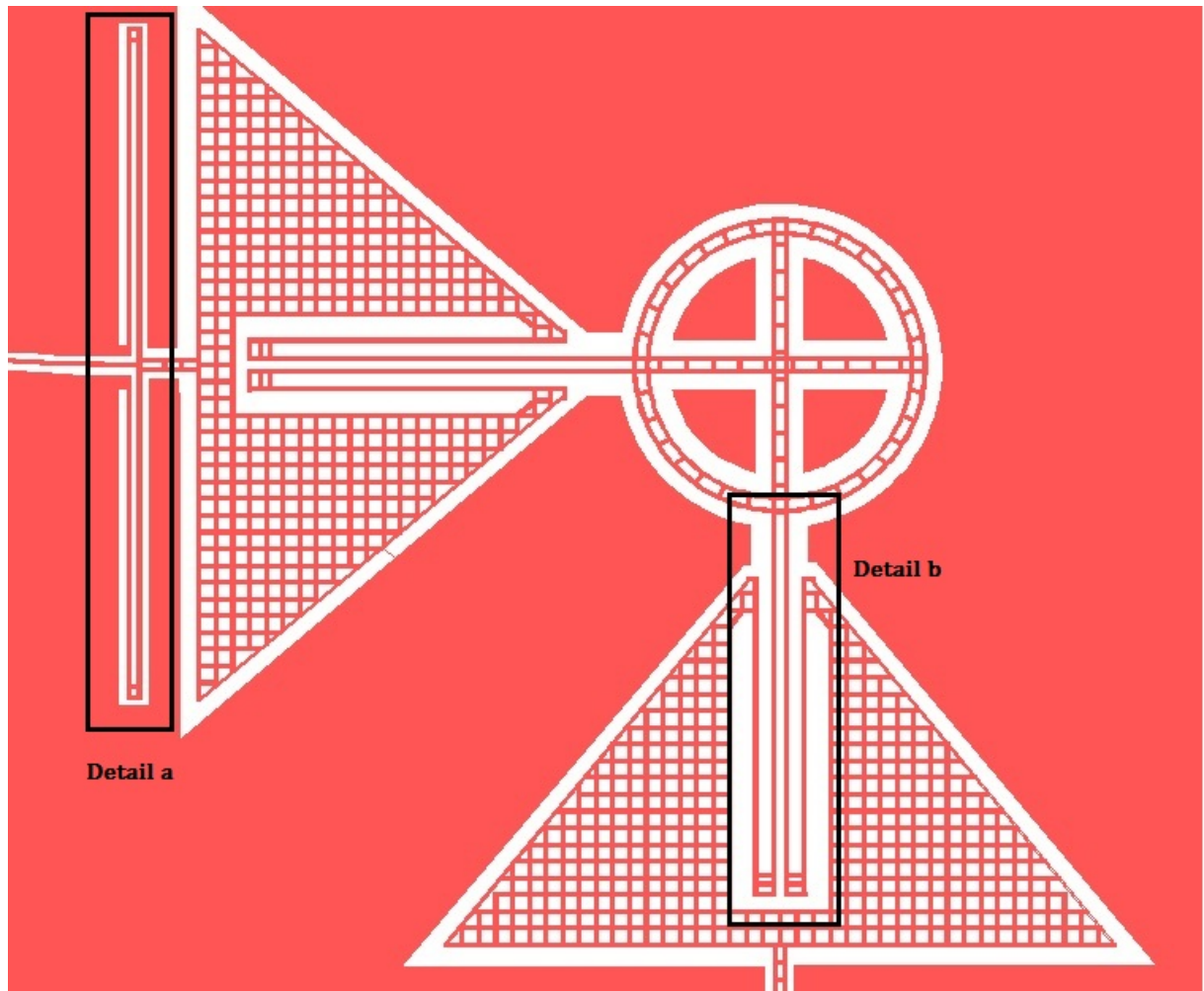
Figure 5.4: Folded beam location on the structure.

In order to find the sensor minimal detectable force the minimal detectable gap variation or the minimal capacitance variation measurable is derived.

Since the minimal capacitance variation is known i.e. its resolution, the function of the minimal displacement detectable depends on the permittivity, the parallel plate area and the gap see Eq.5.6. Where the distances g_1 and g_2 are the initial gap from the mobile plate and the pair of parallel plates on the top and bottom on Fig.4.8 respectively.

$$dy = -\frac{dc \, (y + g_1)^2 \, (g_2 - y)^2}{\epsilon \, S \, (g_1 + g_2) \, (g_2 - 2 \, y - g_1)} \tag{5.6}$$

Because of the behavior of the detectable gap variation in Eq.5.6 depends of the instantaneous gap, being reduced as the gap decreases, the minimal detectable gap variation are smaller while the gap is reduced. Then the lower the gap the lower the measurable gap variation and therefore the higher the force resolution.

Use of the design parameters to found the minimal detectable force, the maximum and the concrete force displacement dependence:

Given the geometrical paraments of the structure:

$$l = 3[mm]$$
$$a = 200[\mu m]$$
$$t = 50[\mu m]$$
$$w = 5[\mu m]$$
$$l_1 = l_2 = 2[mm]$$

$$\tag{5.7}$$

Geometrical paraments of the measure capacitor device and the ΔC provided by the DAS corresponding to the capacitance estimated resolution:

$$\varepsilon = 8.8542 \times 10^{-12}[\frac{F}{m}]$$
$$S = w \times permieter = 5 \times 4.26 \times 10^{-8}[m^2] = 2.12 \times 10^{-7}[m^2]$$
$$g_1 = 22[\mu m]$$
$$g_2 = 43.5[\mu m]$$
$$\Delta C = n \times 4[aF]$$
$$n = 3$$
$$\Delta C = 12 \times 10^{-18}[F] \tag{5.8}$$

Then the force as a function of the lateral displacement of the design is obtained and can be seen in the Fig.5.5.

The maximum traction force i.e. case of 1 micron before the contact between the parallel plates of g_1 is:
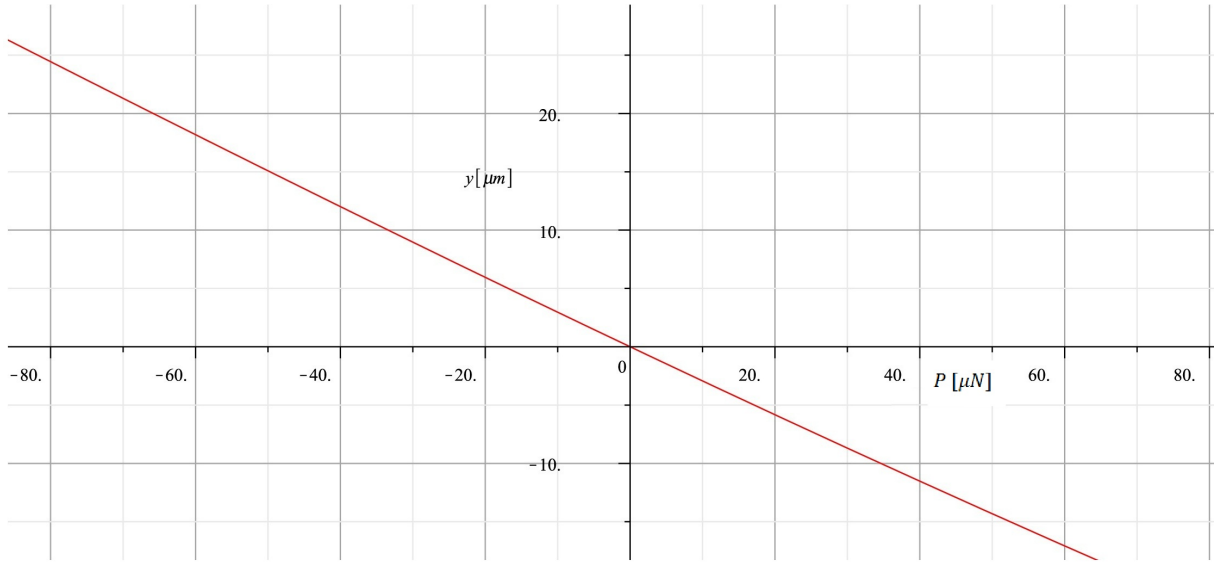
Figure 5.5: Representation of the axial force vs the lateral midpoint displacement.

$$P_{max} = 74.4673[\mu N]$$

Thus the maximum compressive force applicable when g_2 is at 1 micron to be closed is:

$$P_{max} = 136.258[\mu N]$$

The minimum detectable force using Eq.3.3 at the equilibrium point is:

$$P_{min} = 3.39[nN]$$

5.2   Force sensor straight beam design

This chapter focuses on the design of a 2 DOF force sensor based on a straight beam. The analytical equations that describes this behavior are derived. A complete DOF force sensor is designed, taking into account the sensing mechanism.

The presented designs takes advantage of the folded beam suspension low stiffness to generate a low rigidity. Because of the folded beam suspension has a very low stiffness regarding to shear forces and very high regarding to axial direction forces; this property is used with the concept of decouple the 2DOF system of measurement as in previous designs. Therefore the force applied in y direction affects negligible in the x direction, this concept can be applied to any two dimensional force and displacement vectors measurable in the plane .

5.2.1   Principle of actuation

The main idea is to measure in 2 directions in a uncoupled system of measurement, this way the displacements measurable in x and y direction are ideally thought to be non constrained. This concept can be seen in Fig.5.6, where in order to make an stable mechanism of measures it is implemented a stiffness and also a measurement device that will affect the behavior while an electrical force. Because of the displacements to measure has to be in x and y direction for the capacitor alignment it is used folded beams suspension close to the capacitors in order to avoid undesired transverse displacements.

This concept is represented schematically in Fig.5.6. The stiffness K_x seen in Fig.5.6 can be assumed to be due to the addition of the folded beams in x direction, because of the stiffness of bending the vertical beam is two orders of magnitude low than the one due to the folded beams in series. For this direction it is adopted a total of four folded beams suspensions in series.

Although the stiffness in x direction is higher the capacitance can be set in order to measure the relationship between both capacitors placed at each end therefore the capacitance variations measured can compensate the higher stiffness regarding to the y direction.

For the y direction the stiffness cannon be taken due only by the folded beams configuration because of the deflection of the horizontal placed equivalent beam makes a higher contribution to the total stiffness. Then the stiffness is due to the configuration of two folded beams in series plus the addition of the mentioned horizontal placed beam stiffness.

To quantify the stiffness per each direction it is used the Eq.5.13, font [1], which can be applied for folded beam suspensions and for its equivalent fixed-fixed cantilever beam configuration with an applied load at its middle point. The parameters are the I inertia moment in z direction, the same in all the designs as also E the Young modulus, l is the x axis total beam length, l_f is the equivalent folded beam length and n accounts the number of folded beams in series for the equivalent stiffness as it is mentioned $n = 2$ for measurements in y direction and $n = 4$ for the x direction as the design in Fig.5.8 shows.
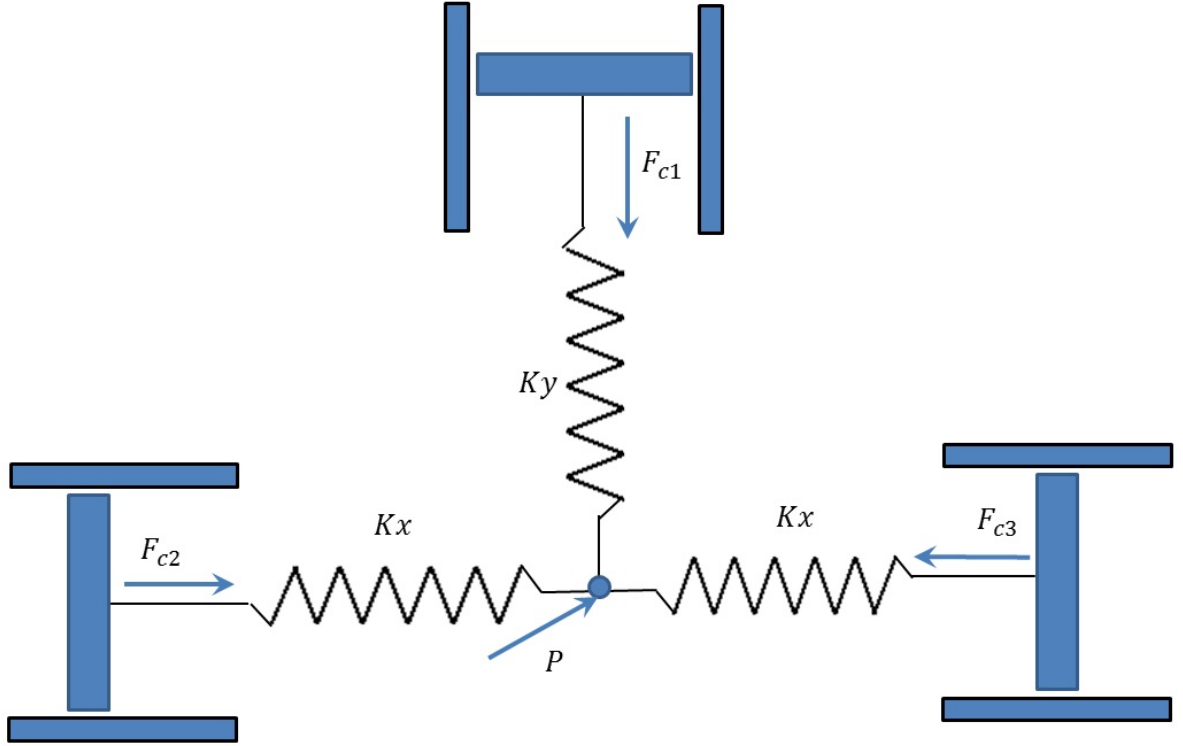
Figure 5.6: Conceptual scheme of the straight beam force sensor.

Figure 6.6 shows the scheme of the configuration adopted for this design.

$$K_n = n \cdot 192 \frac{EI}{l^3} \tag{5.9}$$

Therefore for the x direction the external forces can be described by the use of Eq.5.10, where the forces F_{c2} and F_{c3} are respectively the forces due to the capacitors placed at each horizontal beam ends as describes Eq.2.5, for the y direction it is described the external force by the use of Eq.5.12 being F_{c1} the force due to the capacitor placet at the vertical beam end. This electrical forces will depend on the capacitors configuration applied.

$$P_x = K_4 \cdot x - F_{c2} + F_{c3} \tag{5.10}$$

$$K_x = 768 \frac{EI}{l^3} \tag{5.11}$$

$$P_y = K_y \cdot y + F_{c1} \tag{5.12}$$
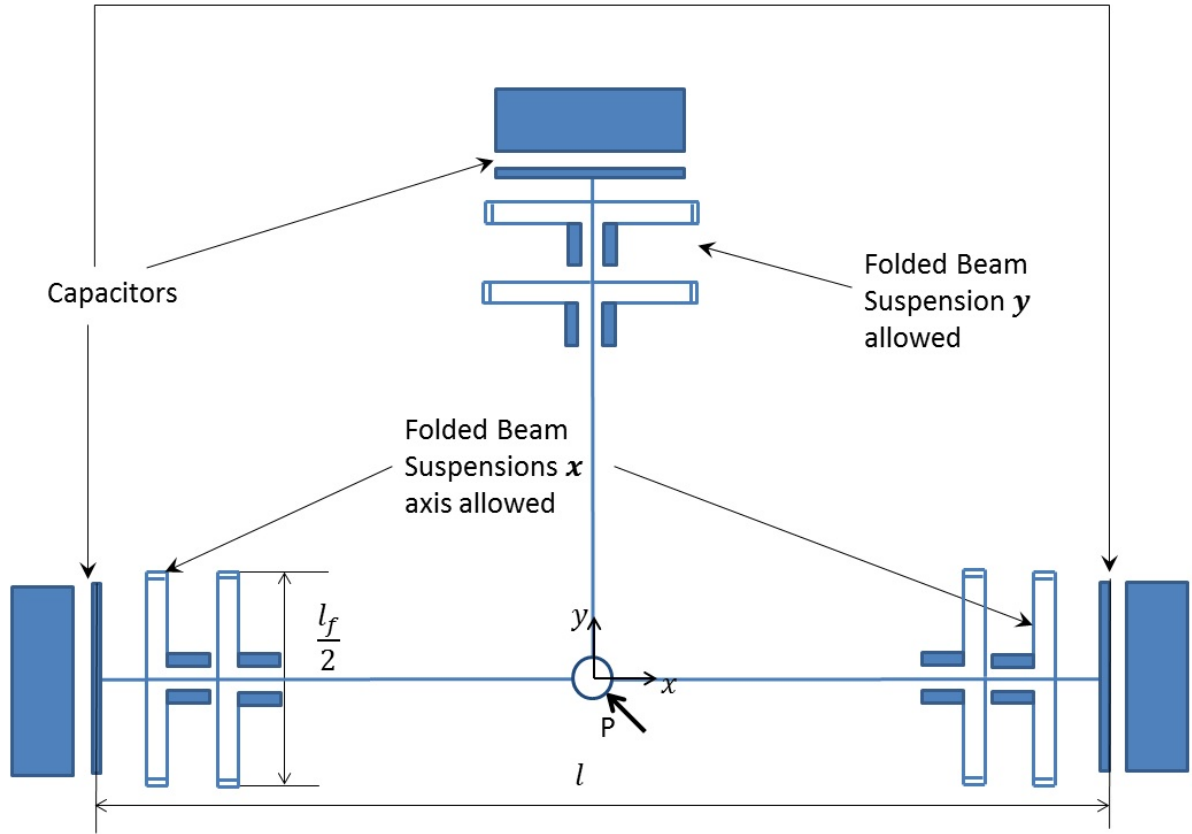
Figure 5.7: Scheme of the Force sensor based on straight beam design.

$$K_y = 192EI(\frac{1}{l^3} + \frac{2}{l_f{}^3})$$

(5.13)

The parameters for the structure independents of the capacitor configuration used are:

$$l = 6[mm]$$
$$l_f = 4[mm]$$
$$t = 50[\mu m]$$
$$w = 5[\mu m]$$
$$I = \frac{tw^3}{12}$$
$$E = 170[GPa]$$

(5.14)

Hence using the parameters it is found the stiffness in x direction in Eq.5.15 and for y direction Eq.5.16.

$$K_x = 1.0625 [\frac{N}{m}] \tag{5.15}$$

$$K_y = 0.60996 [\frac{N}{m}] \tag{5.16}$$

5.2.2 Parallel plates capacitors configuration design

In order to measure the changes in capacitance a parallel plate detection is used see the detail in Fig.5.9. Because of the lower stiffness in the y direction the initial gap between the parallel plates has been increased in comparison to the x direction in order to reduce the instability forces presents due to the electrical capacitance between the pairs of parallel plates.

In order to describe the electrical force F_c it is used Eq.2.5 for the concret case of the parallel plates which need to derive Eq.2.3.

The parameters used are: the initial gap is 25 $[\mu m]$ in y and 20 $[\mu m]$ in x direction, for the gap 2 which is applying a force on the opposite direction the value is the same of $g_2 = 135[\mu m]$. The surface area is the same per each end, is taken as $S = n \cdot t \cdot l$ where n is the number of pair of parallel plates in this case 4, l is the length of each parallel plate in this case is $1[mm]$ and the thickness t which is fixed per wafer, in this case $t = 50[\mu m]$. For the folded beam length l_f is chosen 4 $[mm]$, n is the number of folded beams 2 for y and 4 to x; this leads to a stiffness in y direction of $K_y = 0.532[\frac{N}{m}]$ and of $K_x = 1.534[\frac{N}{m}]$ in x direction. The voltage difference applied between gaps is fixed by the DAS to be $V_1 = V_2 = 1.56[V]$.

In order to measure the maximum measurable force the limitation is due to the margin on displacement, in this case due to the small voltage applied because of the measurement device, the range taken at $1[\mu m]$ before the instability point is found for both compression and traction (-) and (+) respectively.

$$P_{ymax} = \pm 13.2[\mu N]$$

The minimum detectable force is found via Eq.3.3 and using Eq.5.6, the minimum force is plotted in Fig.5.10 for the y direction.

The minimum force at 1 $[\mu m]$ from the instability point is:

$$P_{ymin} = 37.82[pN]$$

Being of 4.7 $[nN]$ at the equilibrium point.

For the x direction measuring in differential mode, the force range is of:
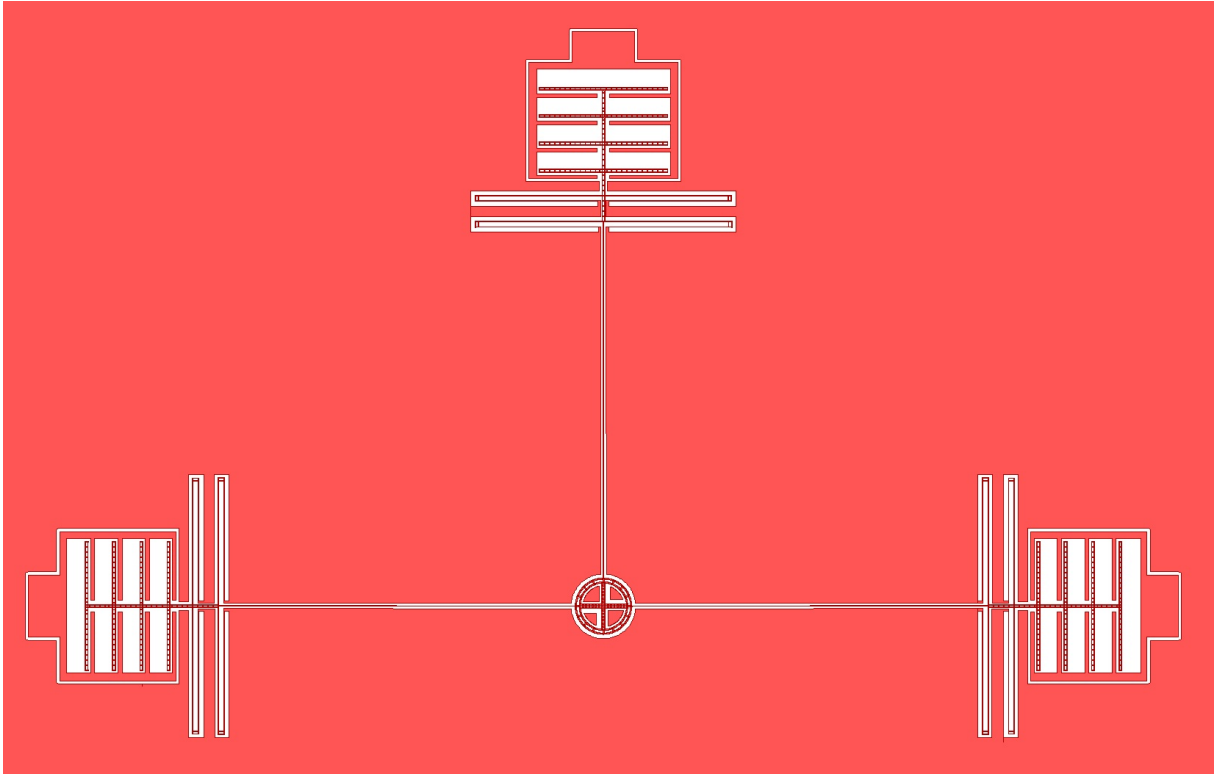
Figure 5.8: Final design of the straight beam base design with parallel plates configuration.
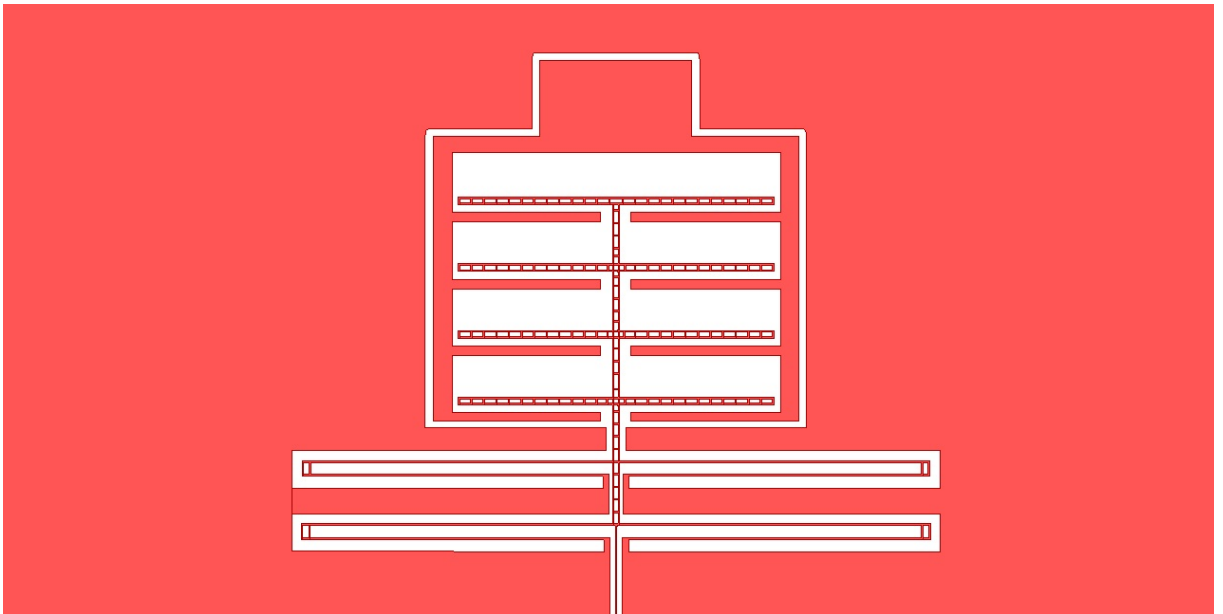
Figure 5.9: Detail of the parallel plates configuration and the folded beams suspension.

$$P_{xmax} = \pm 18[\mu N]$$
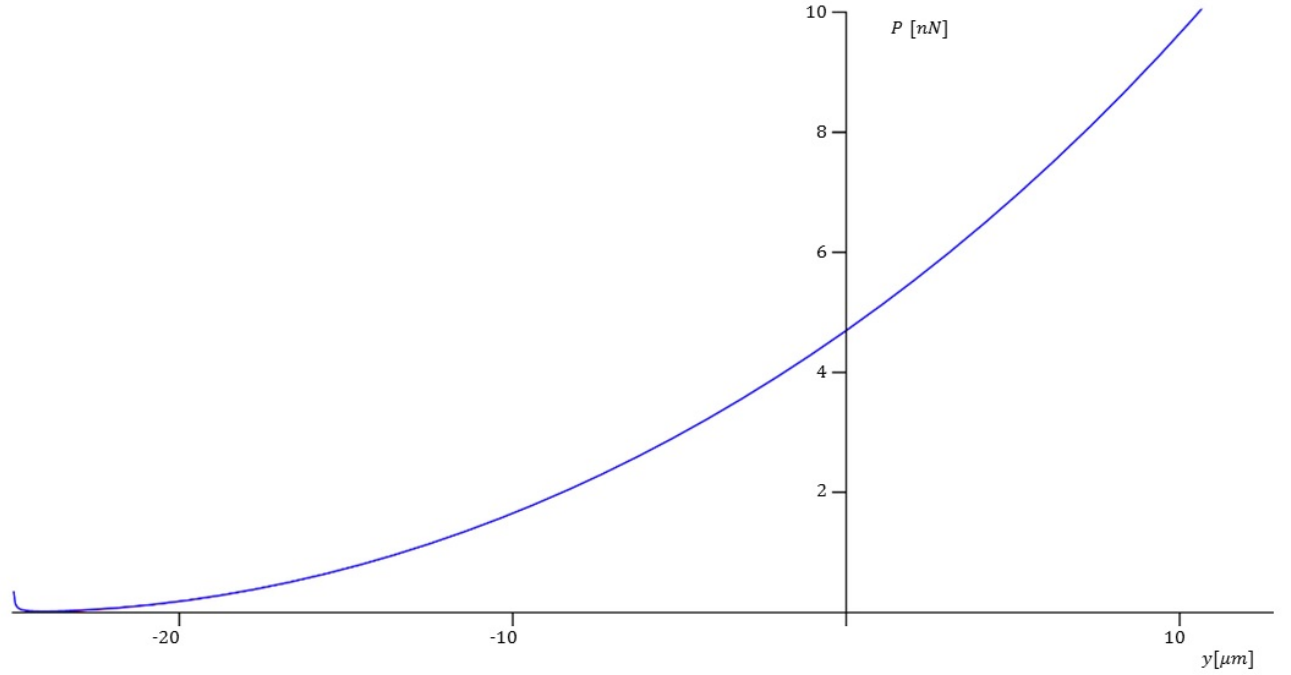
Figure 5.10: Force resolution δP_y in the y axis for the straight beam parallel plates capacitor configuration.

In the case of the minimum detectable force obtained it is plotted in Fig.5.11, for the maximum stable displacement this is at $1[\mu m]$ it is obtained:

$$P_{xmin} = 37.67[pN]$$

Obtaining a remarkable value of $1.48[nN]$ from the equilibrium point.

5.2.3 Comb-drive capacitors configuration design

As mentioned before the limit in the force range is limited due to the instability added by the parallel plates, in order to reduce this issue it is adopted a comb-drive configuration for the detection system. This is shown in Fig.5.12. As it is said the principal advantage is that the stability is increased because of the almost constant force attraction between movable and fixed ends of the measurement structures. In additional and important advantage is that the comb-drive can increase the resolution around the equilibrium point displacements.

Because of the capacitance of the comb-drive can be expressed as the sum of the capacitance between fingers and frontes flat areas with more detail than in the simplified Eq.2.10, i.e. the perimetric length fronted between movable structure and the fixed one it can be decomposed as shows Eq.5.17 in order to take into account the instability effect.

71
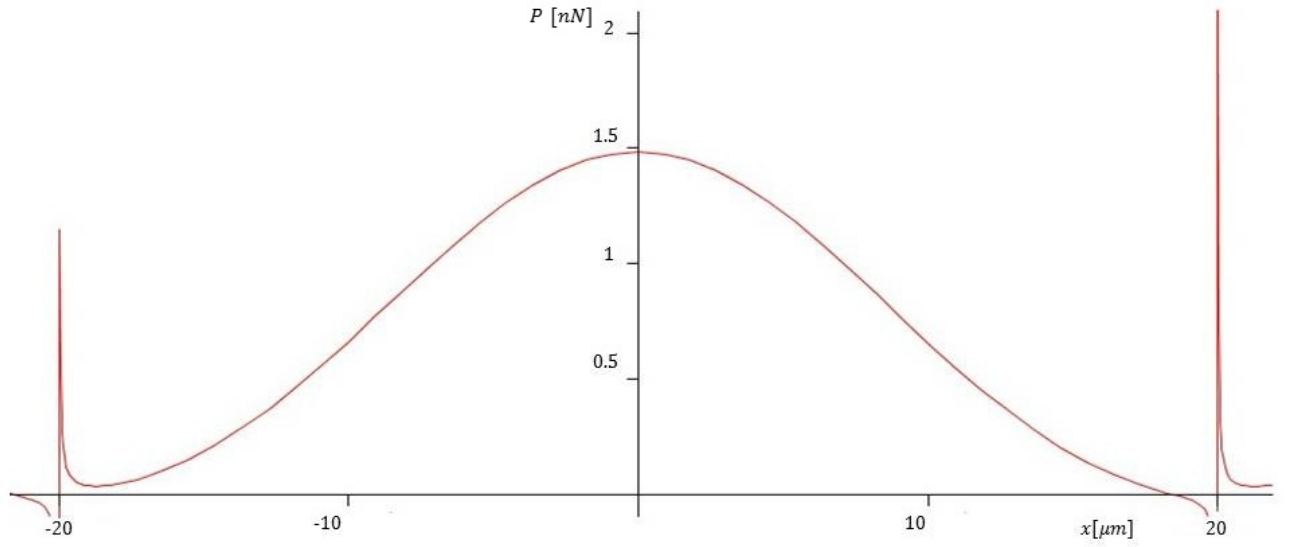
Figure 5.11: Force resolution in x direction δP_x for the parallel plates capacitor configuration.
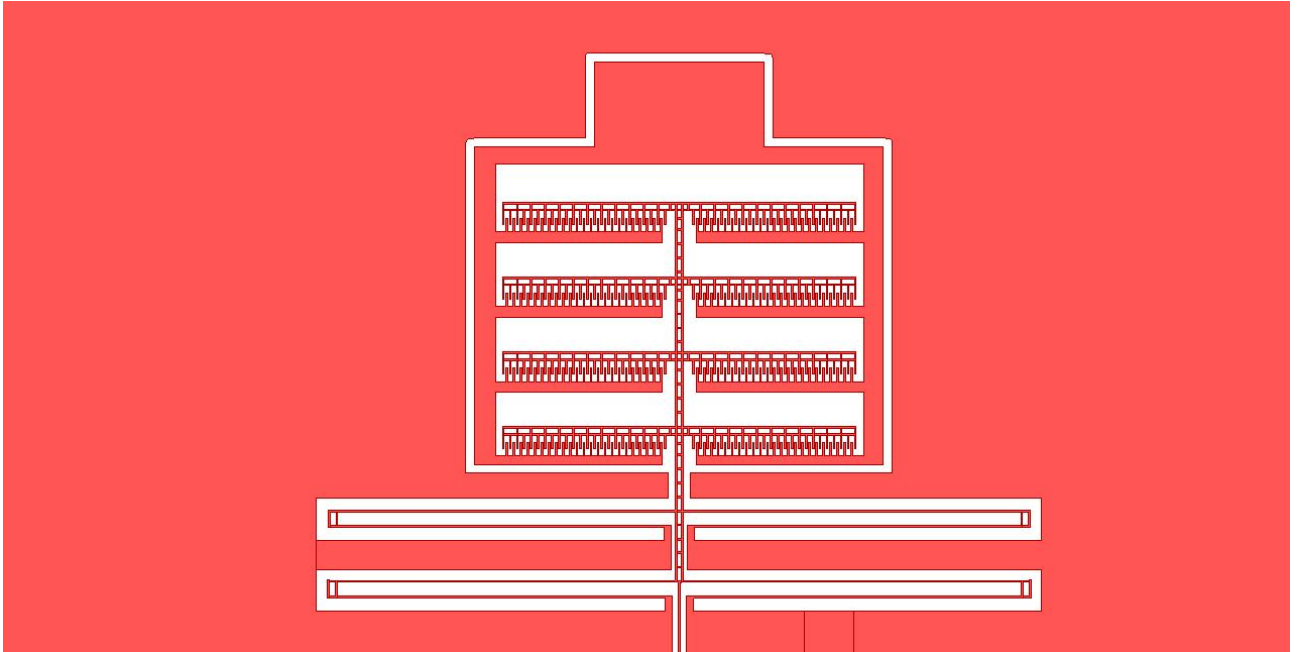
Figure 5.12: Detail of the Comb Drive capacitors configuration.

$$C(x) = \epsilon \cdot t \left(f \left(\frac{go + x}{g_l} + w \left((g + x)^{-1} + (g_2 + x)^{-1} \right) \right) + \frac{l}{g_3 - x} \right) \qquad (5.17)$$

The same parameters has been chosen are:

72

$$f = 400$$
$$w = 5[\mu m]$$
$$t = 50[\mu m]$$
$$g_o = 20[\mu m]$$
$$g_l = 5[\mu m]$$
$$g = 20[\mu m]$$
$$g_1 = 60[\mu m]$$
$$g_2 = 110[\mu m]$$

(5.18)

Using this parameters it is found the capacitance of the design and thus the applied electrical force for each direction and the relationship of the external force.

For the x axis:

The maximum applicable force it is found 1 micron before reach stability limit this is:

$$P_{xmax} = \pm 18.6[\mu N]$$

(5.19)

In the case of the minimum detectable force shown in Fig.5.13, for the x direction at the same point of limit of stability is of:

$$P_{xmin} = 63[pN]$$

(5.20)

At the equilibrium point the minimum force detectable is of $P_{minx} = 2.74[nN]$.

For the y direction case the maximum force is obtained being of:

$$P_{ymax} = \pm 9.2[\mu N]$$

(5.21)

In the case of minimum detectable force in x direction this is of:

$$P_{ymin} = 50.9[pN]$$

(5.22)

At the equilibrium point the resolution obtained is $P_{miny} = 192[pN]$.

The representation of this minimum detectable force as a function of the displacement can be seen in Fig.5.14.
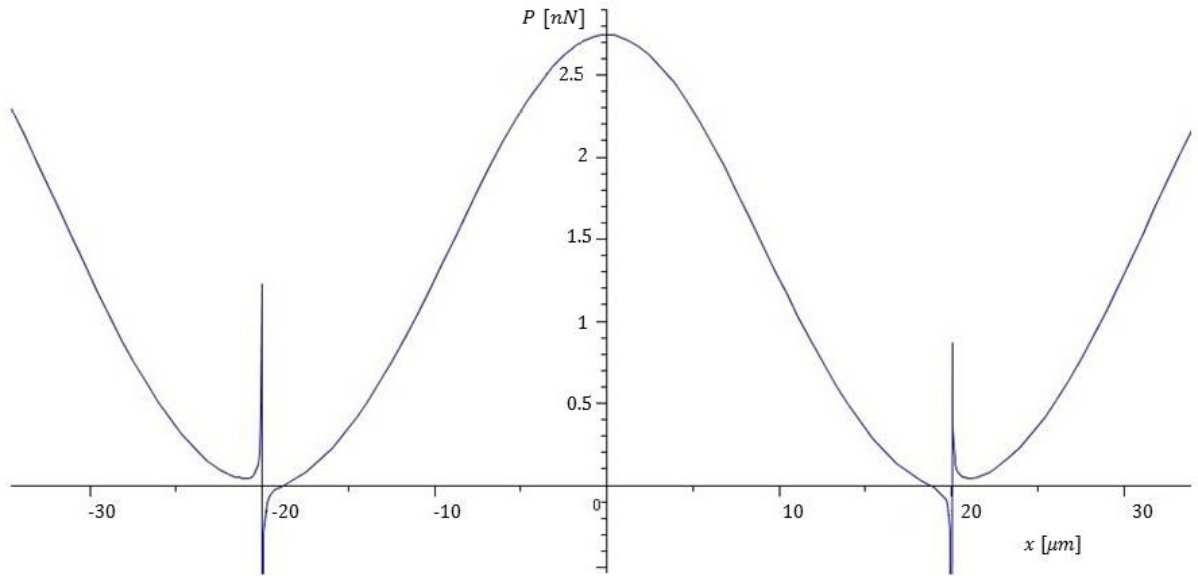
Figure 5.13: $P_{min.}$ detectable in the x axis for the comb-drive capacitor configuration in differential mode.

5.3 Vibration analysis

In this section it is analyzed the interference caused by the DAS when this is connected to the devices. Because this electronic component uses a 32[kHz] signal to be driven. This signal is a voltage that generates a force applied on the MEMS device, we should disregard the fact that this force might be applied at a frequency nearby the eigne modes of vibration causing failure of the device . It shouldn't be of big concern the problem is that when working with MEMS structures these fluctuant forces can be working in the nearby of the eigne modes of vibration and may cause the structural instability and some interferences even cause the structure serious damage.

In order to avoid this problem a FE analysis is made, simulating the structural designed devices in an harmonic analysis.

1 DOF instability based prebuckled beam design

The results are plotted in Fig.5.15, that shows the middle point of the beam displacement as a function of a white noise, showing the response at every stimulant frequency and the most important where the resonant pics are found and if they are coupling with the DAS AC driving frequency.

The force amplitude is accounted as the sum of a constant amount and a cosine perturbation of well known principal frequency, the force then it is particularized depending on the design because of the magnitude is proportional to the first derivate of the capacity and square proportional to the applied voltage, which is a fixed value found in DAS chapter, as Eq.2.5 shows.

74
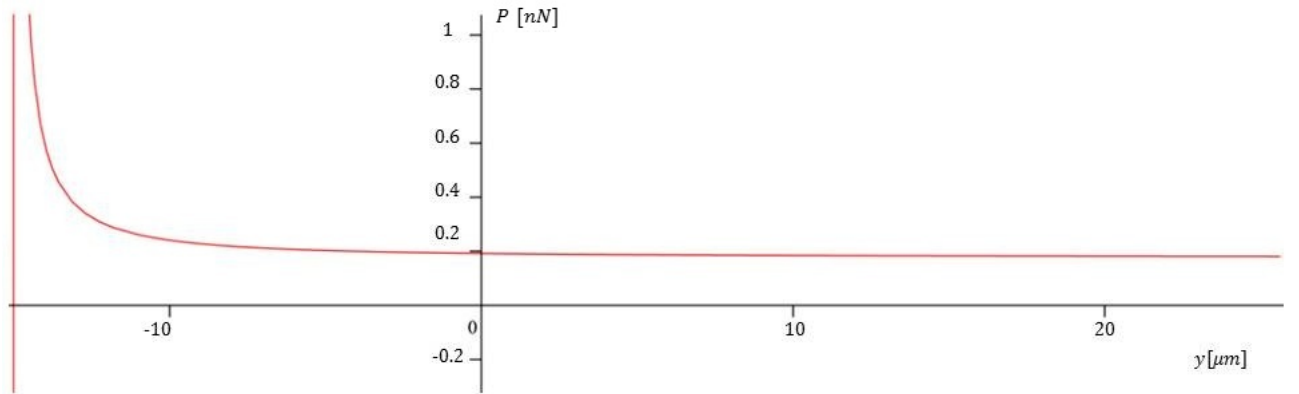
Figure 5.14: $P_{min.}$ detectable for the y for the comb-drive capacitor configuration.
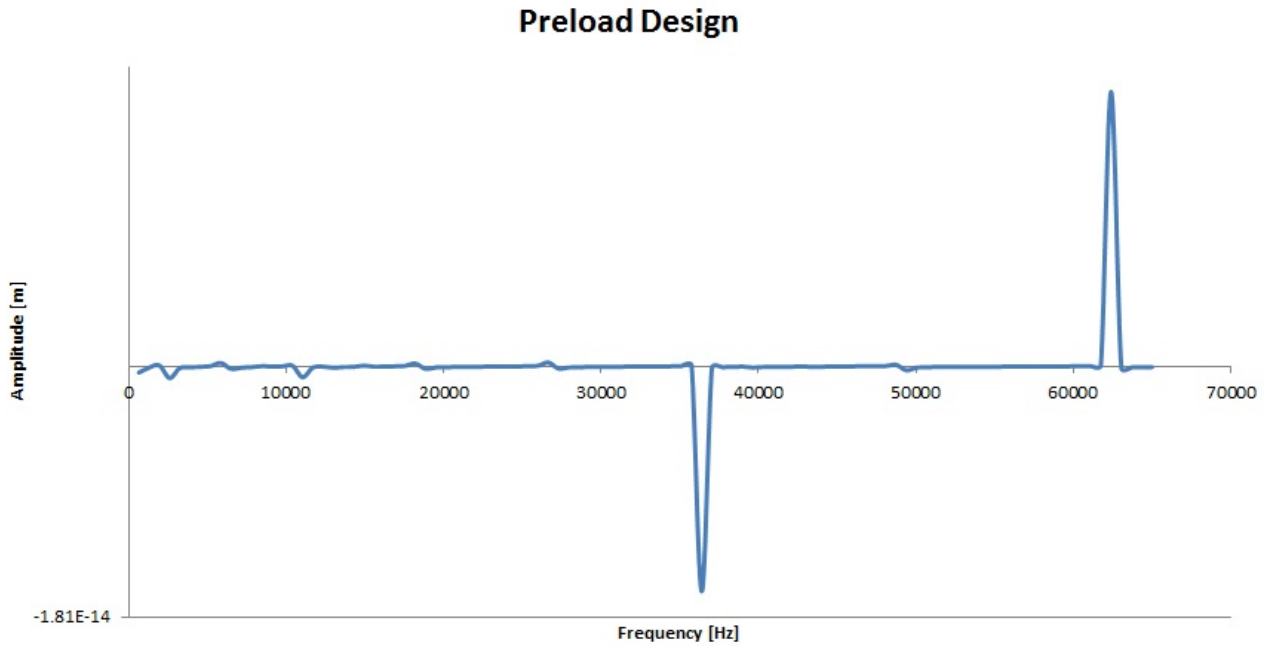
Figure 5.15: Amplitude response to the frequency excitation versus the lateral displacement y of the beam middle point for the critical load based design.

In Fig.5.15 the two main first modes of vibration of the design are at $36.4[kHz]$ and $62.4[kHz]$. Using the specification data of the DAS found in the datasheet and in bibliography [12], the AC applied is of $32[kHz]$, taking into account the second multiple of the excitation frequency which is $64[kHz]$, the excitation frequencies are not coupling the natural ones then the displacement using the FEM for the mentioned frequency is of neglected amplitude of $5.6 \cdot 10^{-18}[m]$ for the first frequency of $32[kHz]$ and of $7.6 \cdot 10^{-17}[m]$ for the doubled frequency excitation signal.

As a conclusion it can be of interest that the results shows there is no risk of collapse

75

in the structure due to the DAS AC working frequency, so the design is frozen.

2 DOF Single prebuckled beam design

In order to avoid the structure collapse due to possible incompatibilities with the DAS, a FEM analysis is made as it was shown in the Preload 1DOF design. The obtained response to the excitation oscillate force is shown in Fig.5.16.
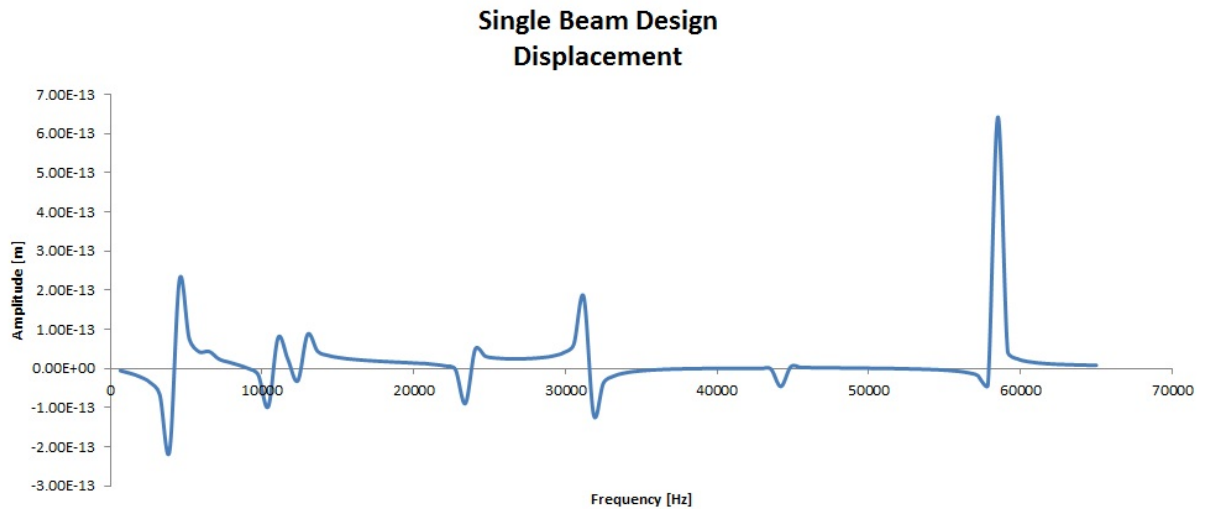
Figure 5.16: Amplitude response to an excitation range of applied harmonic force for the Single Prebuckled Beam Design.

The results shown that close to the first excitation frequency there is a peak of resonance at $31.2[kHz]$ of amplitude of $0.18[pm]$, at the excitation frequency this amplitude is of $0.11[pm]$ and the at the second excitation frequency is of $0.9 \cdot 10^{-14}[m]$. The results shown more interference with the DAS that the Preload design, however the amplitude of the displacement in the worst case scenario is of 3 magnitude orders of the expected displacement measurements.

As a conclusion it can be said that there is no threat to the structural integrity when using the external excitation of the DAS, so the design is frozen.

2 DOF Straight beam design

The obtained response to the excitation oscillate force is shown in Fig.5.17.

The results shown that close to the first excitation frequency there is a peak of resonance at $44.2[kHz]$, at the first excitation frequency the amplitude is of $2.4 \cdot 10^{-15}[m]$ and the at the second excitation frequency is of $2 \cdot 10^{-15}[m]$ with the same closest peak at $44.2[kHz]$. The results shown very few interference with the DAS, the amplitude of the displacement in the worst case scenario is of 5 magnitude orders of the expected displacement measurements.

As a conclusion it can be said that there is no threat to the structural integrity when using the external excitation of the DAS, so the design is frozen.

Cross Design Displacement
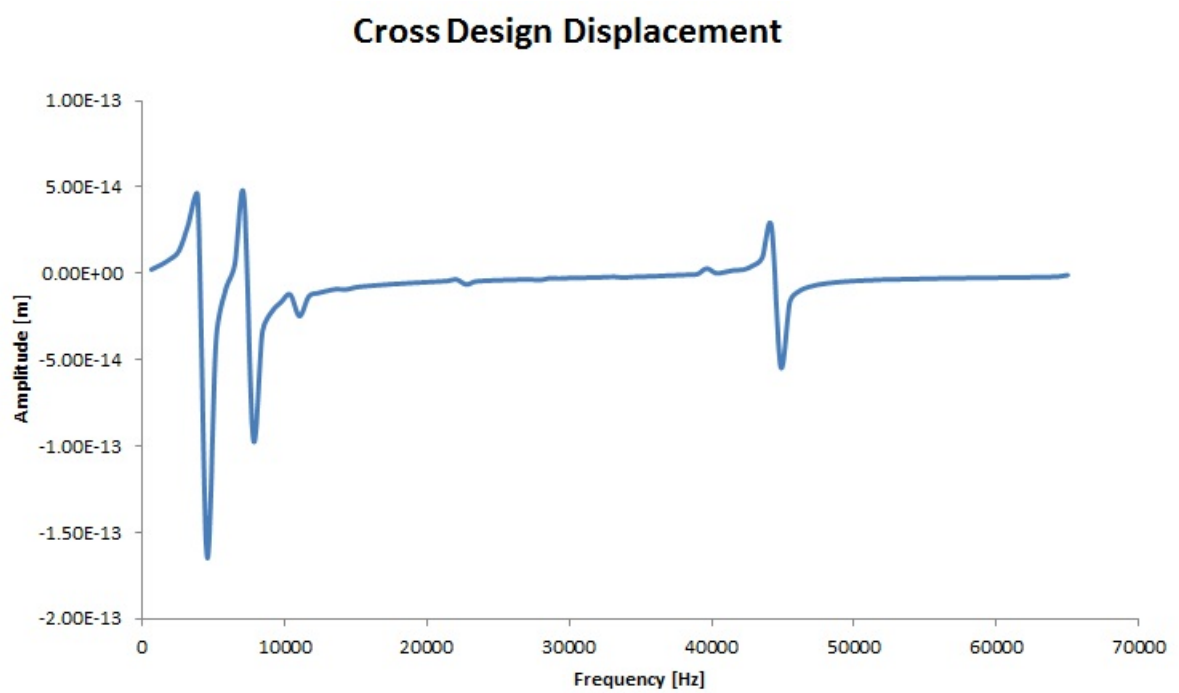
Figure 5.17: Amplitude response to an excitation range of applied harmonic force for the Straight Beam Design.

Chapter 6

The capacitance as a function of the displacement

This chapter describes the relationship between the capacitance changes measured of the sensors and the magnitudes of the displacements which cause them, and hence the forces.

The Newton-Raphson algorithm is implement to invert the capacitance relationships to solve the displacement, because of the nonlinearity of the expressions.

Once the equations are found they are plotted for every design.

6.1   Compressive critical load based design

In this basic design is depicted in Fig.6.1. Two different sensing sensors are adopted, based on parallel plates and comb-drive detection respectively. For both cases, we can express the capacitance as a function of the sensor point displacement.
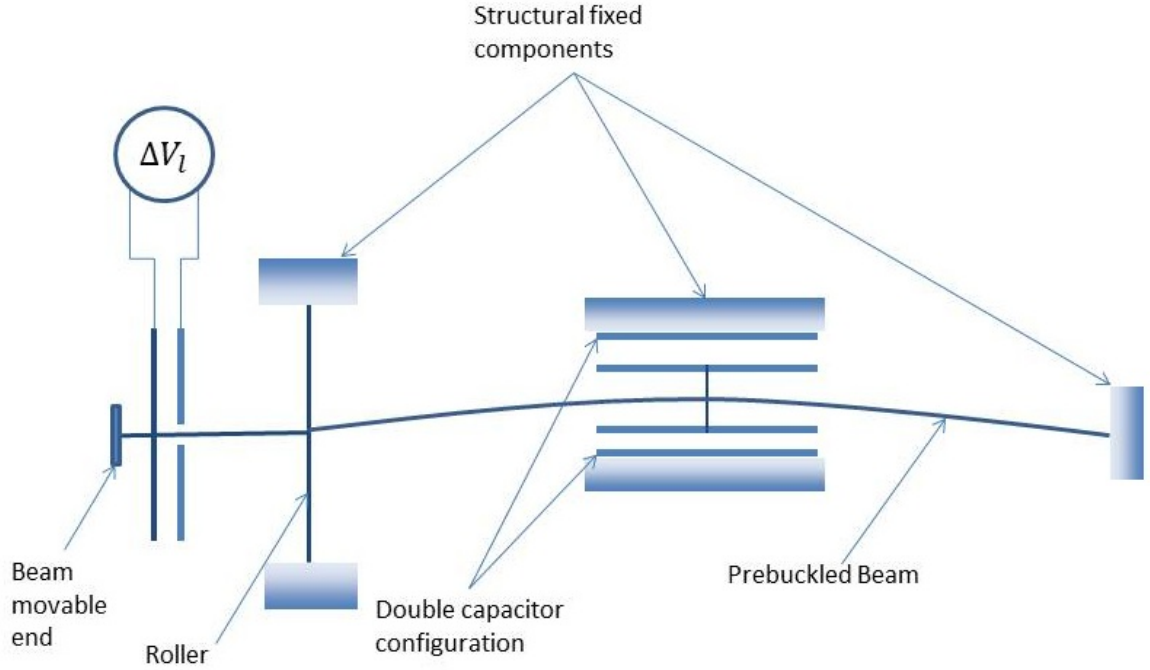
Figure 6.1: Scheme of the single prebuckled beam sensor based on the induced critical load device.

6.1.1   Parallel plates configuration

In this configuration, using the parameters described in Eq.4.29 are set, and using a capacitors length of $l = 8[mm]$ for parallel plates.

It is found the relationship between the middle point y displacement and the capacitance being plotted in Fig.6.2.

6.1.2   Comb-drive configuration

For the Comb-drive configuration, the capacitance is found using the parameters described in Eq.4.29, this is plotted in Fig.6.3.
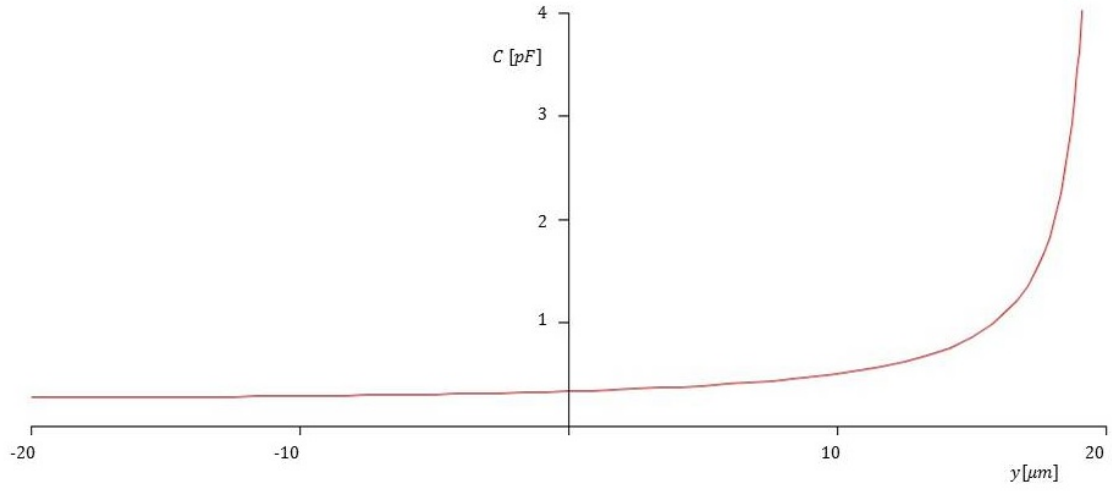
Figure 6.2: Capacitance as a function of the middle point displacement for the Preload Design Parallel Plates Configuration
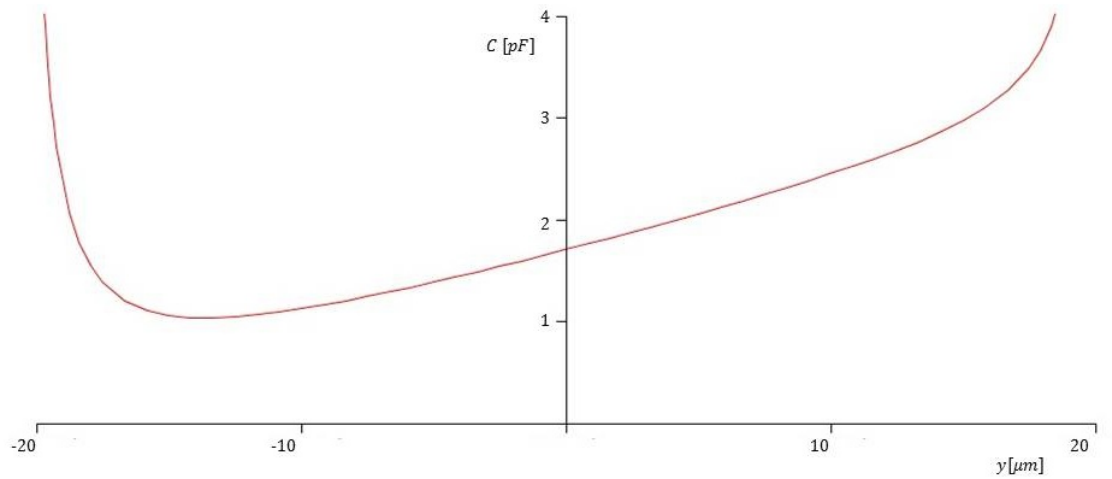
Figure 6.3: Capacitance as a function of the middle point displacement for the Preload Design Comb Drive Configuration

6.2 Single prebuckled beam design

The single prebuckled design is shown schematically in Fig.6.4 the capacitance is measured by the parallel plate configuration.

Using the beam parameters described in Eq.5.8, and adding the relationship between all the parallel plates surfaces for the particular design, the capacitance and the mid point displacement can be obtained. This is represented in Fig.6.5.
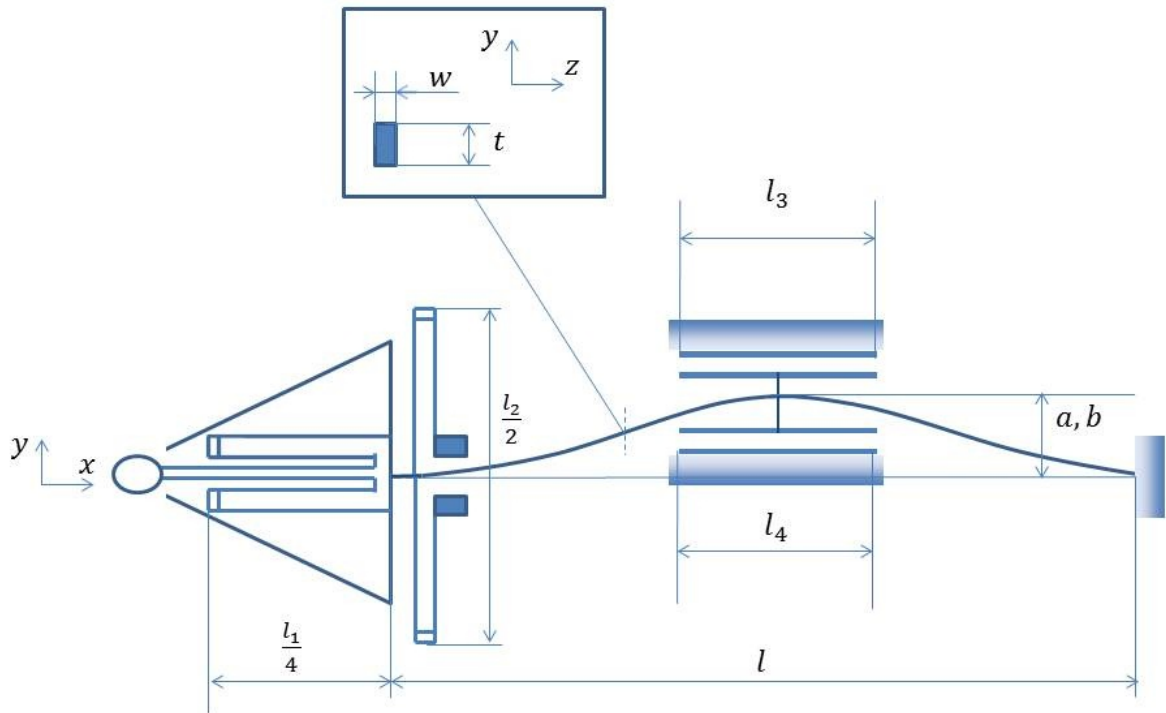
Figure 6.4: Scheme of the Single Prebuckled Design showing 1DOF branch detailed design parameters.
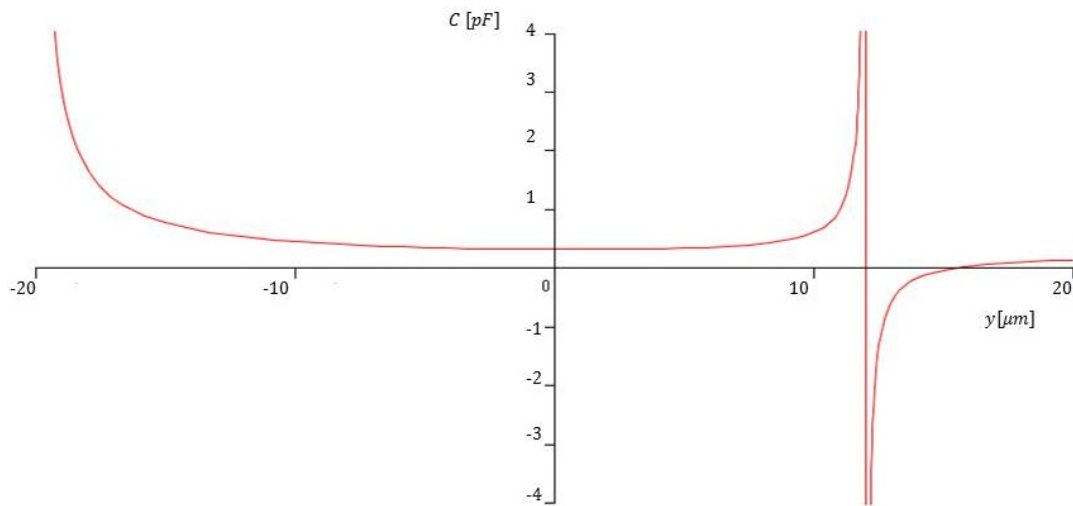
Figure 6.5: Capacitance as a function of the middle point displacement for the Prebuckeld Simple Beam Configuration.

6.3 Straight beam design

The straight beam design is shown schematically in Fig.6.6. The Capacitance equations are presented for the different configuration adopted in the two final designs; the

Parallel Plate and Comb-Drive.
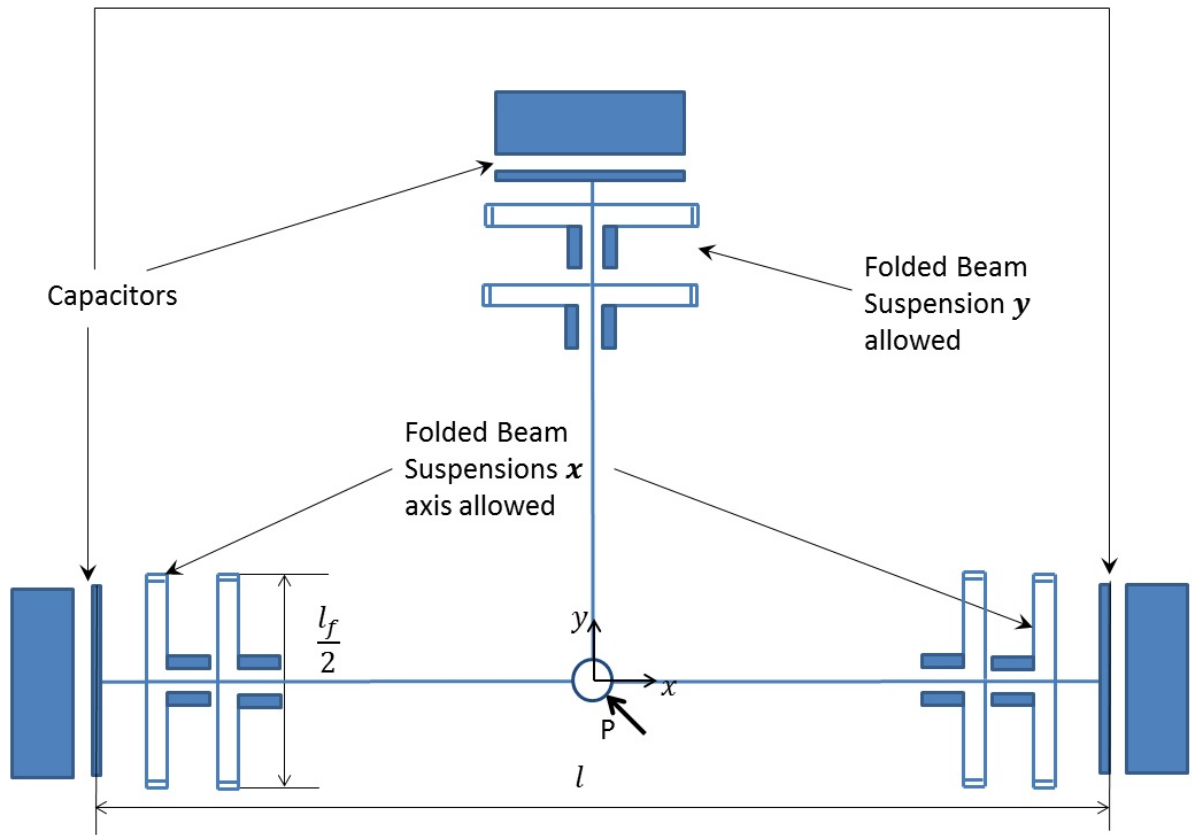
Figure 6.6: Scheme of the Force sensor based on straight beam design.

6.3.1 Parallel plates configuration

For this design the parallel plate capacitor configuration, the capacitance displacement relationship is obtained using the parameters described in section 5.2.2.

The x component the capacitance is obtained being plotted in Fig.6.7, the y component of the capacitance is obtained and also plotted in Fig.6.8.

6.3.2 Comb-drive configuration

For the Comb-Drive capacitor configuration adopted the function the geometrical parameters of the subsection 5.2.3 are used, therefore the capacitance as a function of the displacement for each direction is found. For the x component the capacitance is plotted in Fig.6.9. For the y component the capacitance is obtained and represented in Fig.6.10.
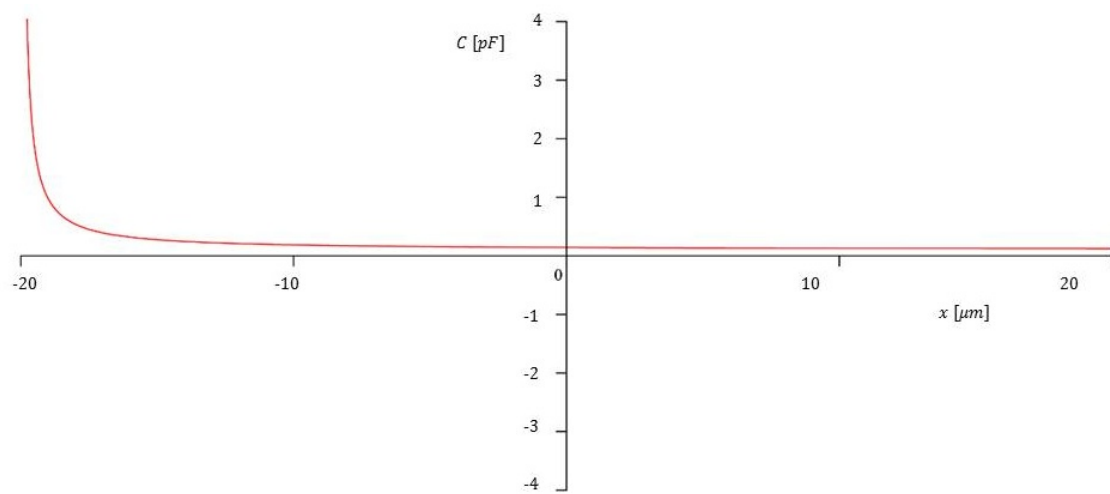
Figure 6.7: Capacitance as a function of the x displacement for the Straight Beam Parallel Plates Configuration.
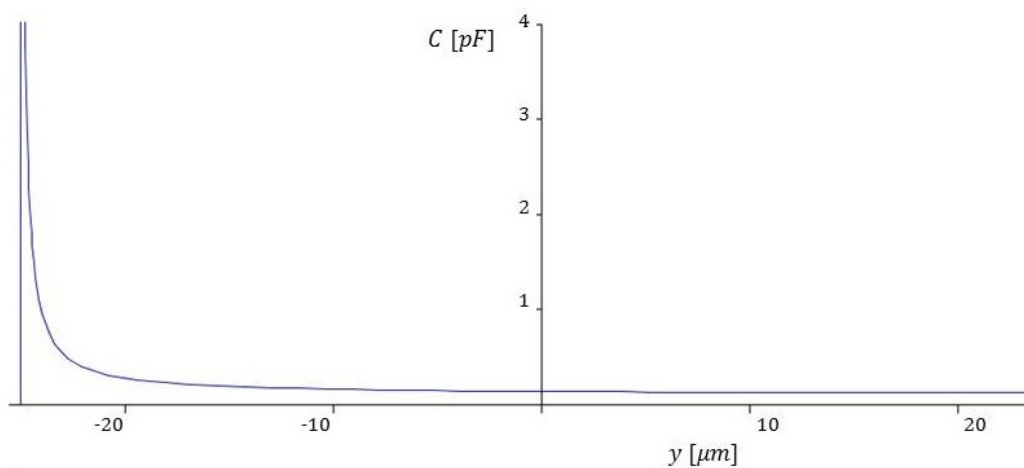
Figure 6.8: Capacitance as a function of the x displacement for the Straight Beam Parallel Plates Configuration.
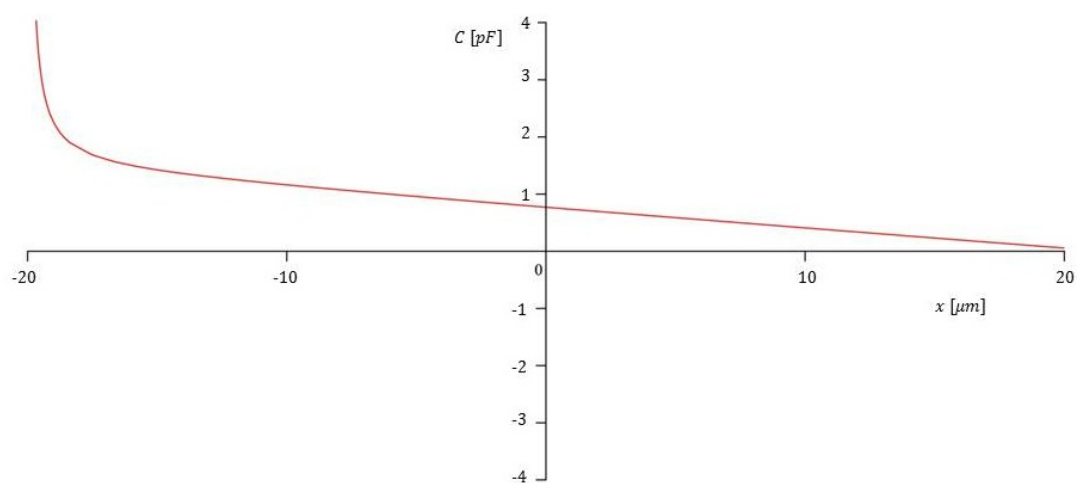
Figure 6.9: Capacitance as a function of the x displacement for the Straight Beam Comb-Drive Configuration.
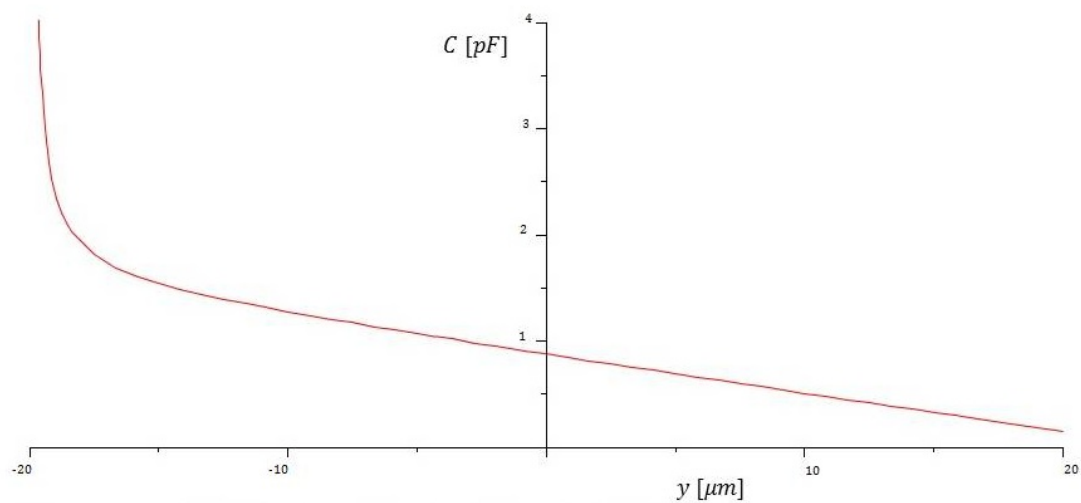
Figure 6.10: Capacitance as a function of the y displacement for the Straight Beam Comb-Drive Configuration.

Chapter 7

Fabrication process

In this chapter is presented the fabrication process followed in order to fabricate the force sensor devices.

7.1 Fabrication process description

The fabrication process is based on standard silicon-on-insulator micromachining process find in more details in [8].The process will start from a SOI wafer, which cross section is plotted in Fig.7.1.

1.- A silicon-on-insulator (SOI) wafer is used as the starting substrate. This wafer has the following layer thicknesses:

- Silicon thickness: $50 \pm 1[\mu m]$
- Oxide thickness: $2 \pm 0.05[\mu m]$
- Handle wafer (Substrate) thickness: $380 \pm 5[\mu m]$

2.- The silicon layer is etched down to the oxide layer using plasma DRIE which needs a photoresist mask to protect the silicon parts that you don't want to etch, see Fig.**??**, with the mask design to fabricate the designed devices.

3.- The wafer can be patterned and etched from the top and from the bottom side using the DRIE etching process.

4.- After applying the DRIE etching process the release of the silicon structure is performed using the HF wet etching process, which will remove the oxide layer between the silicon and substrate. Movable structures shoud not be wider than $10[\mu m]$ otherwise they will no get released. Teh cross section of a wafer after top and bottom DRIE process and the release step is plotted in Fig.7.1.

A basic representation of the resultant after applying the whole process can be seen in Fig.7.2 where it can be seen the release process of the future movable parts of the
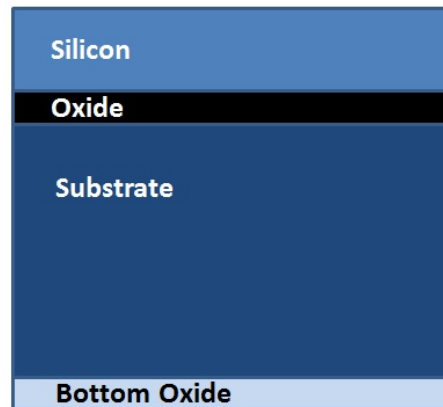
Figure 7.1: Scheme of the layers contained into the wafers.
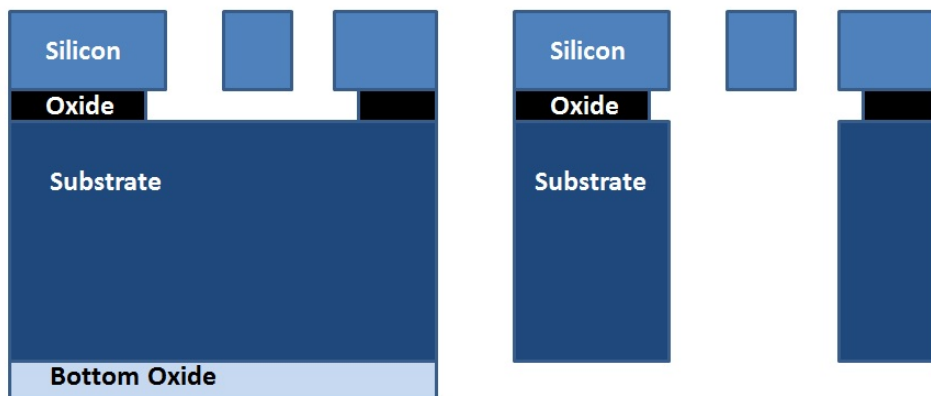
Figure 7.2: Scheme of the layers contained into the wafer after the etching process.

structure, for both one side and both side etching process. The fabrication process has been manufactured in Irvine faculties in UCI campus.

After applying the fabrication procedure described above on all the designs composing the wafer see Fig.7.3, a capacitor component of the straight beam design can be seen in Fig.8.21.
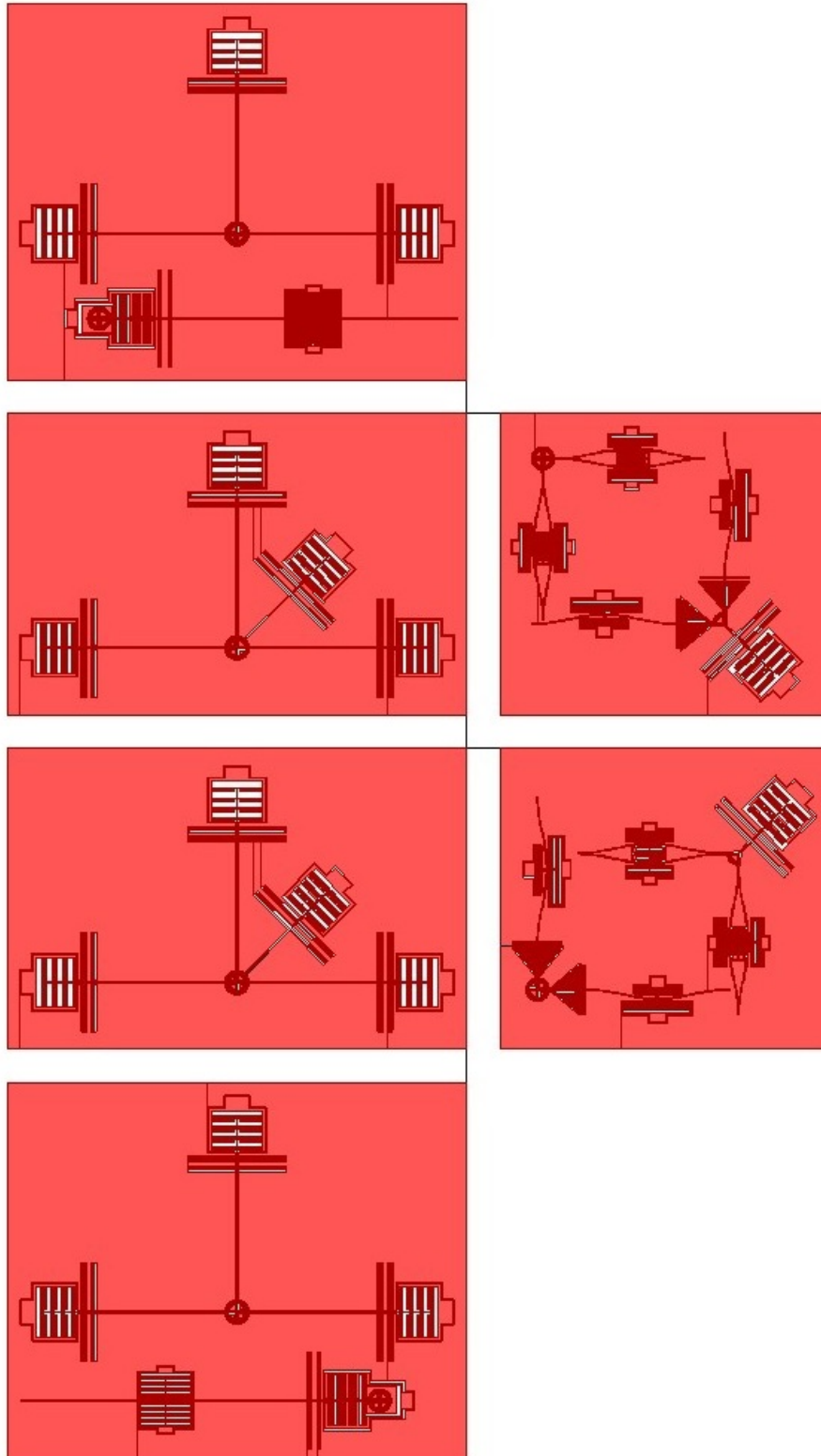
Figure 7.3: View of the distribution of the devices ready for the fabrication process.
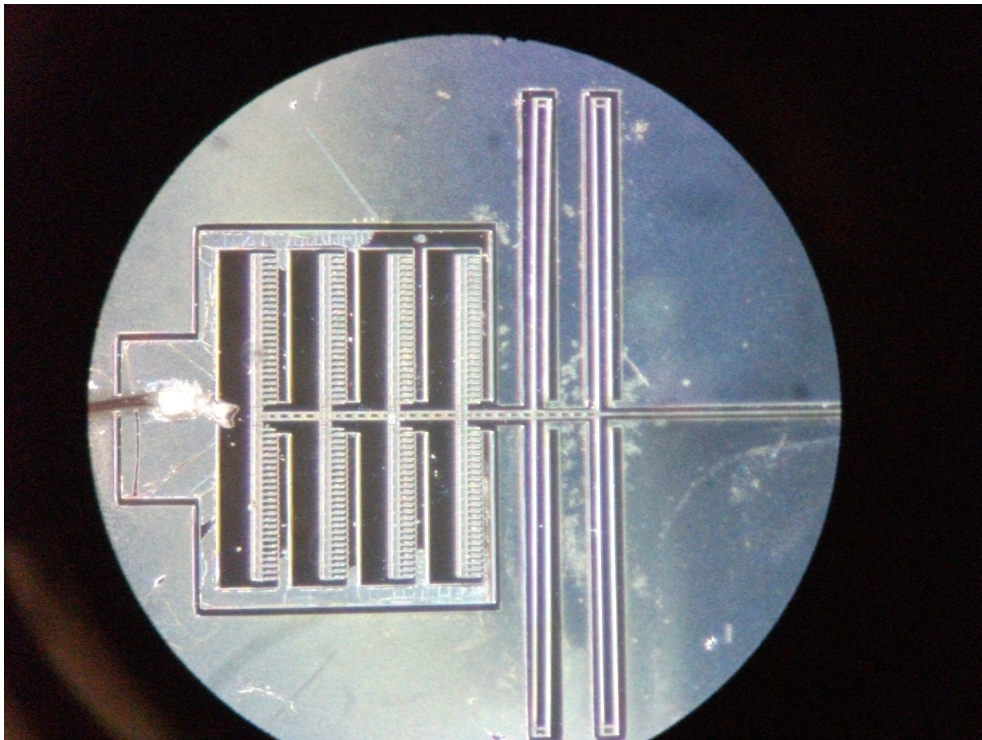
Figure 7.4: Amplified picture 2 of the fabricated and packed Straight Beam Test Design with Comb-Drive Capacitor Configuration, ready to connect to the DAS.

Chapter 8

Calibration and preliminary testing

This chapter describes the calibration procedure for the force sensors designed.

8.1   Calibration procedure for 1 DOF sensors

In order to calibrate the 1 DOF compressive load design it is used the same component that generates the instability to impose a deformation of the middle point of the beam by means of the prebuckled instability.

Thus applying a voltage difference the forced applied axially changes and so the displacement it can be seen in Fig.8.1.
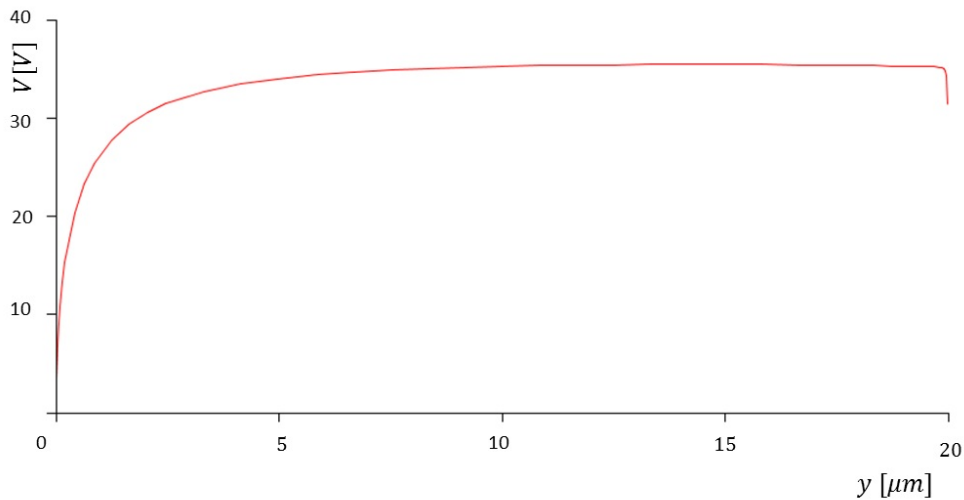
Figure 8.1: Displacement of the middle point of the beam due to the applied voltage.

Then this displacement is measure by using the inverse of the capacitance obtained in both configurations parallel plates and comb-drive found in section6.1 and 5.2.3. Then

by applying the voltage shown in Fig.**??**it will be expected to obtain the displacement announced.

8.2 Calibration procedure for 2 DOF sensors

For the designs it is presented the calibration procedure to apply to for the 2 DOF sensors.

8.2.1 Calibration procedure for the prebuckled beam design

To calibrate the designs and validate them, a force sensor with an external load generated through a set of comb-drive will be fabricated. The comb drive will transfer a force via a straight beam thanks to a applied voltage between both sides of the comb drive capacitor, see Fig.8.2, this is connected to the previous seen design i.e. Prebuckled Beam 2DOF design, at 45º from the vertical x or y direction, transferring the force in this oblique constrained direction see Fig.8.3.
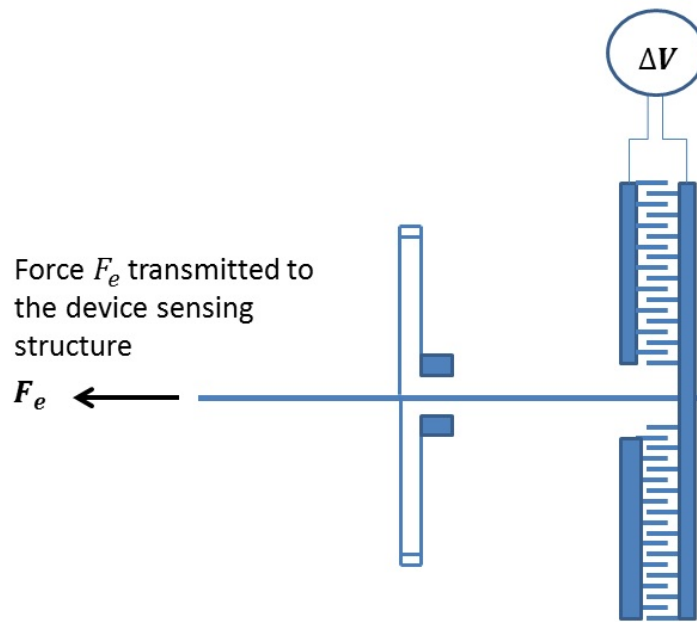
Figure 8.2: Scheme of the Calibration Force device based on Comb Drive capacitor configuration.

The resultant force is applied then in an oblique direction regarding to the main principal directions x and y, and a double folded beam configuration constrain the displacement is assumed to be in the 45º direction as it can be seen in Fig.8.3 where the implementation of the comb drive actuator is shown. Thus the result is a combination of the stiffness in three directions x, y and oblique and an electrical one in oblique. Therefore it can be added to the Eq.5.1 as the projected stiffness and an electrical force for
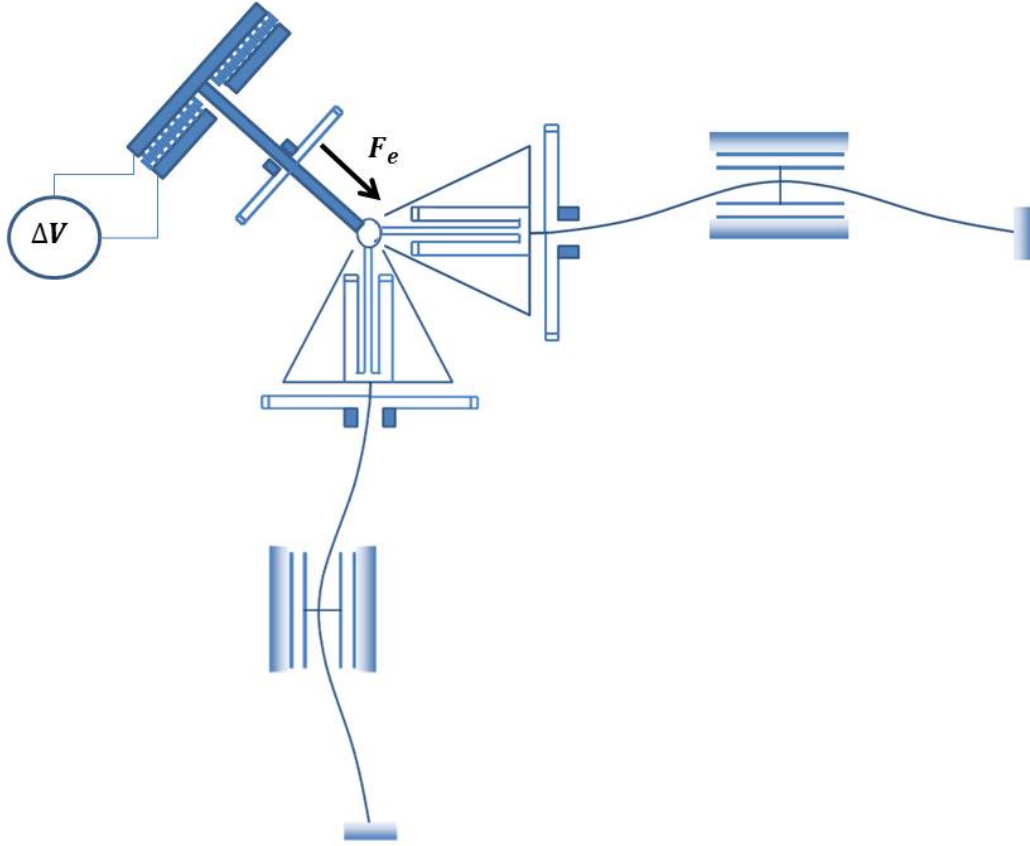
Figure 8.3: Scheme of the Calibration Force device based on Comb Drive capacitor configuration implemented on the Simple Prebuckled Beam Design.

both directions x and y stiffness then the equation for the response displacement to an applied voltage at the mentioned oblique direction is Eq.8.1. Where the 0 is due to the absence of external forces in the equilibrium.

$$0 = 192EI_z(\frac{1}{l_1^3} + \frac{1}{l_2^3})x + \alpha EI_z + \beta F_c + 192EI_z(\frac{1}{l_1^3})x + \frac{F_{c2}}{\sqrt{2}} \qquad (8.1)$$

In Eq.8.1 the therm $\frac{F_{c2}}{\sqrt{2}}$ involves the applied force in either x or y direction as a function of the displacement in oblique direction that can be decomposed as $x/\sqrt{2}$ and $y/\sqrt{2}$ modifying the variables of the displacements in Eq.2.5 and Eq.4.23 it is found the electrical applied force as a function of the input voltage V in Eq.8.2.

$$F_{c2} = \frac{1}{4} \cdot (3.54168 \cdot 10^{-8} + \frac{8.8542 \cdot 10^{-19}}{(38 \cdot 10^{-6} - \frac{y}{\sqrt{2}})} + \frac{8.8542 \cdot 10^{-19}}{(77 \cdot 10^{-6} - \frac{y}{\sqrt{2}})} - \frac{8.8542 \cdot 10^{-19}}{(110 \cdot 10^{-6} + \frac{y}{\sqrt{2}})})V^2\sqrt{2} \ (8.2)$$

Since the applied voltage is known therefore the displacement of the middle point of the pre-curved beam is obtained by isolating the variable y of the Eq.8.1. The same

equivalent procedure is applicable in order to find the x direction displacement by replacing y by x in Eq.8.1 and solving per each input voltage V.

The results as a plot of the displacement of the middle point as a function of the applied voltage difference in the test device component are shown in Fig.8.4.
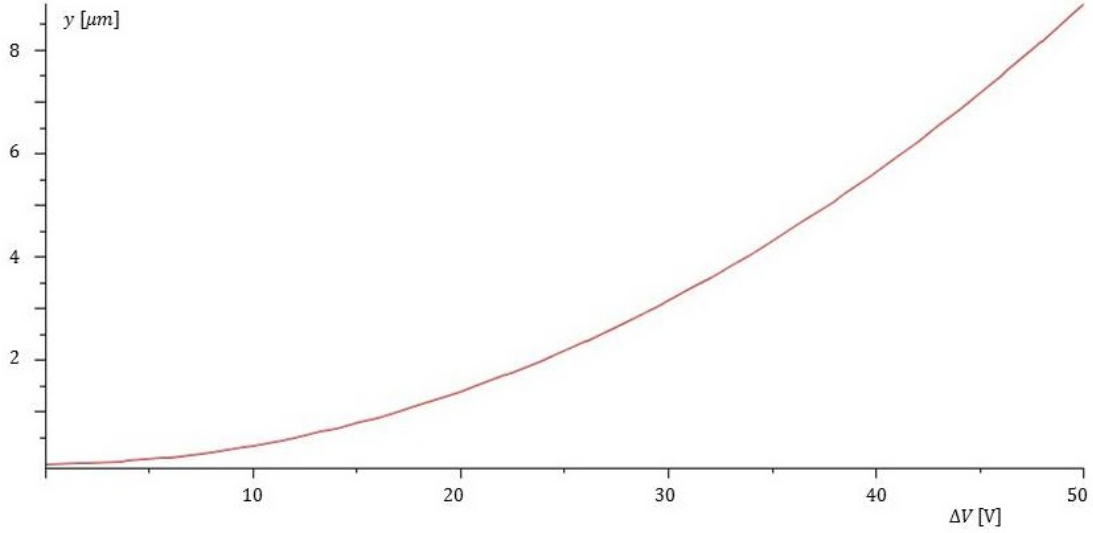
Figure 8.4: Displacement of the beam middle point as a function of the electric potential applied

8.2.2 Force sensor calibration of the straight beam design

For the calibration design the stiffness added to the system by the double folded beam suspension is accounted by using Eq.5.13 for $n = 2$ in oblique direction, in addition the electrical force due to the calibration component F_{cn} in the oblique direction. Projection in oblique direction and imposing equilibrium non considering external forces it is obtained the relationship between the displacements and the applied voltage per each component of the displacement x and y. Obtaining Eq.8.3 and Eq.8.4, solving them for the displacement these are represented in Fig.8.5 and Fig.8.6 respectively.

$$0 = (K_x + K_{nx}) \cdot x + F_{cnx})$$
(8.3)

$$0 = (K_y + K_{ny}) \cdot y + F_{cny})$$
(8.4)

By modifying the on test component input potential difference, the displacement can be obtained solving for either component because of the symmetry. The results are shown in Fig.8.5 where the displacement in the x direction and Fig.8.6 are plotted.
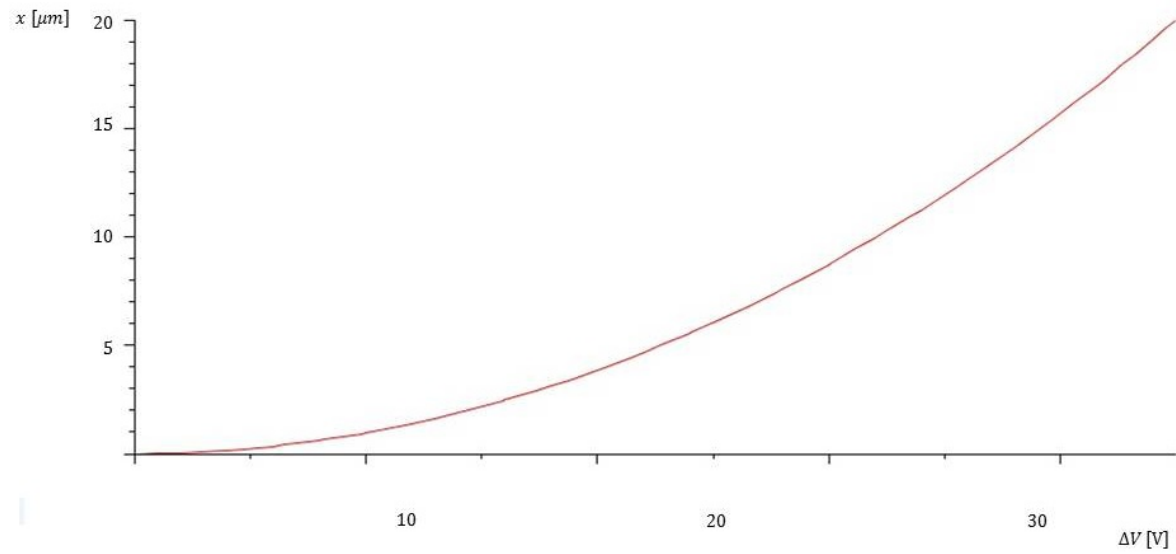
Figure 8.5: Displacement of the x component due to the application of a voltage test component for the Straight Beam Design.
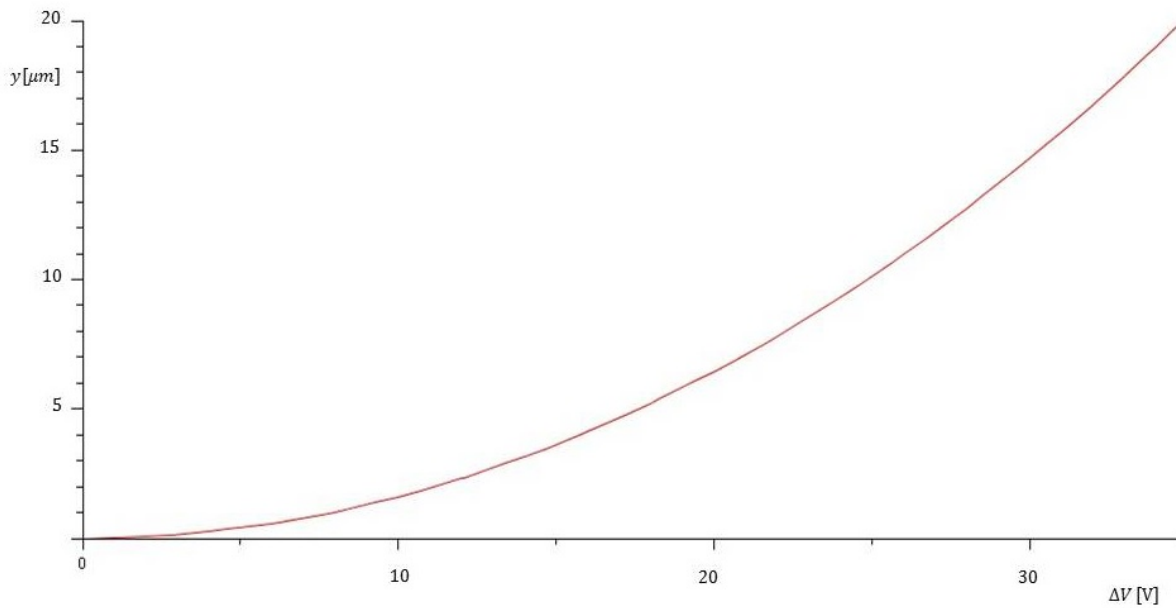
Figure 8.6: Displacement of the y component due to the application of a voltage test component for the Straight Beam Design.

8.3 Preliminary device testing and experimental set-up

In order to validate the principle of operation some devices have been wire bounded to a chip package and interfaced to the on-the self data acquisition system ANALOG Devices AD7745/AD7746 evaluation board, which is illustrated in Fig.8.7, and the complete

experimental set up is shown in Fig.8.8.

The DAS provides a capacitance output, which is read with a PC:

Before applying any force, the DAS is self calibrated according the chip's datasheet, see [12].

After the device is calibrated. Besides the capacitance to be measured there are other parasitic capacitances (i.e. between wire bonds, between the beam and the substrate) that are measured and added to the expected varying capacitance; these capacitance are expected to be constant over the time and an important value taht would saturate the DAS.

Therefore the differential mode is adopted to test the devices, so these capacitances are mainly canceled.

Once the connection is done the next step is to measure the offset capacitance and a noise estimation. Therefore the devices are connected to the DAS connectors as shown a picture taken in the laboratory Fig.8.7 and the components needed for the whole experiment are shown in Fig.8.8. Then starting with the measurements it is analyze the signal obtained for a period of time. After that the signal is converted to capacitance obtaining the numerical values via the DAS. The offset capacitance is then obtained before forcing any displacement in it.

8.4   Preliminary experimental set-up

Any MEMS device should be designed to overcome the variability of the fabrication process. Sensors normally include a self-calibration mechanism that fixes the intrinsic variation of the performance due to imperfections

According to the results obtained after the fabrication process, the designs tested has been modified its original stiffness because of the imperfections parts of the structure. The response to an external force such the electrostatically is expected to be also affected because of the impurities between the gaps and imperfections.

Experimental set up of the straight beam test design with the parallel plates configuration.

The test device using straight beam with the parallel plates capacitors configuration, this is shown in Fig.8.9, and a more close detail pictures in Fig.8.10 and Fig.8.11.

For this design the results after analyzing the pictures Fig.8.9, Fig.8.10 and Fig.8.11, it can be used a modification in the formulation of the internal stiffness, taking into account the new geometry Fig.8.12, it can be obtained an equivalent stiffness on x, y and oblique direction. Applying displacements compatibility for at the connection point i.e.where the beams ends in the circle, it can be found the equivalent stiffness in x direction due to a small displacement δx, the equivalent stiffness in y direction due to a small displacement δy and the equivalent stiffness in oblique direction n due to a small displacement δn.
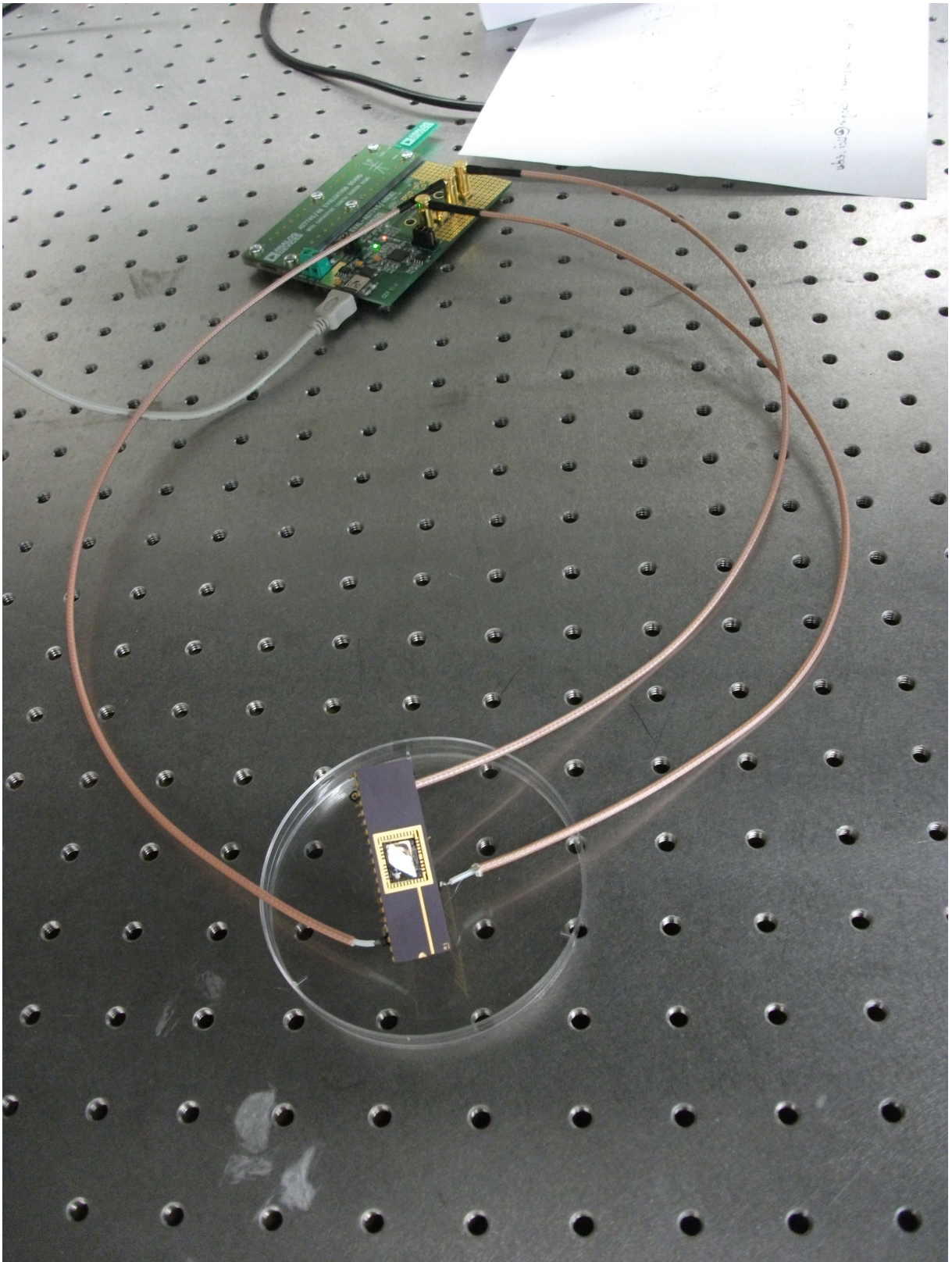
Figure 8.7: Picture of the experimental montage for measurement.
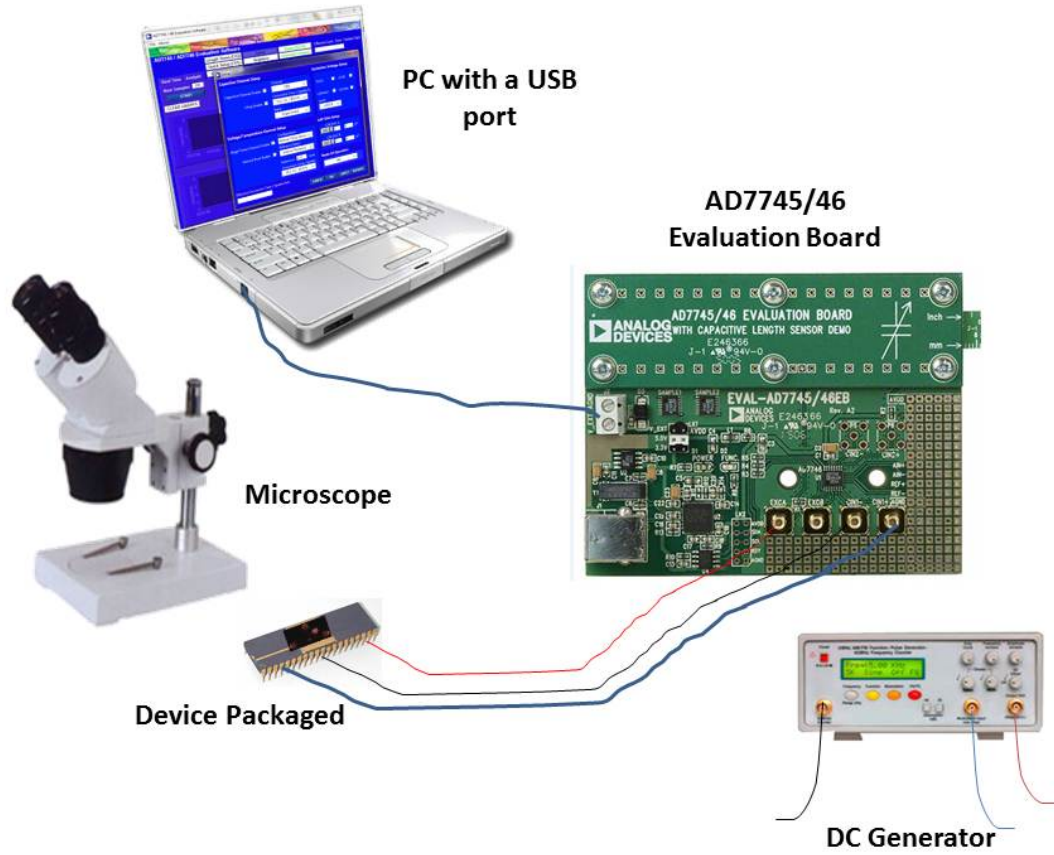
Figure 8.8: Image of the overall experimental montage and components needed.

For the stiffness in x direction, there is a double folded beam suspension on the right side of the structure which is undamaged, and at the opposite side there is another double folded beam suspension, but in this case it is partially broken therefore it has to be modified from the double folded beam stiffness equation. This is made using the equivalent stiffness of a cantilever with and applied load at its end plus a single folded beam suspension stiffness. Hence the resultant stiffness in x direction is composed of Eq.5.13 using $n = 3$ for folded beams, plus Eq.8.5 that belongs to the cantilever beam. Obtaining Eq.8.6.

$$K_{x2} = 24\frac{EI}{l^3} \tag{8.5}$$

$$K_X = 600\frac{EI}{l^3} \tag{8.6}$$

The stiffness in y direction doesn't seems to be affected structurally, so the equivalent magnitude is the usual for a double folded beam suspension using Eq.5.13 for $n = 2$.

For the stiffness in n oblique direction, there is a double folded beam suspension,

Figure 8.9: Picture of the fabricated and packed Straight Beam Test Design with Parallel Plates Capacitor Configuration.

but as it happened in this case of x direction it is partially broken therefore it has to be modified from the double folded beam stiffness equation. This is made as in the case of x direction, using the equivalent stiffness of a cantilever with and applied load at its end plus a single folded beam suspension stiffness. Thus the resultant stiffness in n direction is then Eq.8.7.

$$K_{XY} = 216\frac{EI}{l^3}$$ (8.7)

$$K_{xy} = 12\frac{EI}{l^3}$$ (8.8)

Because of the displacements compatibility of the displacements expected in one direction is affected by the stiffness of other components via the restriction of the connection point. Therefore the equations described above don't represent exactly the behavior of the real structure. To solve this issue it has been assumed the next:

- The displacements in x direction are affected by the stiffness of the vertical beam as the Eq.8.5 shows for the length of the vertical beam.

- The displacements in x direction are affected by the stiffness of the oblique positioned beam as the Eq.8.5 shows for the length of the oblique beam, being projected on the x axis therefore its contribution is Eq.8.8.

99
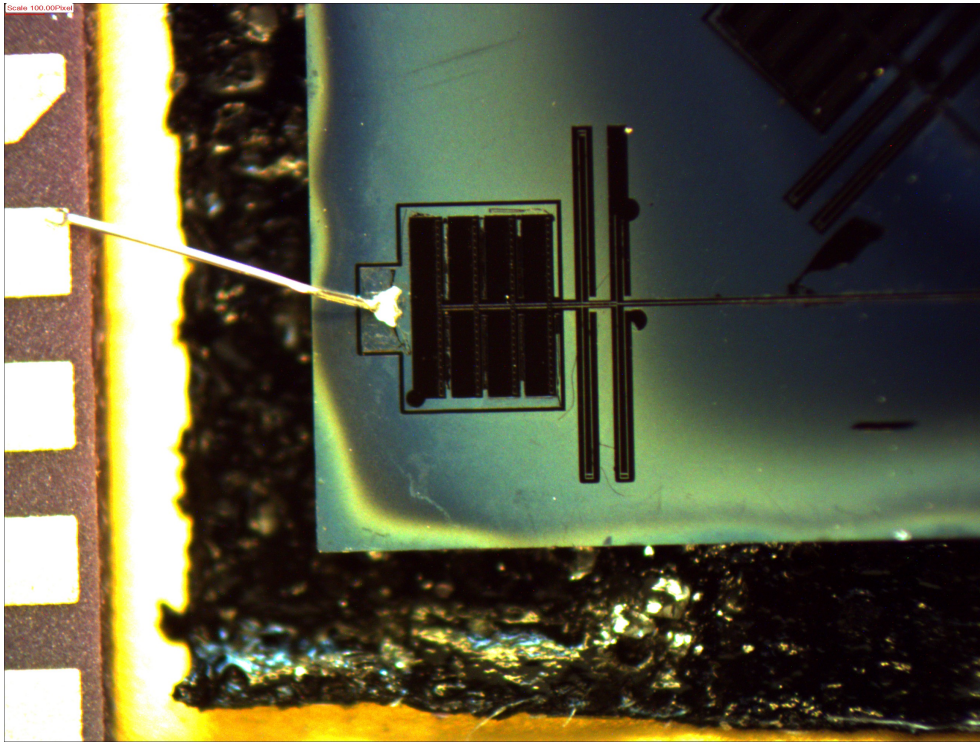
Figure 8.10: Amplified Picture 1 of the fabricated and packed Straight Beam Test Design with Parallel Plates Capacitor Configuration, ready to connect to the DAS.

- The displacements in y direction are affected by the stiffness of the x oriented double beam as the Eq.8.6 using $n = 1$ for the length of the double beam.

- The displacements in y direction are affected by the stiffness of the oblique positioned beam as the Eq.8.5 shows for the length of the oblique beam, being projected on the x axis therefore its contribution is Eq.8.8.

- The displacements in n direction are affected by the stiffness of the x beam as the Eq.5.13 being projected in n using $n = 1$ for the length of the double beam.

- The displacements in n direction are affected by the stiffness of the x direction beam as the Eq.8.6 shows and projecting it in n direction.

- The displacements in n direction are affected by the stiffness of the x direction via the vertical beam as the Eq.8.5 being projected in n direction.

- The displacements in n direction are affected by the stiffness of the y direction beam as the Eq.5.13 shows and using $n = 2$ in the equation and projecting it in n direction.

- no further interferences are taking in consideration.

Preliminary validation procedure for the parallel plate configuration

Fig.8.13 shows the signal for the straight beam parallel plates design. There is an

100

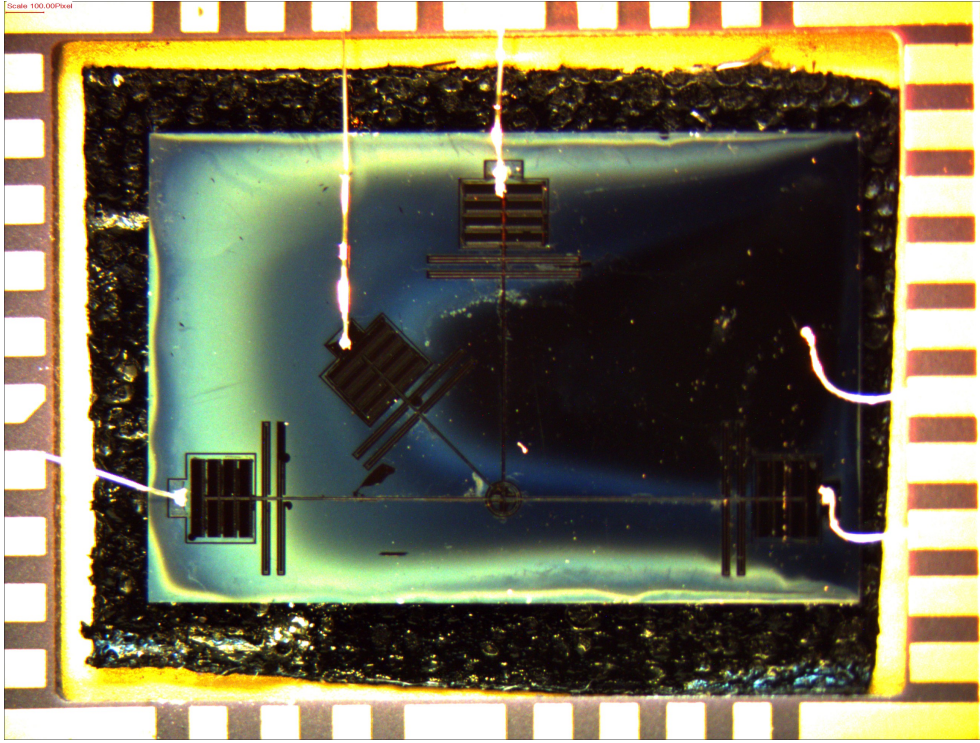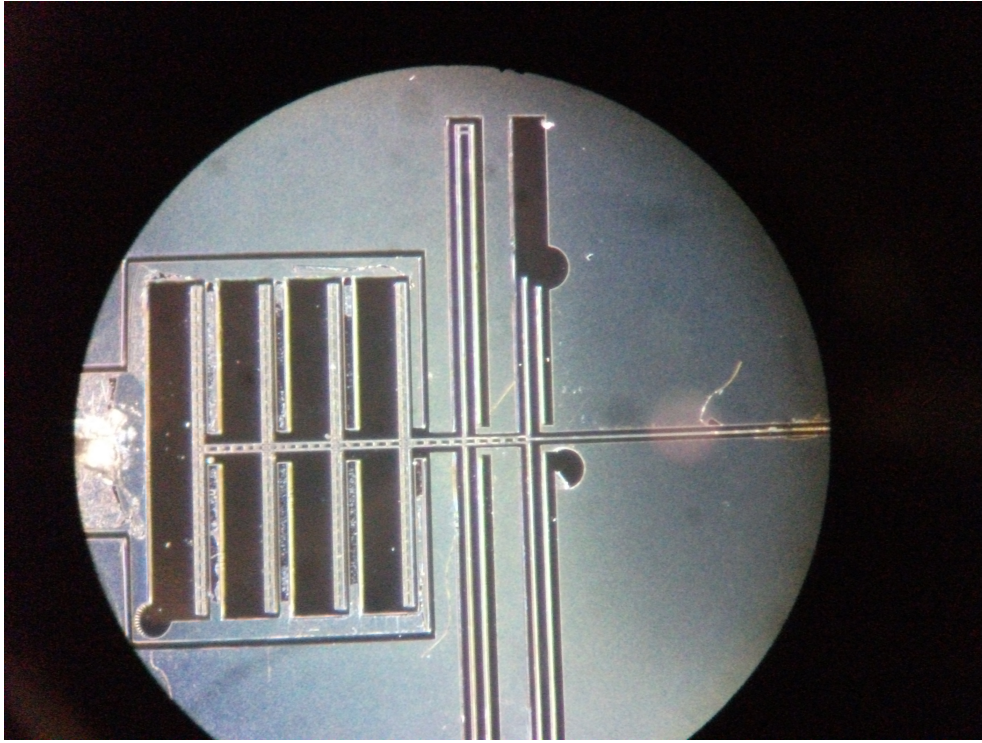Figure 8.11: Amplified Picture 2 of the fabricated and packed Straight Beam Test Design with Parallel Plates Capacitor Configuration, ready to connect to the DAS.

important random noise, the standard deviation σ is calculated and subtracted to the signal, so any magnitude over that value is due external stimulus.

The results shown in Fig.8.13, for a 50 seconds test yields a standard deviation of $\sigma = 21.8[aF]$, and a descending tendency on the magnitude measured. This can be originated by the current through the Silicon and Silicon Oxide, rising the temperature and therefore the permittivity and the most important the variation on the internal tension of the structure. This modify the measurement of the capacitances. Nevertheless the noise is higher than expected, that was the mentioned on datasheet of $4[aF]$, and due to this fact the resolution is lower than expected in a factor $n = 5.45$, for this design, so the expected that the minimum displacements and then the minimum forces detectable will be increased at least by this factor.

The next step is to obtain the response to an external force due to the electrostatically force via the implemented test device. Therefore the connection is performed by differential capacitance mode between the 2 capacitors at the x axis, and the voltage difference applied by the DAS device at, between the movable structure part and the fixed one. To apply the force a differential of electrostatic potential DC is applied using a DC Generator connecting the two ends one at the test capacitor and the other to the movable structure. This way the device should measure the variations in capacitance on the x axis due to the force-displacement due to the test device.

After connecting and turning on the complete system, it is received the capacitance with a very high amplitude of random noise from the maximum to the minimum before
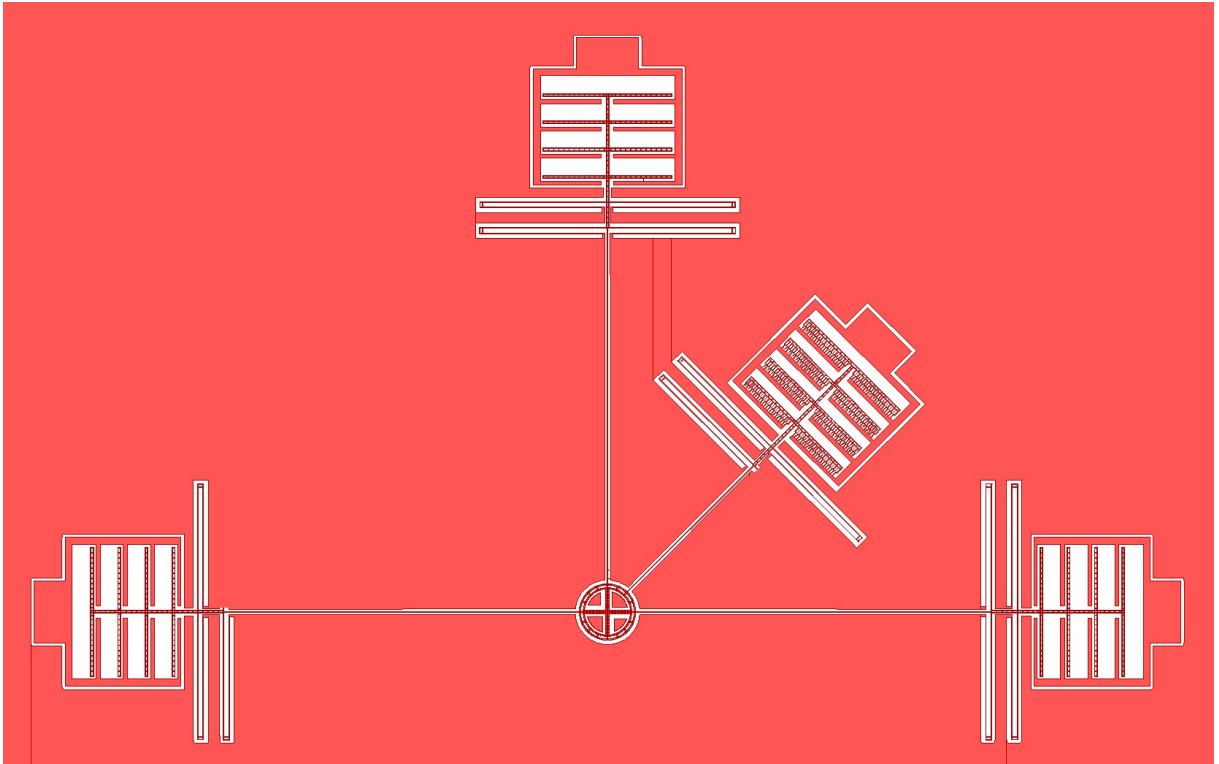
Figure 8.12: Representation of the Straigh Beam Test Design with the Parallel Plates Configuration after the fabrication process.
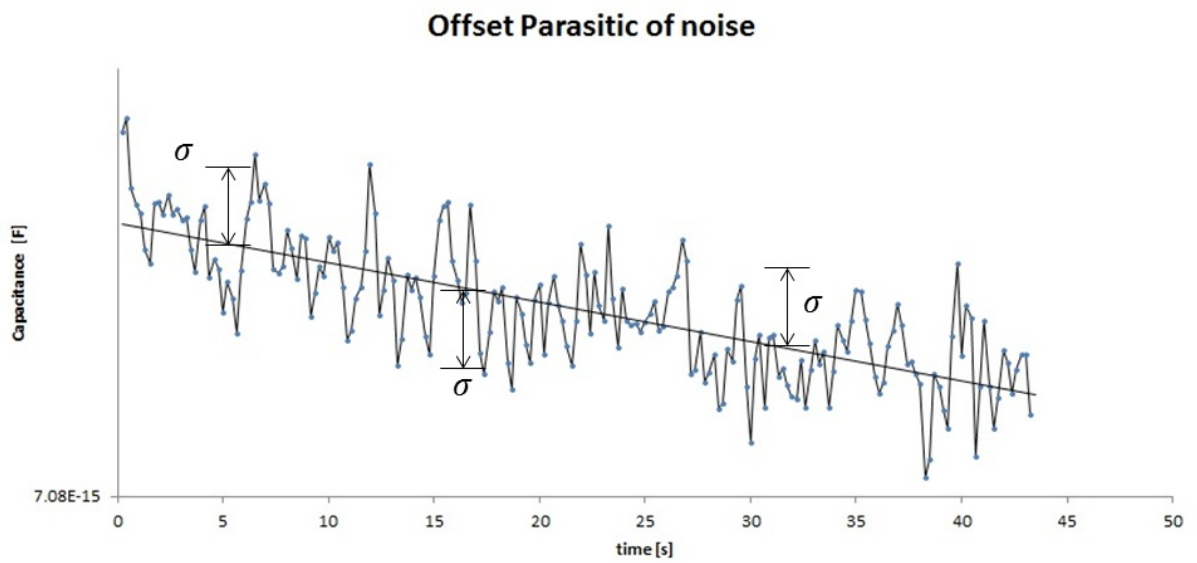
Figure 8.13: Measurement of the noise capacitance due to the internal thermal noise.
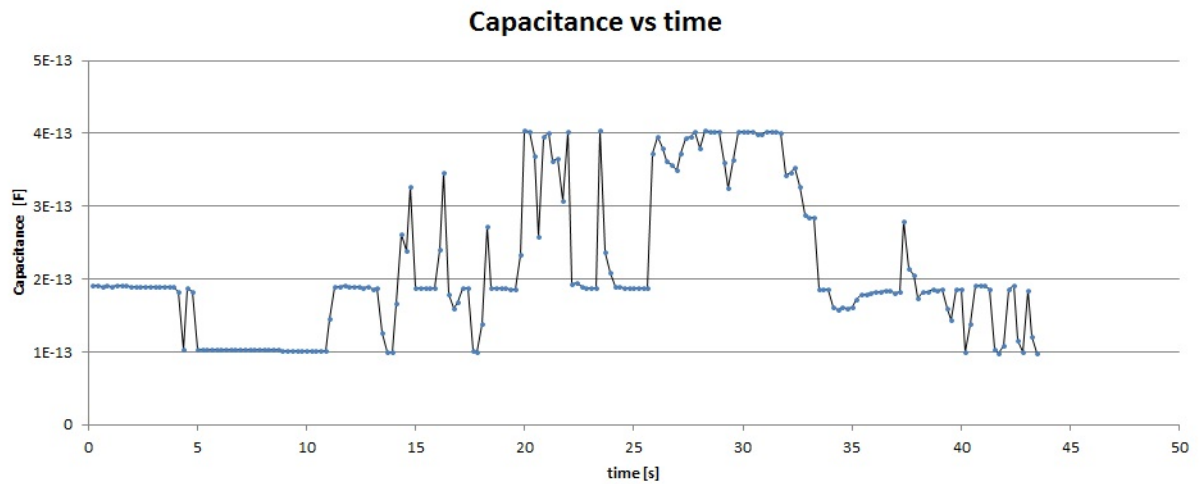
Figure 8.14: Measurement of the capacitance in the x axis due to the forced displacements for the Straight Beam Parallel Plates Configuration.

applying any voltage at the DC generator. Therefore no valid measures can be obtained because the connection of the DC generator to the same voltage reference of the capacitance device measure DAS are not compatible generating, this should be cause by the internal impedance that DC generator are adding to the capacitance signal. This suggest that a different way of calibrate has to be performed in order to validate the calibration process.

In order to verify whether the DAS is really measuring the capacitance variations the connection to the test force device is unplugged, this way the connections are in differential mode for the x axis. A way to measure if the displacement variations are well represented by capacitance variation, the connection ring i.e. where the beams are connected together, is forced to move from the equilibrium position to the lateral sides reaching its limits of displacements in this directions whilst the signal is being recorded. The capacitance signal as a function of time is plotted in Fig8.14. This signal indeed shows significative variations of the capacitance during the displacement experiment.

The signal obtained in Fig.8.14 is treated in order to compare the forced displacements with the expected ones using the capacitance equations found in The Capacitance as a Function of the Displacement section. the signal is centered to the mean offset magnitude, therefore the offset in differential mode is almost 0 as it has to be, and how it is planned to be in the capacitance equations for differential mode. Then using the equation **??** for differential mode Eq.8.9, for the obtained and treated capacitance values i.e. with almost 0 offset, it is found the relationship between time and displacement due to the variations of the capacitance magnitude in Fig.8.15.

After looking at the displacements due to the capacitance variations it is easy to seen that the magnitude found is in a reasonable order of magnitude than the expected vale forced manually. During the test, the displacements where approximately from the top lateral on the left to the top lateral on the right approximately. Therefore the expected displacements where forced to be between $-20[\mu m]$ to $20[\mu m]$. Comparing the obtained ones on Fieg8.15 that shows a maximum and minimum displacements of during the
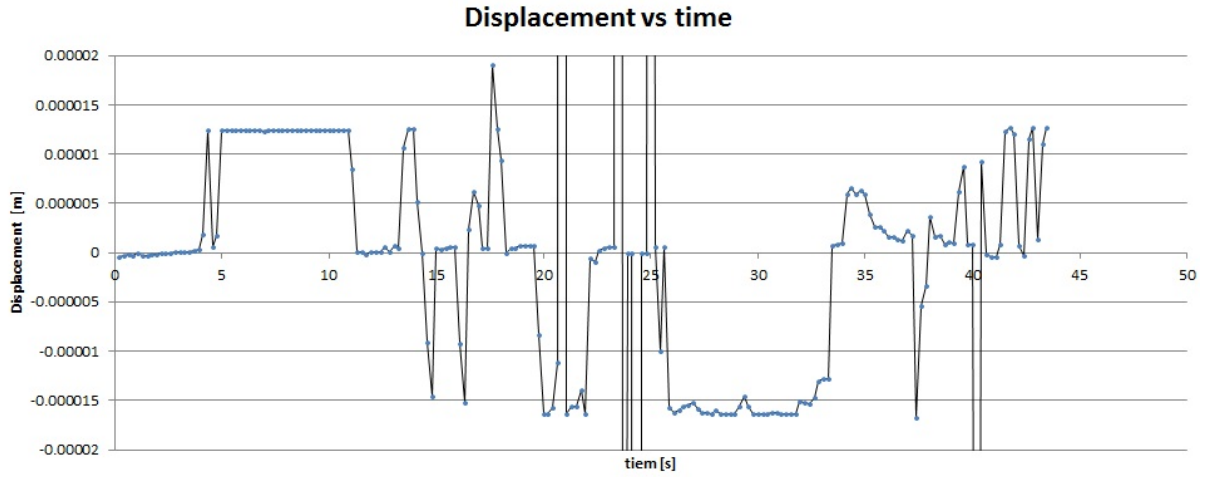
Figure 8.15: Measurement of the displacement in the x axis due to the forced displacements for the Straight Beam Parallel Plates Configuration.

experiment, showing a range from $-12.4[\mu m]$ to $16.3[\mu m]$, which are a very similar values, despite the uncertain of the exact forced displacements of the experiment.

$$C_{xppd} = \frac{8.7655 \cdot 10^{-19}}{(2 \cdot 10^{-5} + x)} + \frac{8.7655 \cdot 10^{-19}}{(13.5 \cdot 10^{-5} - x)} - \frac{8.7655 \cdot 10^{-19}}{(2 \cdot 10^{-5} - x)} + \frac{8.7655 \cdot 10^{-19}}{(13.5 \cdot 10^{-5} + x)} \tag{8.9}$$

Continuing with the experiments due to the difficulty in measure a pull in study has been done in order to verify whether the internal stiffness is the one expected by the calibration equations and assumptions. Hence the DC generator in connected again to the test capacitor on the device and via microscope the limit in the equilibrium up to the pull in voltage will be obtained.

Using the stiffness in the assumptions section for this design, the equilibrium between the electrical force and the internal response due to the stiffness is found and isolating for the applied voltage on the capacitors it is obtained Eq.**??** and plotted in Fig.**??**, for the oblique forced test device direction.

$$V = \sqrt{-1.023\,x \left(-1.629 \cdot 10^{-8} - 4.0729 \cdot 10^{-19} \left(38 \cdot 10^{-6} - x\right)^{-2} + 8.1459 \cdot 10^{-19} \left(83 \cdot 10^{-6} + x\right)^{-2}\right)^{-1}} \tag{8.10}$$

The first minimum found indicates the pull in point and the regarding pull in voltage, which in this case is of $V_{pin} = 37.6[V]$.

During the test the pull in voltage found was of $45.6[V]$, higher than the expected.

Arrived at this point it is also performed a pull in test in the x and y direction, connecting the DC Generator to the end capacitors one per time.

For the x axis the equilibrium equation found using the internal stiffness and the force due to the applied DC at the capacitor after isolation the applied voltage as a function of the displacement is Eq.8.11 and plotted in Fig.8.17. The pull in voltage found is using Eq.8.11 is of $V_{pin} = 35.996[V]$, the experimental one found was of approximately $V_{pin} = 35[V]$ for the left capacitor and approximately of $V_{pin} = 34[V]$, which are close to the the the
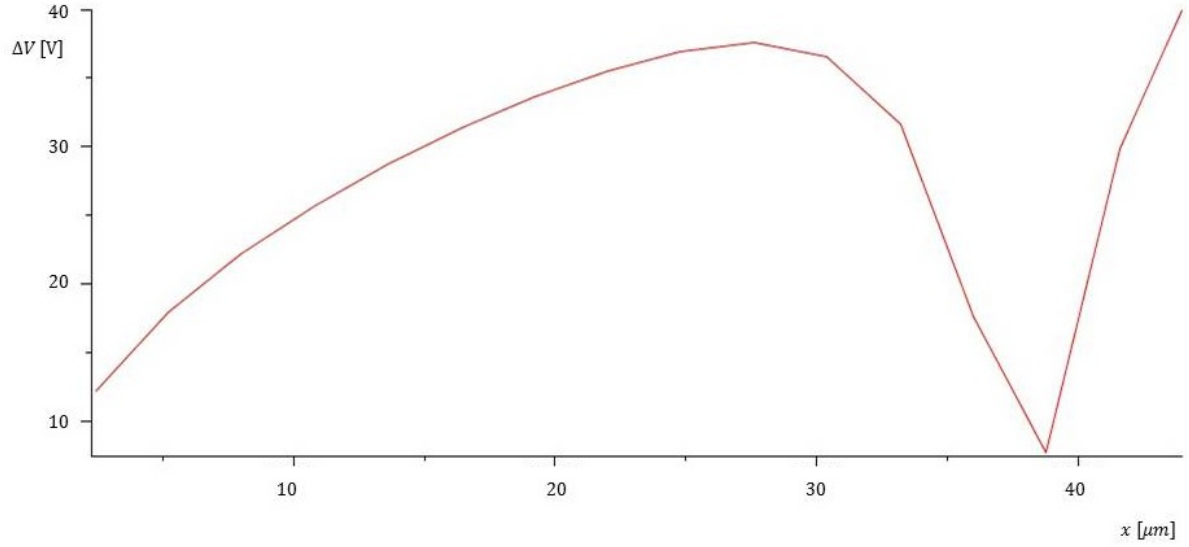
Figure 8.16: Applied input voltage as a function of the x axis displacement.

expected values.

$$V = 1.04559 \cdot 10^9 \sqrt{x \left(0.00002 - x\right)^2} \tag{8.11}$$

For the y direction the equilibrium equation found of the voltage as a function of the displacement is Eq.8.12 and plotted in Fig.8.18.

$$V = 8.6936 \cdot 10^8 \sqrt{x \left(25 \cdot 10^{-6} - x\right)^2} \tag{8.12}$$

The pull in voltage found is using Eq.8.12 is of $V_{pin} = 41.83[V]$, the experimental one found was of approximately $V_{pin} = 43[V]$, which are again close to the the expected values.

Experimental set up of the straight beam test design with the comb-drive configuration.

The second tested device is the straight beam design with the test attached component and comb-drive capacitors configuration and can be seen in Fig.8.19, and a more close detail pictures in Fig.8.20 and Fig.8.21:

Preliminary validation procedure

As in the previous seen design, in order to verify whether the DAS is really measuring the capacitance variations the connection to the test force device is unplugged, this way the connections are in differential mode for the x axis. A way to measure if the displacement variations are well represented by capacitance variation. The displacement is forced to from the equilibrium position to the lateral sides reaching its limits of displacements in this directions whilst the signal is being recorded. The capacitance signal

105
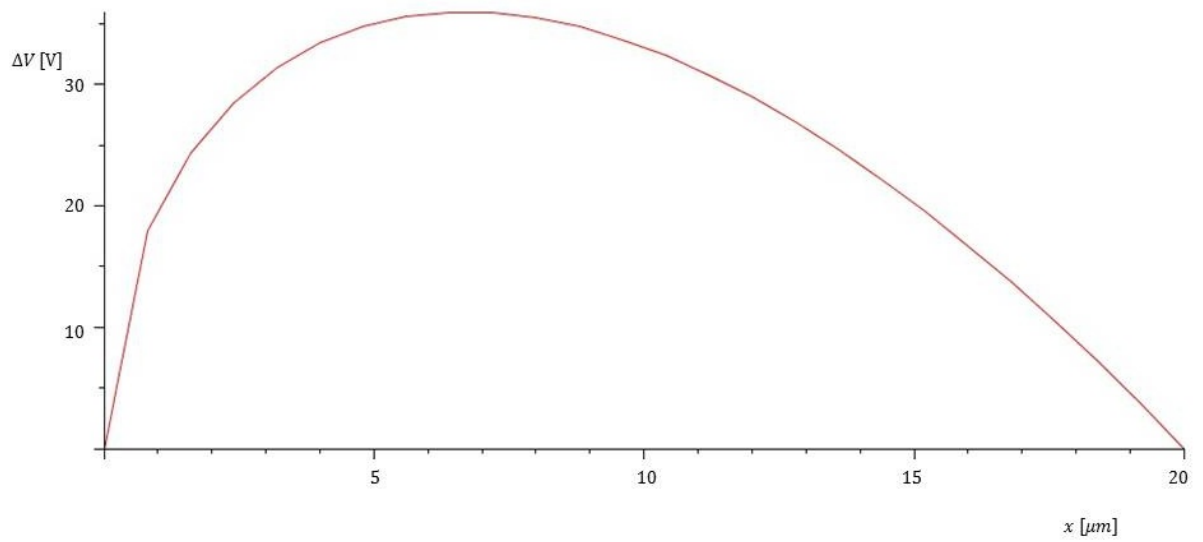
Figure 8.17: Applied input voltage as a function of the x axis displacement.
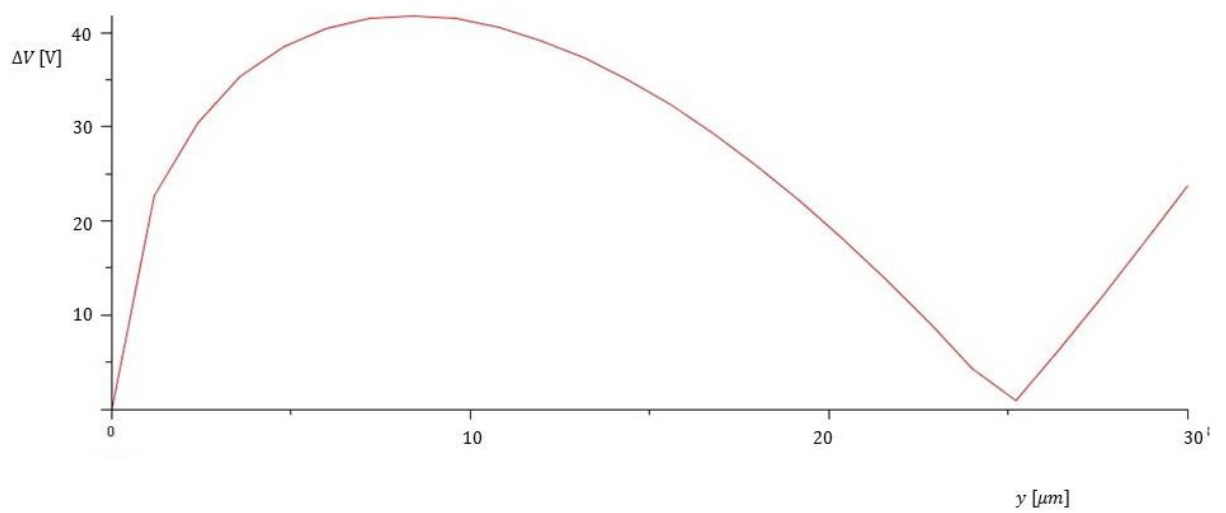
Figure 8.18: Applied input voltage as a function of the y axis displacement.
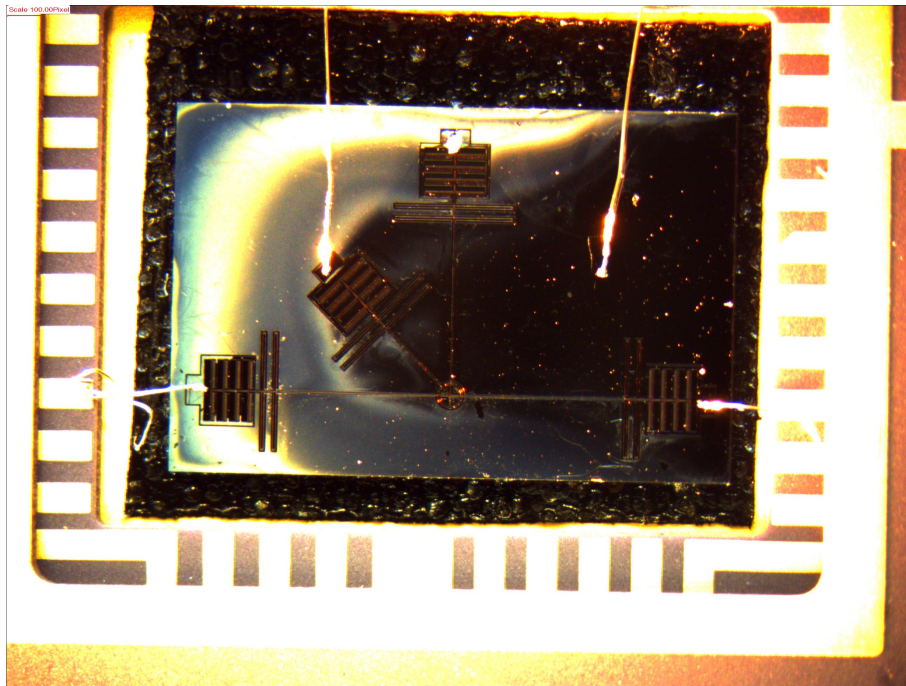
Figure 8.19: Picture of the fabricated and packed Straight Beam Test Design with Comb-Drive Capacitor Configuration, ready to connect to the DAS.
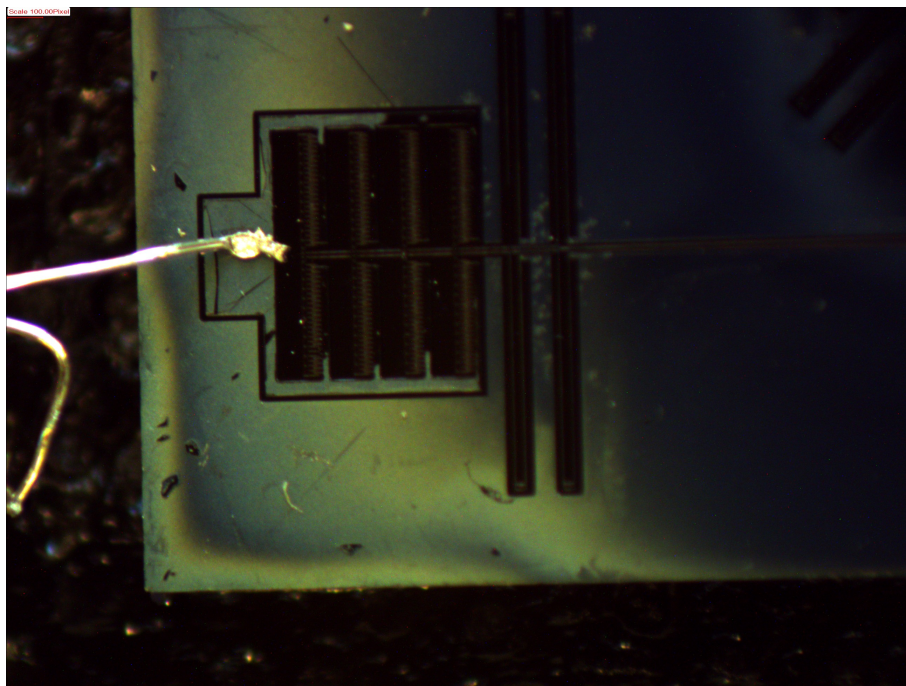
Figure 8.20: Amplified picture 1 of the fabricated and packed Straight Beam Test Design with Comb-Drive Capacitor Configuration, ready to connect to the DAS.

as a function of time is plotted in Fig8.22. This signal indeed shows again significative variations of the capacitance during the displacement experiment.
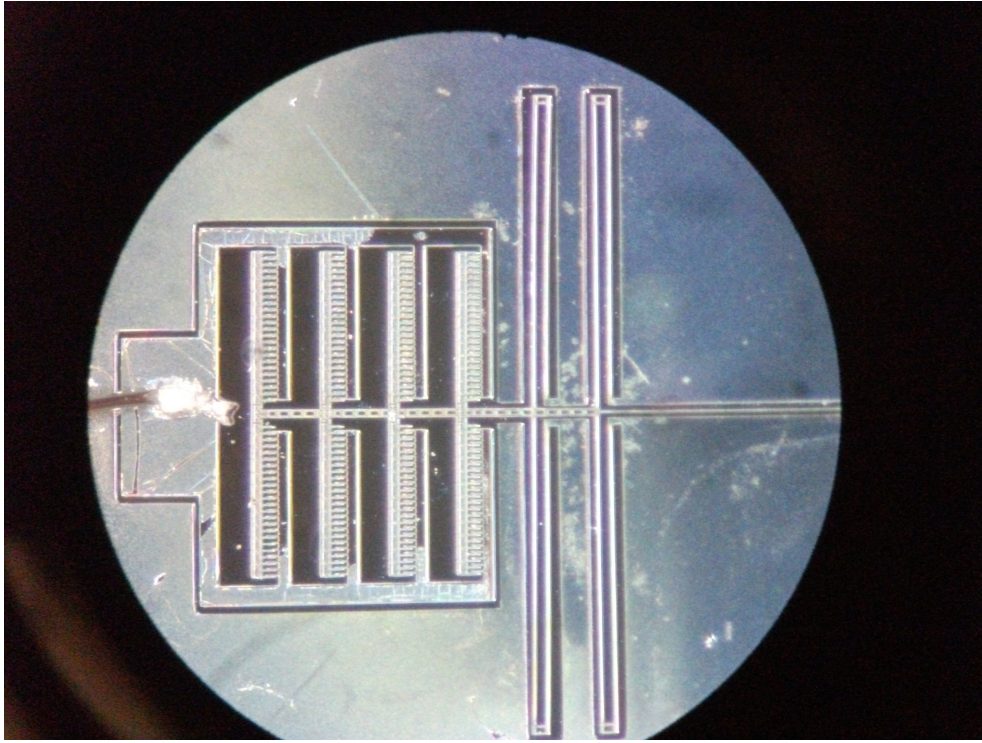
Figure 8.21: Amplified picture 2 of the fabricated and packed Straight Beam Test Design with Comb-Drive Capacitor Configuration, ready to connect to the DAS.

The signal obtained in Fig.8.22 is treated in order to compare the forced displacements with the expected ones using the capacitance equations found in The Capacitance as a Function of the Displacement section. Hence signal is centrad from the mean offset magnitude, therefore the offset in differential mode is almost 0 as it has to be. How it is expected to be in the capacitance equations for differential mode.

Then using the equation for differential mode Eq.8.13, for the obtained and treated capacitance values i.e. with almost 0 offset, it is found the relationship between time and capacitance in Fig.8.22 and using Eq.8.13 displacement due to the variations of the last magnitude in Fig.8.23.

$$C_{xcd} = (-3.47 \cdot 10^{-8} x + \frac{8.6771 \cdot 10^{-19}}{(2 \cdot 10^{-5} + x)} + \frac{8.6771 \cdot 10^{-19}}{(6 \cdot 10^{-5} + x)} + \frac{1.7708 \cdot 10^{-18}}{(9.7 \cdot 10^{-5} - x)})$$
$$-(-3.47 \cdot 10^{-8} x + \frac{8.6771 \cdot 10^{-19}}{(2 \cdot 10^{-5} + x)} + \frac{8.6771 \cdot 10^{-19}}{(6 \cdot 10^{-5} + x)} + \frac{1.7708 \cdot 10^{-18}}{(9.7 \cdot 10^{-5} - x)})$$

(8.13)

After looking at the displacements due to the capacitance variations it is easy to seen that the magnitude found is in a reasonable order of magnitude than the expected vale forced manually. During the test, the displacements where approximately from the top lateral on the left to the top lateral on the right approximately. Therefore the expected displacements where forced to be between $-20[\mu m]$ to $20[\mu m]$. Comparing the obtained ones on Fig.8.23 that shows a maximum and minimum displacements of during

108
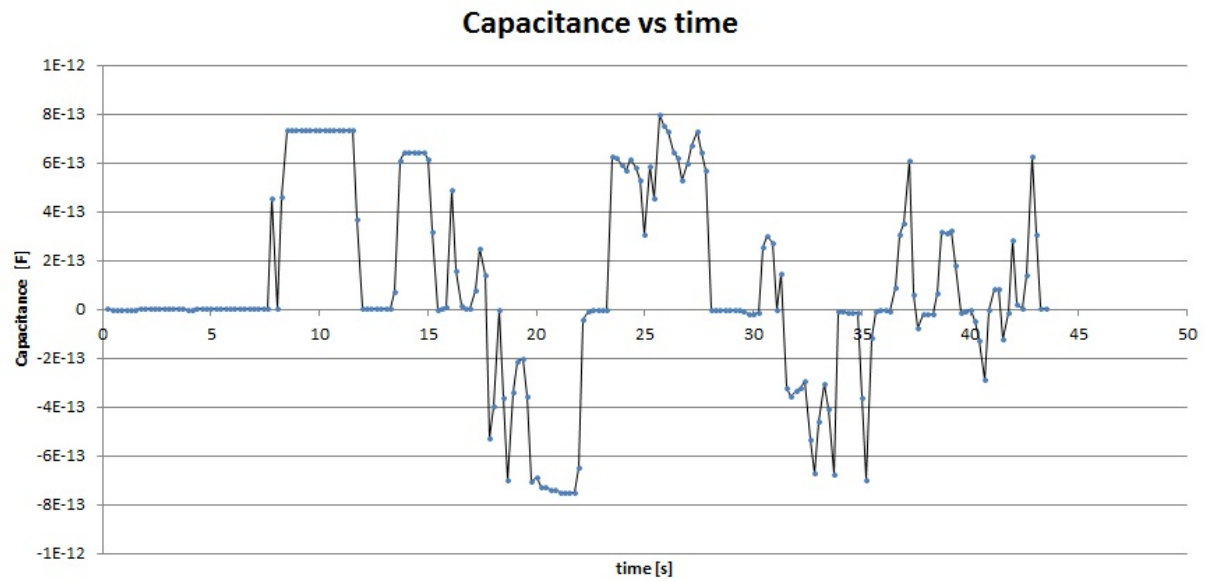
Figure 8.22: Capacitance measured as a function of time for the x axis due to a forced experimental displacement for the Comb-Drive Configuration.
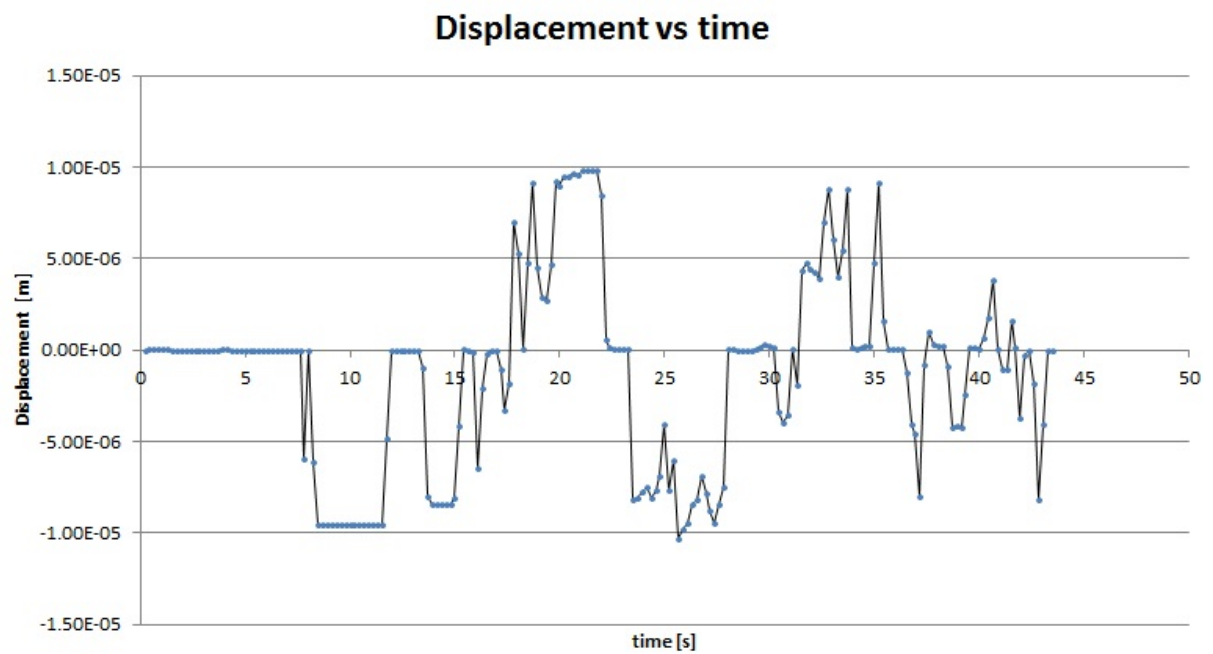
Figure 8.23: Displacement in the x axis due to a forced experimental displacement for the Comb-Drive Configuration.
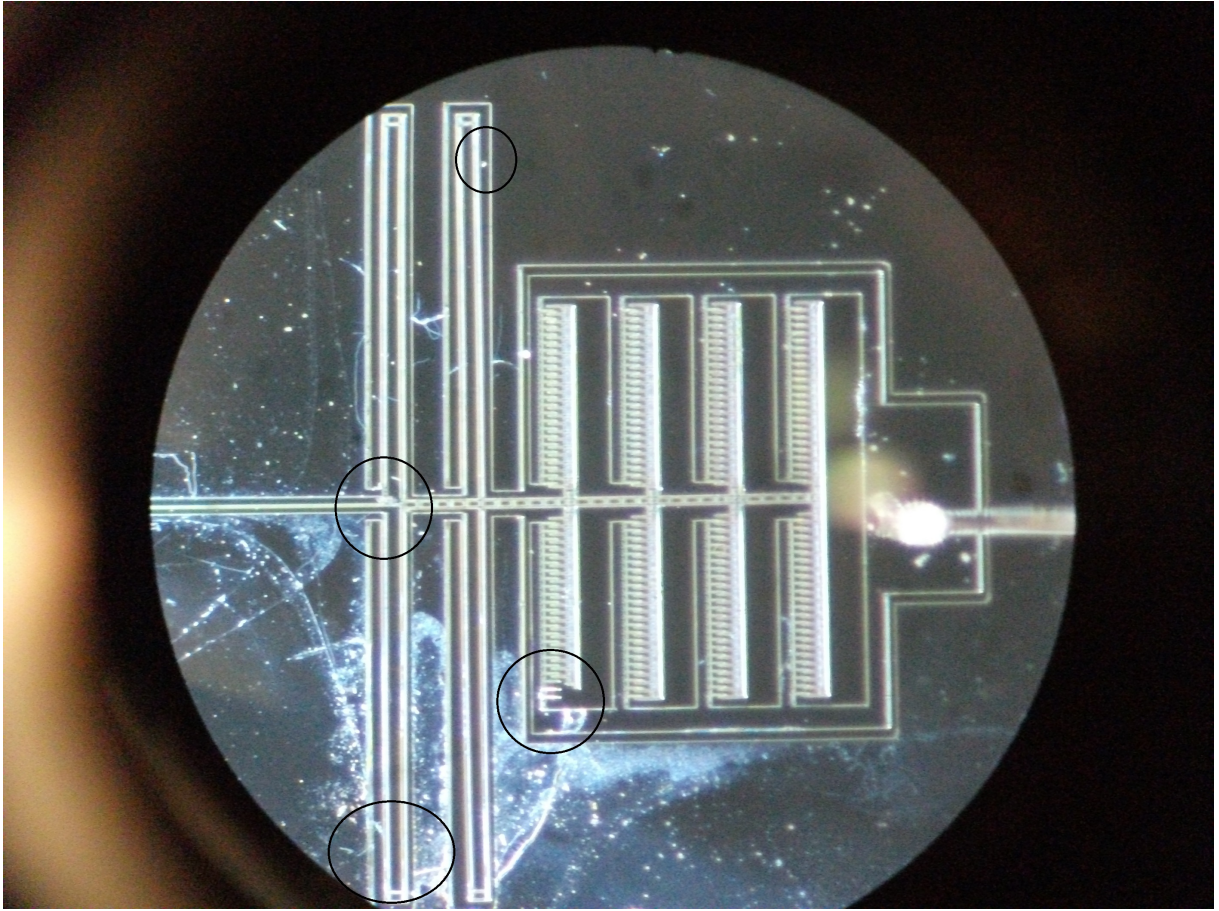
Figure 8.24: Imperfections on the in the gaps after the etching process.

the experiment, showing a very symmetrical range from $-9.6[\mu m]$ to $9.8[\mu m]$, which are a similar values, again despite the uncertain of the exact forced displacements of the experiment. Mostly due to the possible geometrical instability of any of the main beams, and other mentioned impurities and imperfections during the fabrication process as seen in Fig.8.24.

Chapter 9

Project Planning

The project planning and the Gantt diagram are presented next:

CODE	Descripction	Duration	Start	End
Beginning	Beginning of the project.	0 days	Mon 2/14/11	Mon 2/14/11
Introduction & Planification.	Objective, justification, scope, background, introduction to MEMS and Colloidal Propulsion.	5 days	Mon 2/14/11	Fri 2/18/11
State of the art reasearch.	Search for information regarding to the field of the proect, capacitive sensors, state of the art of MEMS and Space Minisatellitesin order to find previous	6 days	Fri 2/18/11	Fri 2/25/11
Buckling Analytic Study Verification & Validation.	Strucutral study of the buckling instability in slender beams, validation of results using FEA.	7 days	Thu 2/17/11	Fri 2/25/11
Prebuckled Analytic Study Verification & Validation.	Strucutral study of the Prebuckled slender beams, validation of results using FEA.	7 days	Fri 2/25/11	Mon 3/7/11
First Model Study & Design	Study and Design of a 1 DOF force sensor device using a prebuckled slender beam, design based on the laterally pull in instability.	10 days	Tu 3/8/11	Mon 3/21/11
Second Model Study & Design	Study and Design of a 1 DOF force sensor device based on the axial buckling instability forcing the buckling effect.	12 days	Mon 3/21/11	Tu 4/5/11
Two DOF Simple Prebuckled Beam Model Study & Design	Study and Design of a 2 DOF force sensor device based on a pair of prebuckled beams one per each direction x ^ y.	9 days	Wed 4/6/11	Mon 4/18/11
Two DOF Double Prebuckled Beam Model Study & Design	Study and Design of a 2 DOF force sensor device based on a pair of double prebuckled beams, one per each direction x and y.	10 days	Tu 4/19/11	Mon 5/2/11
Two DOF Straight Beam Study & Design.	Study and Design of a 2 DOF force sensor device based on straight beams one per each direction x and y.	9 days	Wed 5/4/11	Mon 5/16/11

Test Design Device & Study design and implementation.	Study and Design of the test device which force the strucure of the devices for the calibration process.	12 days	Th 5/5/11	Fri 5/20/11
Masks Revission Process and Enviromental Compatibilities.	Process of revission and design of the devices Masks in order to meet the requirements and avoid interaction problemas with the DAS.	75 days	Tu 3/8/11	Sun 6/19/11
Fabrication process	Process of fabricatin that involves the Masks fabrication and the final SOI MUMPS fabrication method used for the final designs.	48 days	Mon 6/20/11	Wed 8/24/11
Calibration Process	Calibration process with the devices after the fabrication process, in order to obtain measurements of a well know externally applied inputs.	3 days	Wed 8/24/11	Fri 8/26/11
Validation PostProcess	Validation of the devices using the measurements and the expected results.	9 days	Wed 8/24/11	Mon 9/5/11
Conclusions & Future Work.	Valorization of the whole project done and future actions in order to improve the results obtained..	10 days	Mon 9/5/11	Fri 9/16/11
Ending	Project Ending.	0 days	Fri 9/16/11	Fri 9/16/11

114
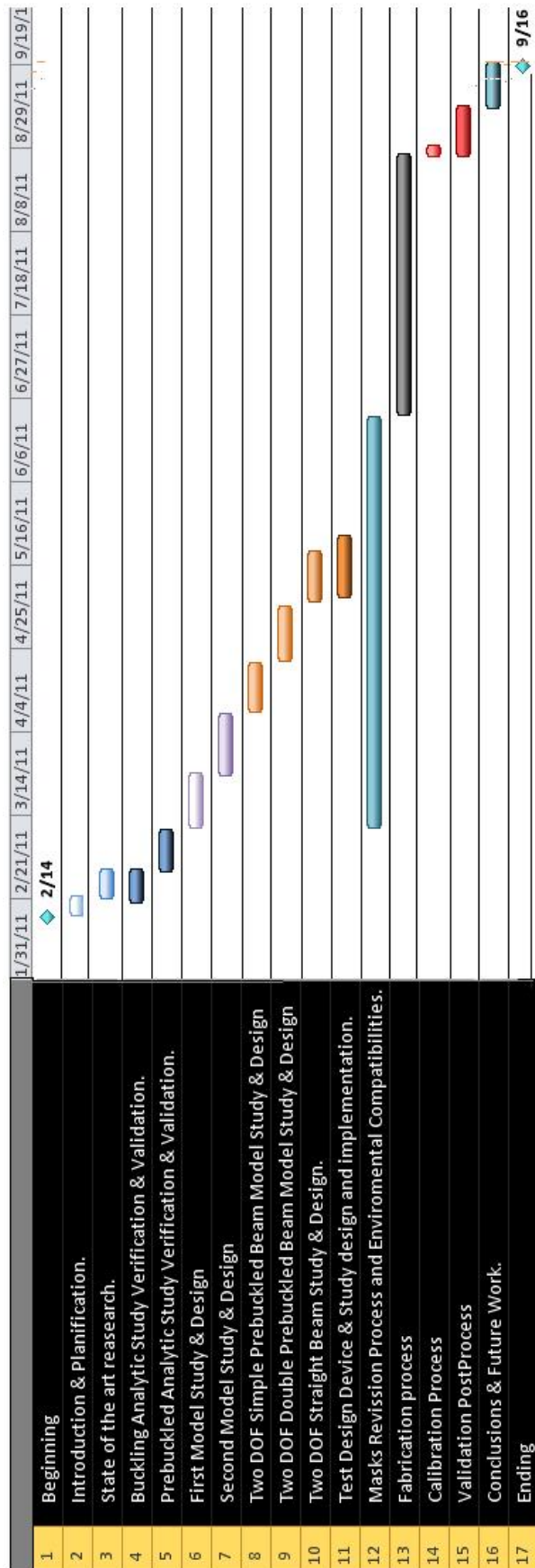
Chapter 10

Budget

In this study estimate the total prototypes construction and design cost has been considered, including the different parts done by the student and also, the ones done by qualified laboratory staff. The software licenses have not been included.

Description	Amount	Conversion	Cost
Student working hours	600	15€/h	9,000 €
Test materials	1	2,200 €	3,500 €
Other working expenses	50	20 €/h	1,000 €
Documents preparation materials	-	-	56 €
Fees and others	-	-	1,500 €
Total			15,056 €

Chapter 11

Conclusions and Future Work

11.1   Conclusions

In this project different sensor designs have been designed and the principle has been validated analytically and preliminary test have been done, which foresee that the proposal ranges of forces and resolution can be achieved using MEMS technology.

The analytical model has been in chapter three, which has been validated through FEA analysis. To design force sensors which take advantage of the amplification of the displacement in the middle point a prebuckled beam to sense the small forces generated in colloidal motors with high resolutions.

In this chapter it is performed the plot of the range of forces measurable for each design in front of its resolution taken at the equilibrium point. In the special case of the 1 DOF design based on instability the values obtained are from the comb-drive and parallel plates capacitors configuration and are plotted for different values of the applied voltage hence it can be obtained a desired range and resolution setting the appropriate voltage for the parameters applied in the final designs. The representation is found in Fig.11.1 in some of the designs are write the ratio r which is the relationship between the range of forces and the resolution.

- A methodology of self calibration and change of resolution has been developed to broad the applications of the sensors and to overcome the variation in performance intrinsic to microfabrication process.

- The design has been fabricated in INRF facilities in UCI (University of California Irvine) thanks to CALCAT Engineering innovation program.

- An experimental setup has been set based on an on-the -self data acquisition system and the experimental results validate the principle of actuation and the expected range of measurable forces.

  To summarize the force sensors based on MEMS technology the used pre-buckled beams represents itself a very competitive, economic and easy solution in force
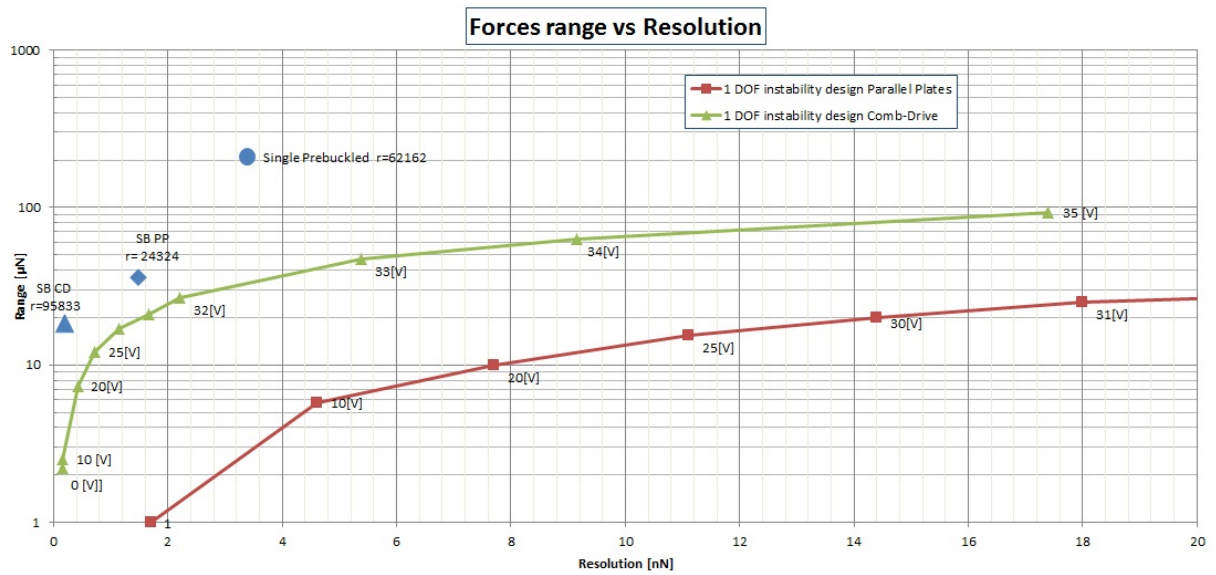
Figure 11.1: Representation of the force range and resolution for the different designs.

sensors actual industry. Which involves an infinite range of applications and therefore an almost unlimited kinds of potential clients at least for the aerospace industry field.

11.2 Future Work

- From the preliminary testing results showed that the calibration would be much simpler if the same capacitors used to tune the resolution where also used to self-calibrate the device, trough future design should be in this direction.

- During the testing procedure unexpected random noise complicated measurements. More testing should be done to clarify the source of that noise (i.e. due to fabrication imperfections, wire bonding..).

- The sensors where normally exited, but there is the need to design appropriate fixtures to transmit the force from the colloidal engine to the force application tip.

Chapter 12

ANNEX

ANSYS Finite Element Studies Code

1 DOF Preload Beam:

/clear /begin / Title, Curved Beam

!**************************PREPROCESS************************

/PREP7

w=50e-6 h=5e-6

!******************************** !* Element type and Properties * !********************************

ET,1,BEAM3

Izz=1/12*w*(h**3) R,1,h*w,Izz,h MP,EX,1,1.7e+11

!******************************** !* Geometry * !********************************

l2=10e-4 l3=20e-4 lc=3e-3

k,1,0,0,0 k,2,0,l3/2,0 k,3,-l2,l3/2,0 k,4,0,l3,0 k,5,lc,1e-6+l3/2,0 k,6,2*lc,l3/2,0

L,1,2 L,2,3 L,2,4 L,2,5 L,5,6

!************* !* Meshing * !*************

SMRT,1 FLST,2,5,4,ORDE,2 FITEM,2,1 FITEM,2,-5 LMESH,P51X

!*********************** !* Boundary Conditions * !***********************

FLST,2,3,3,ORDE,3 FITEM,2,1 FITEM,2,4 FITEM,2,6 !* /GO DK,P51X, , , ,0,ALL, , ,
, , ,

!* /GO DK,P51X, , , ,0,ALL, , , , , , FLST,2,1,3,ORDE,1 FITEM,2,3 !* /GO FK,P51X,FX,30.81734e-

******************************** !* Nonlinear Geometry Analysis * !********************************

/SOLU ANTYPE,STATIC

NLGEOM,on !OUTRES„1 !ARCLEN,ON,4 !NROPT, auto !NSUBST,200 !NEQIT,400

2 DOF Simple Prebuckled Beam:

/clear /begin / Title, Curved Beam

!**************************PREPROCESS*************************

/PREP7

!*********************** !* Geometric Properties * !***********************

h= 5e-6 !In-plane thickness of the beam (AMPLADA VIGA EN EL PLA) w= 50e-6 !Out-plane thickness of the beam (GRUIX VIGA EN Z) b=2e-4 !Initial height d=0.5e-3 L=3e-3 e=1e-5 Pi=3.1415926535897

!********************** !* Model Generation * !**********************

*dim,x,array, 2006,1 !*dimensions for x *dim,y,array, 2006,1 !*dimensions for y

*do,k,1,501

x(k)=((k-1)*L)/500 y(k)=(5e-6)+0.5*b*(1-cos(2*Pi*(k-1)/500))

K,k,x(k),y(k),0 !*Define keypoints

*enddo !*get,Knumber,KP„count !*Number of keypoints

*do,k,1,500 L,k,k+1

*enddo

*do,k,1504,2004

x(k)=(5e-6)+l+(5e-6)+0.5*b*(1-cos(2*Pi*(k-1504)/500)) y(k)=-(5e-6)-l+ ((k-1504)*L)/500

K,k,x(k),y(k),0 !*Define keypoints

*enddo

!*get,Knumber,KP„count !*Number of keypoints

*do,k,1504,2003 L,k,k+1 *enddo

L,501,2004

!******************************** !* Element type and Properties * !********************************

```
ET,1,BEAM3

Izz=1/12*w*(h**3)

R,1,h*w,Izz,h

MP,EX,1,1.7e+11 ! Material propierties

!************** !* Meshing * !**************

ESIZE,1,1e-6 SMRTSIZE,1

LMESH,ALL

!*********************** !* Boundary Conditions * !***********************

/PREP7 FLST,2,2,3,ORDE,2 FITEM,2,1 FITEM,2,1504 !* /GO DK,P51X, , , ,0,ALL,
, , , , ,

!***************************** !* Nonlinear Geometry Analysis * !*****************************

/SOLU ANTYPE,STATIC

NLGEOM,on !OUTRES„1 !ARCLEN,ON,4 !NROPT, auto !NSUBST,200 !NEQIT,400

2 DOF Double Prebuckled Beam:

/clear /begin / Title, Curved Beam

!*************************PREPROCESS*************************

/PREP7

!*********************** !* Geometric Properties * !***********************

    h= 5e-6 !In-plane thickness of the beam (AMPLADA VIGA EN EL PLA) w= 50e-6
!Out-plane thickness of the beam (GRUIX VIGA EN Z) b=2e-4 !Initial height d=0.5e-3
L=3e-3 e=1e-5 Pi=3.1415926535897

!*********************** !* Model Generation * !***********************

*dim,x,array, 2006,1 !*dimensions for x *dim,y,array, 2006,1 !*dimensions for y

*do,k,1,501

x(k)=((k-1)*L)/500 y(k)=(5e-6)+0.5*b*(1-cos(2*Pi*(k-1)/500))

K,k,x(k),y(k),0 !*Define keypoints

*enddo !*get,Knumber,KP„count !*Number of keypoints

*do,k,1,500 L,k,k+1
```

```
*enddo

!k,1002,L,d,0 !k,1003,L-e,d,0 !k,1004,L-e,e/2,0 !k,1005,L,-d,0 !k,1006,L-e,-d,0 !k,1007,L-
e,-e/2,0

!L,501,1002 !L,1002,1003 !L,1003,1004 !L,501,1005 !L,1005,1006 !L,1006,1007

*do,k,502,1002

x(k)=((k-502)*L)/500 y(k)= -0.5*b*(1-cos(2*Pi*(k-502)/500))

K,k,x(k),y(k),0 !*Define keypoints

*enddo

!*get,Knumber,KP,,count !*Number of keypoints

*do,k,502,1001 L,k,k+1 *enddo

*do,k,1003,1503

x(k)=(5e-6)+l-0.5*b*(1-cos(2*Pi*(k-1003)/500)) y(k)=-(5e-6)-l+((k-1003)*L)/500

K,k,x(k),y(k),0 !*Define keypoints

*enddo !*get,Knumber,KP,,count !*Number of keypoints

*do,k,1003,1502 L,k,k+1

*enddo

*do,k,1504,2004

x(k)=(5e-6)+l+(5e-6)+0.5*b*(1-cos(2*Pi*(k-1504)/500)) y(k)=-(5e-6)-l+ ((k-1504)*L)/500

K,k,x(k),y(k),0 !*Define keypoints

*enddo

!*get,Knumber,KP,,count !*Number of keypoints

*do,k,1504,2003 L,k,k+1 *enddo

L,1002,1503 L,501,1002 L,1503,2004

!******************************** !* Element type and Properties * !********************************

ET,1,BEAM3

Izz=1/12*w*(h**3)

R,1,h*w,Izz,h

MP,EX,1,1.7e+11 ! Material propierties
```

!************* !* Meshing * !*************

ESIZE,1,1e-6 SMRTSIZE,1

LMESH,ALL

!*********************** !* Boundary Conditions * !***********************

/PREP7 FLST,2,2,3,ORDE,2 FITEM,2,1 FITEM,2,1504 !* /GO DK,P51X, , , ,0,ALL, , , , , ,

!***************************** !* Nonlinear Geometry Analysis * !*****************************

/SOLU ANTYPE,STATIC

NLGEOM,on !OUTRES,,1 !ARCLEN,ON,4 !NROPT, auto !NSUBST,200 !NEQIT,400

2 DOF Straight Beam:

/clear /begin / Title, Curved Beam

!**************************PREPROCESS************************

/PREP7

w=50e-6 h=5e-6

!******************************** !* Element type and Properties * !********************************

ET,1,BEAM3

Izz=1/12*w*(h**3) R,1,h*w,Izz,h MP,EX,1,1.7e+11

!******************************** !* Geometry * !********************************

a=0.4e-3 !separació barreres al=2e-3 !alçada barreres l=3e-3 ! longitud viga desde origen xy p=20e-4 !longitud plate d=1e-4 !separació plate barrera xp=l+al/2 yp=l-al/2+a

k,1,0,0,0 k,2,0+1e-6,al/2,0 k,3,-d,al/2,0 k,4,-d,al/2-p/2,0 k,5,-d,al/2+p/2,0 k,6,0,al,0 k,7,a,al,0 k,8,a+1e-6,al/2,0 k,9,a+l,al/2,0 k,10,a,0,0 k,11,a/2,0,0 k,12,a/2,al,0

L,1,2 L,2,3 L,3,4 L,5,3 L,2,6 L,2,8 L,7,8 L,8,9 L,8,10

k,13,yp,xp,0 k,21,yp+al/2,xp-1e-6,0 k,31,yp+al/2,d+xp,0 k,41,yp+al/2-p/2,d+xp,0 k,51,yp+al/2+p/2,d+xp k,61,yp+al,xp,0 k,71,yp+al,-a+xp,0 k,81,yp+al/2,-a+xp-1e-6,0 k,101,yp,-a+xp,0 k,111,yp,-a/2+xp,0 k,121,yp+al,-a/2+xp,0

L,13,21 L,21,31 L,31,41 L,51,31 L,21,61 L,21,81 L,71,81 L,81,9 L,81,101

k,131,yp,al-xp,0 k,211,yp+al/2,al-xp+1e-6,0 k,311,yp+al/2,al-d-xp,0 k,411,yp+al/2-p/2,al-d-xp,0 k,511,yp+al/2+p/2,al-d-xp,0 k,611,yp+al,al-xp,0 k,711,yp+al,al+a-xp,0 k,811,yp+al/2,al+a-xp+1e-6,0 k,1011,yp,a-xp+al,0 k,1111,yp,a/2-xp,0 k,1211,yp+al,al+a/2-xp,0

L,131,211 L,211,311 L,311,411 L,511,311 L,211,611 L,211,811 L,711,811 L,811,9 L,811,1011

!************* !* Meshing * !*************

SMRT,1 FLST,2,18,4,ORDE,2 FITEM,2,1 FITEM,2,-18 LMESH,P51X FLST,2,27,4,ORDE,2 FITEM,2,1 FITEM,2,-27 LMESH,P51X

!*********************** !* Boundary Conditions * !***********************

FLST,2,12,1,ORDE,12 FITEM,2,1 FITEM,2,26 FITEM,2,38 FITEM,2,50 FITEM,2,55 FITEM,2,80 FITEM,2,92 FITEM,2,102 FITEM,2,107 FITEM,2,132 FITEM,2,144 FITEM,2,154 !* /GO D,P51X, , , , , ,ALL, , , , ,

/GO

FLST,2,1,3,ORDE,1 FITEM,2,9 FK,P51X,FX,1e-5 !* /GO FLST,2,1,3,ORDE,1 FITEM,2,9 FK,P51X,FY,-1e-005

******************************** !* Nonlinear Geometry Analysis * !********************************

/SOLU ANTYPE,STATIC

NLGEOM,on

12.1 Double Prebuckled Beam Design

12.1.1 Double prebuckled beam design

For this design the double direction force sensor is used with the double prebuckled beam geometry shown schematically on Fig.12.1 and in the final design on Fig.12.2.Using the second chapter theory it can be found the relationship between the applied force and the lateral displacement in Eq.12.9. Where now the stiffness due to the structure is doubled because of the parallel equivalent spring configuration.

Using this configuration the specimen is considered to be 2 dof because of the small stiffness of each pair of beams on shear direction, it prevents coupled the displacement problem. Then the axial displacement applied on one direction affects on the same direction to the geometry as shown in Fg.12.3 and on the perpendicular placed beam the same load generates a displacement shown in Fig.12.4, by the geometrical relationship between x and y it can be found the vector of displacements.

Because there is an axial and shear displacement on each beam, the system of measurement has to discriminate between pure axial and pure shear forces and displacements. This issue is solved assuming the superposition of the displacements i.e. one due to the axial plus other due to the shear displacement. Because of the symmetry of the geometry it is easy to see the fact that the shear displacement affects equal on both middle points pair of beams and the axial displacement affects on opposite direction
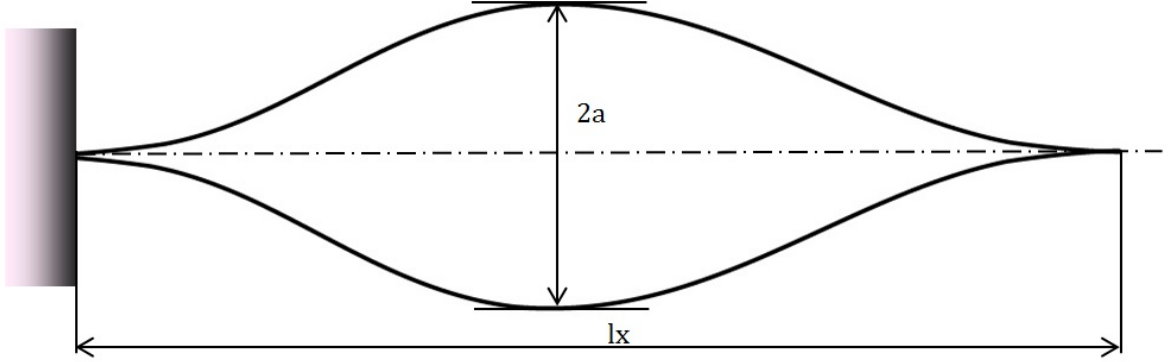
124

Figure 12.1: Schematic geometry of the pre-buckled double beam.

and equal value. In order to found each middle beam point lateral displacements and thus recomposing the vectorial character of the force parallel plates capacitors are used see Fig.12.5.

The capacitance the measured by the capacitors C_{11}, C_{12}, will be measured commonly i.e. as the addition of the two magnitudes, this way it will be obtained a single amount named C_1. Thes same is made for the capacitances used C_2, C_3 and C_4. This way it can be solved a 4X4 decoupled system obtaining the solution in Eq.12.1, Eq.12.2,Eq.12.3 and Eq.12.4.

$$\frac{\epsilon}{2}\left(\frac{S_2}{C_2}+\frac{S_1}{C_1}\right)-g_0 = d_{y1}Px \tag{12.1}$$

$$\frac{\epsilon}{2}\left(\frac{S_2}{C_2}-\frac{S_1}{C_1}\right) = d_{y1}Py \tag{12.2}$$

$$\frac{\epsilon}{2}\left(\frac{S_4}{C_4}+\frac{S_3}{C_3}\right)-g_0 = d_{y2}Py \tag{12.3}$$

$$\frac{\epsilon}{2}\left(\frac{S_4}{C_4}-\frac{S_3}{C_3}\right) = d_{y2}Px \tag{12.4}$$

For the considered design the area of actuation surface is the same in all parallel plate capacities $S_1 = S_2 = S_3 = S_4$ then equations Eq.12.1 to Eq.12.4 it simplifies as
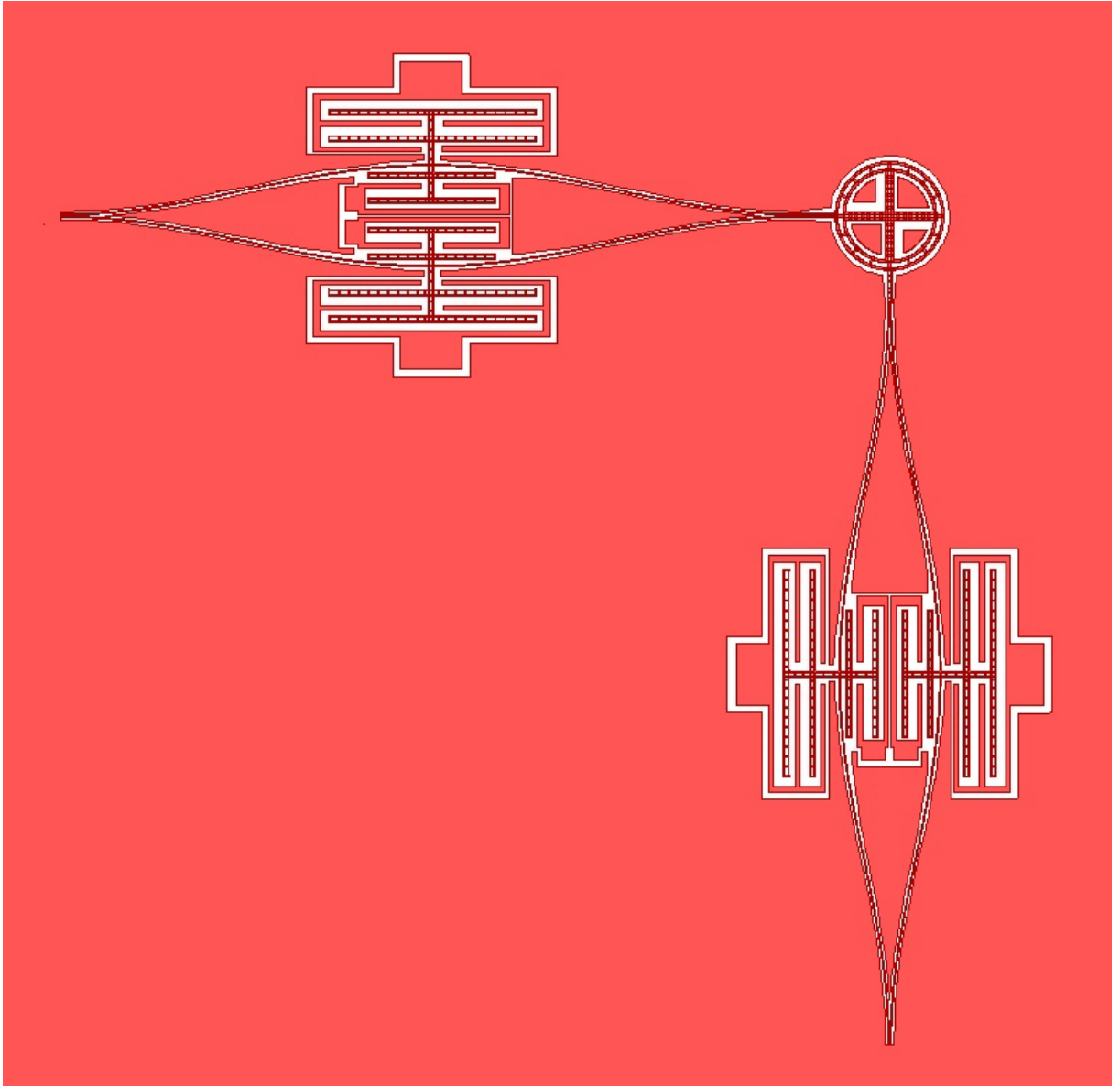
125

Figure 12.2: Geometry of the pre-buckled double beam design.

Eq.12.5, Eq.12.6, Eq.12.7, Eq.12.8.

$$\frac{S\epsilon}{2}\left(\frac{1}{C_2} + \frac{1}{C_1}\right) - g_0 = d_{y1}Px \tag{12.5}$$

$$\frac{S\epsilon}{2}\left(\frac{1}{C_2} - \frac{1}{C_1}\right) = d_{y1}Py \tag{12.6}$$

$$\frac{S\epsilon}{2}\left(\frac{1}{C_4} + \frac{1}{C_3}\right) - g_0 = d_{y2}Py \tag{12.7}$$

$$\frac{S\epsilon}{2}\left(\frac{1}{C_4} - \frac{1}{C_3}\right) = d_{y2}Px \tag{12.8}$$

Taking into account that the sum of capacitance measures must be higher the Eq.12.6
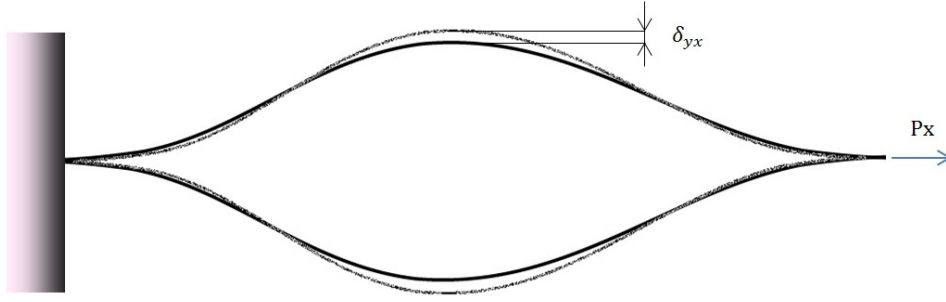
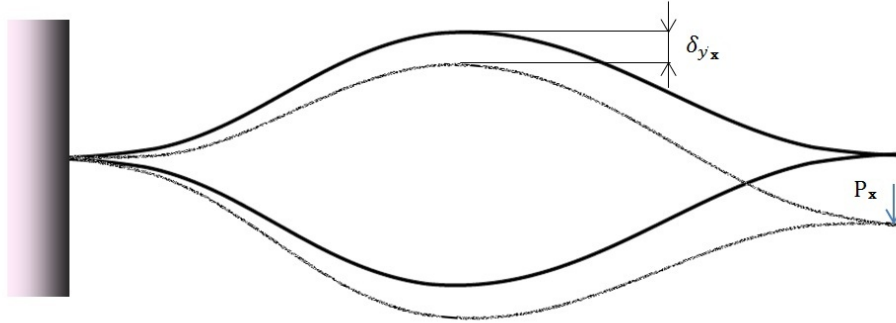Figure 12.3: Deflection due to the axial load Fx on the x symmetry beam.

Figure 12.4: Deflection due to the axial load Fx on the y symmetry beam.

and Eq.12.8 should provide more uncertainty, because of its small size in magnitude regarding to Eq.12.6 and Eq.12.8, therefore it is more efficient to work with Eq.12.5 and Eq.12.7 to found the mid point lateral displacements. Once the values d_y1 and d_y2 are obtained per each axial displacement it can be easily found the force applied by the use of Eq.12.9, Eq.12.5 to obtain P_x and Eq.12.7 to found P_y, and therefore the force vector.

$$P = \frac{1}{30720} \frac{(AEI + BF_c)\, l}{(a + y)\, \pi^2} \quad (12.9)$$

$$A = 3840\, \frac{\pi^8 \left(a\, (a + y)^4 - (a + y)^5 \right)}{l^7} + 30720\, \frac{\pi^6 \left(a^3 - (a + y)^3 \right)}{l^5} - 245760\, \frac{\pi^4 y}{l^3}$$

$$B = 2 - \frac{\left(16384\, \pi^4 + 2880\, \pi^6 \right) (a + y)^4}{l^4} - \frac{\left(81920\, \pi^2 + 15360\, \pi^4 \right) (a + y)^2}{l^2}$$

$$F_c = \frac{\epsilon}{2} \left(\frac{S_1}{(g_2 - y)^2} - \frac{S_2}{(g_1 + y)^2} \right)$$

$$(12.10)$$
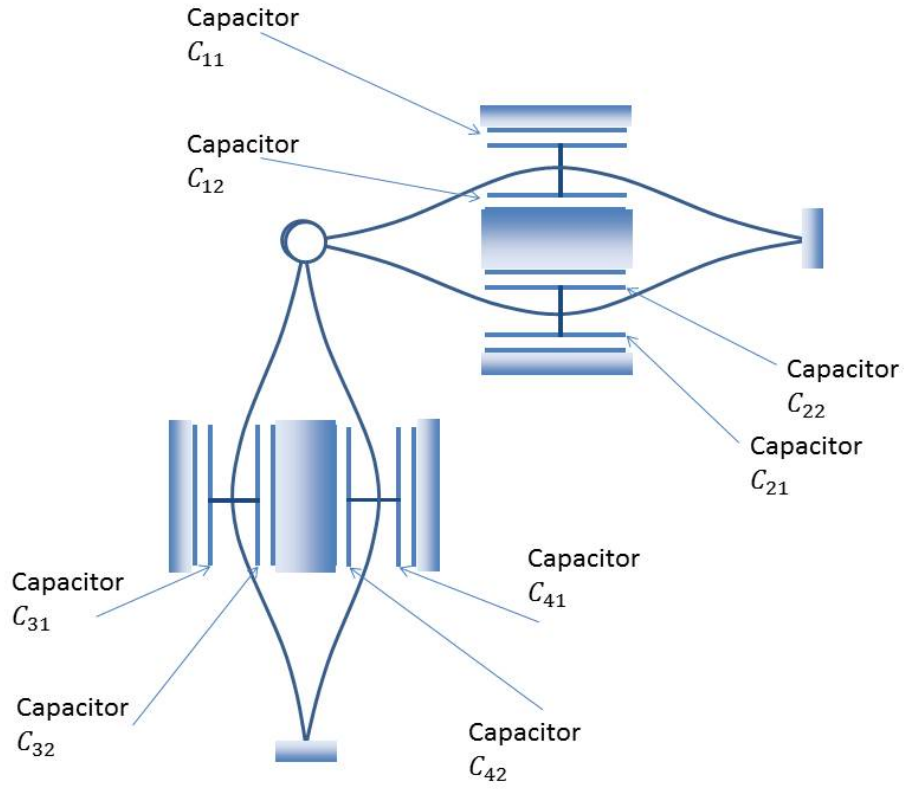
Using the next geometrical parameters shown in Fig.12.6:

127

Figure 12.5: Configuration of the capacitors in the Double Prebuckled Beam Design.

$$l = 3[mm]$$
$$a = 200[\mu m]$$
$$t = 50[\mu m]$$
$$w = 5[\mu m]$$

The external force can be characterized as a function of the lateral displacement according to Eq.12.11, where a second order Mc.Laurin approximation is used. Relationship between the theorical displacement y and the force applied is plotted in Fig.12.7.

$$P = -1.9739\,y + 9708.841\,y^2 \tag{12.11}$$

Thus the maximum traction applied force is:

$$P_{max} = 46.24[\mu N]$$

Thus the maximum compressive force applicable is:
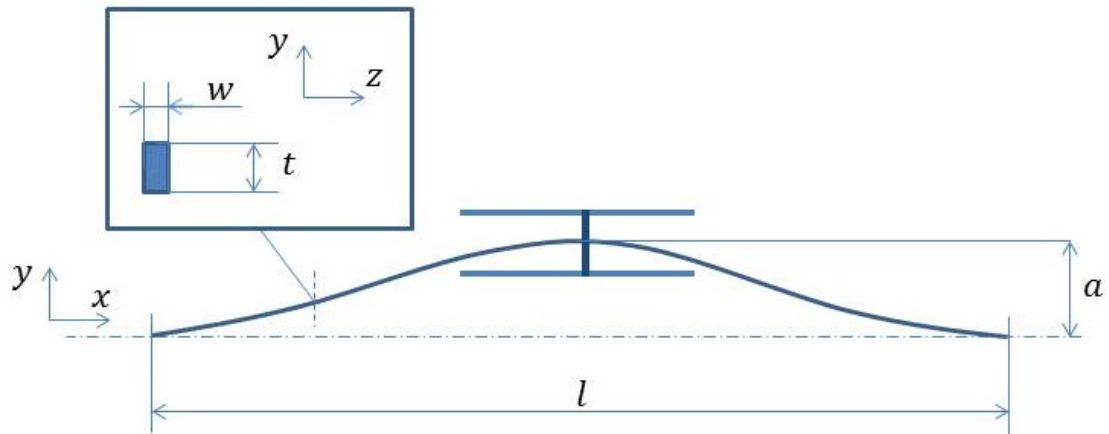
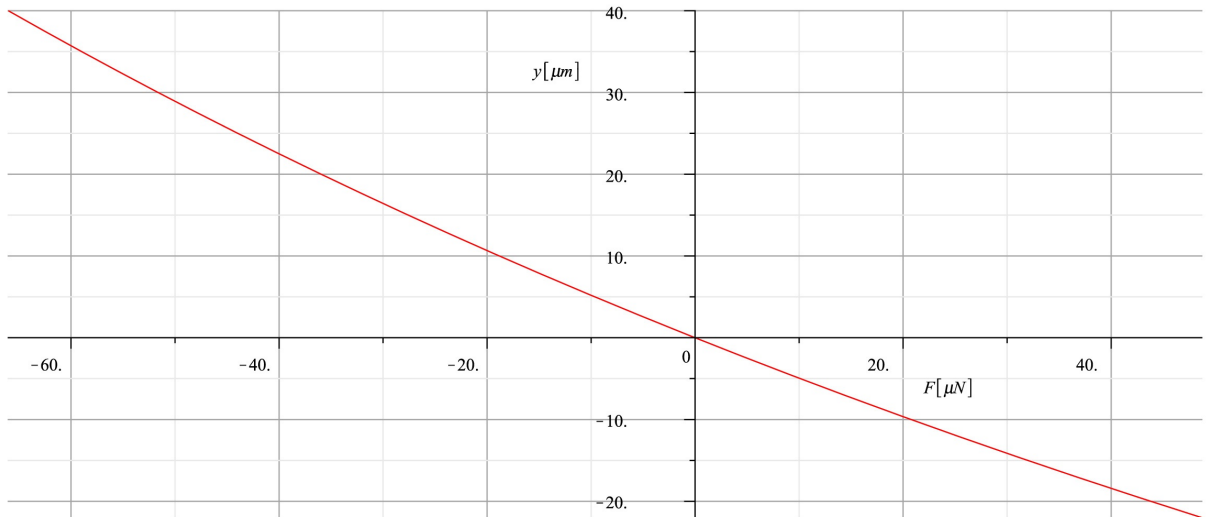Figure 12.6: Geometrical Beam parameters in the Double Prebuckled Beam Design.

Figure 12.7: Axial load P versus the lateral displacement for the double prebuckled beam configuration.

$$P_{max} = 66.02[\mu N]$$

Using the same principle shown in the previous chapter it is assumed a minimal gap resolution to found the minimal detectable force of 1[nm], hence the minimum detectable force is:

$$P_{min} = 1.97[nN]$$

Vibration Study

129

In order to avoid the structure collapse due to possible incompatibilities with the DAS, a FEM analysis is made as it was shown in the previous seen designs. The obtained response to the excitation oscillate force is shown in Fig.12.8.
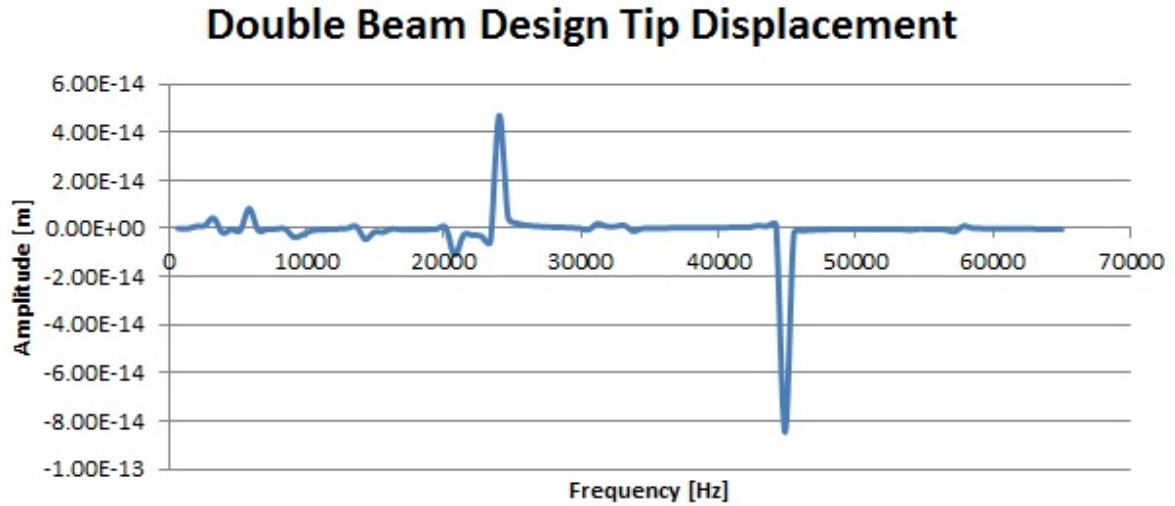
Double Beam Design Tip Displacement

Figure 12.8: Amplitude response to an excitation range of applied harmonic force for the Double Prebuckled Beam design.

The results shown that close to the first excitation frequency there is a peak of resonance at $24.1[kHz]$, at the first excitation frequency the amplitude is of $9.3 \cdot 10^{-16}[m]$ and the at the second excitation frequency is of $2.8 \cdot 10^{-16}[m]$ with the closest peak at $44.8[kHz]$. The results shown very few interference with the DAS, the amplitude of the displacement in the worst case scenario is of 6 magnitude orders of the expected displacement measurements.

As a conclusion it can be said that there is no threat to the structural integrity when using the external excitation of the DAS, so the design is frozen.

12.1.2 Double prebuckled beam test design

For this design the test device added is exactly the same as the one used in the section 8.2.1, the formulation to apply is to add the stiffness of the double folded beam and to project the electrical force due to the test device on each independent coordinate x and y, because of the symmetry such the simple beam configuration the resolution of the equation obtained is the same.

The only difference of the name of the variable form y to get de displacement in this direction and x to obtain the displacement due to the applied potential difference. The displacement can be obtained as a function of the applied voltage using Eq.12.9 adding the projections of the stiffness and the electrical force yields its representation in Fig.12.10.
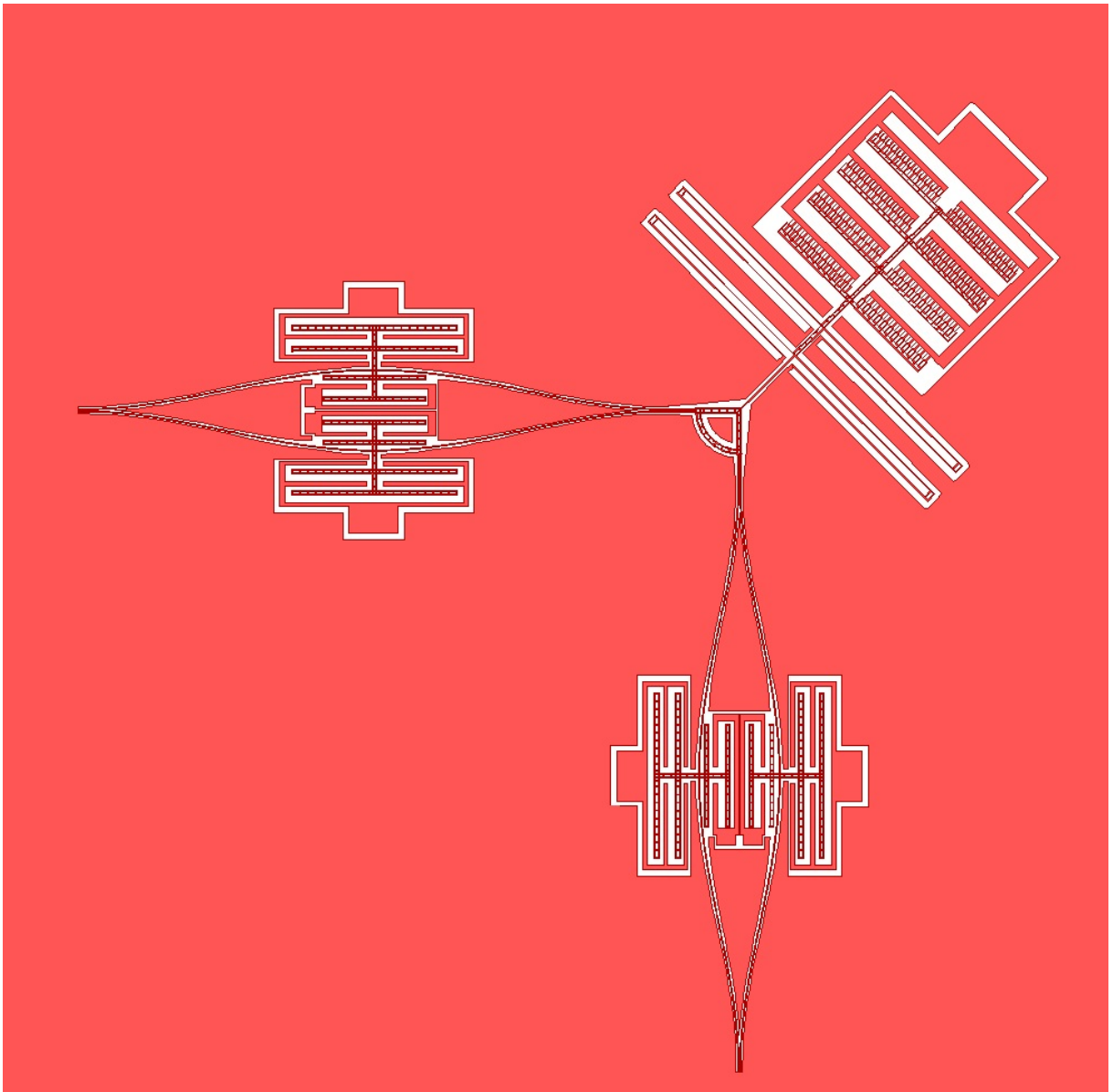
Figure 12.9: Geometry of the pre-buckled double beam test design.

12.2 Final design masks

In this section it is presented the masks used in the fabrication process to obtain the sensing and the test devices.
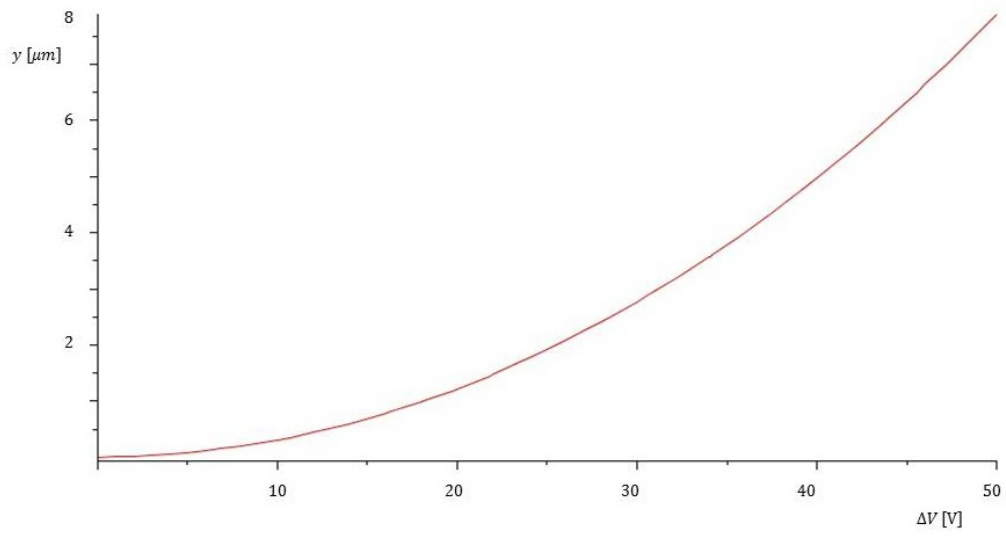
Figure 12.10: Displacement of the middle point of the beam for the double prebuckled beam test design as a function of the applied input voltage V.
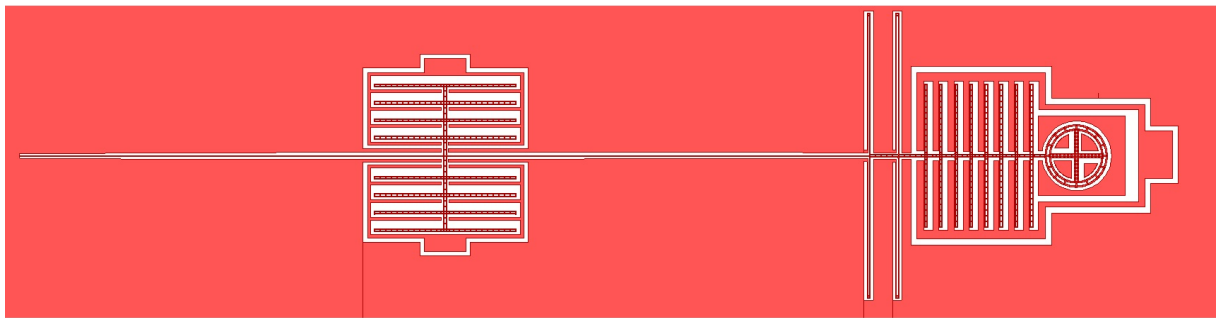

Figure 12.11: 1 DOF compressive load design with parallel plates configuration
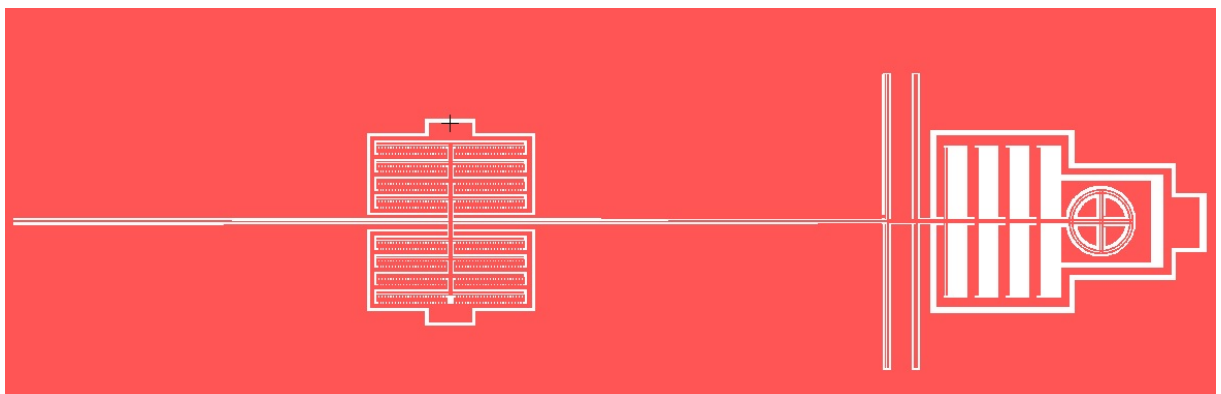

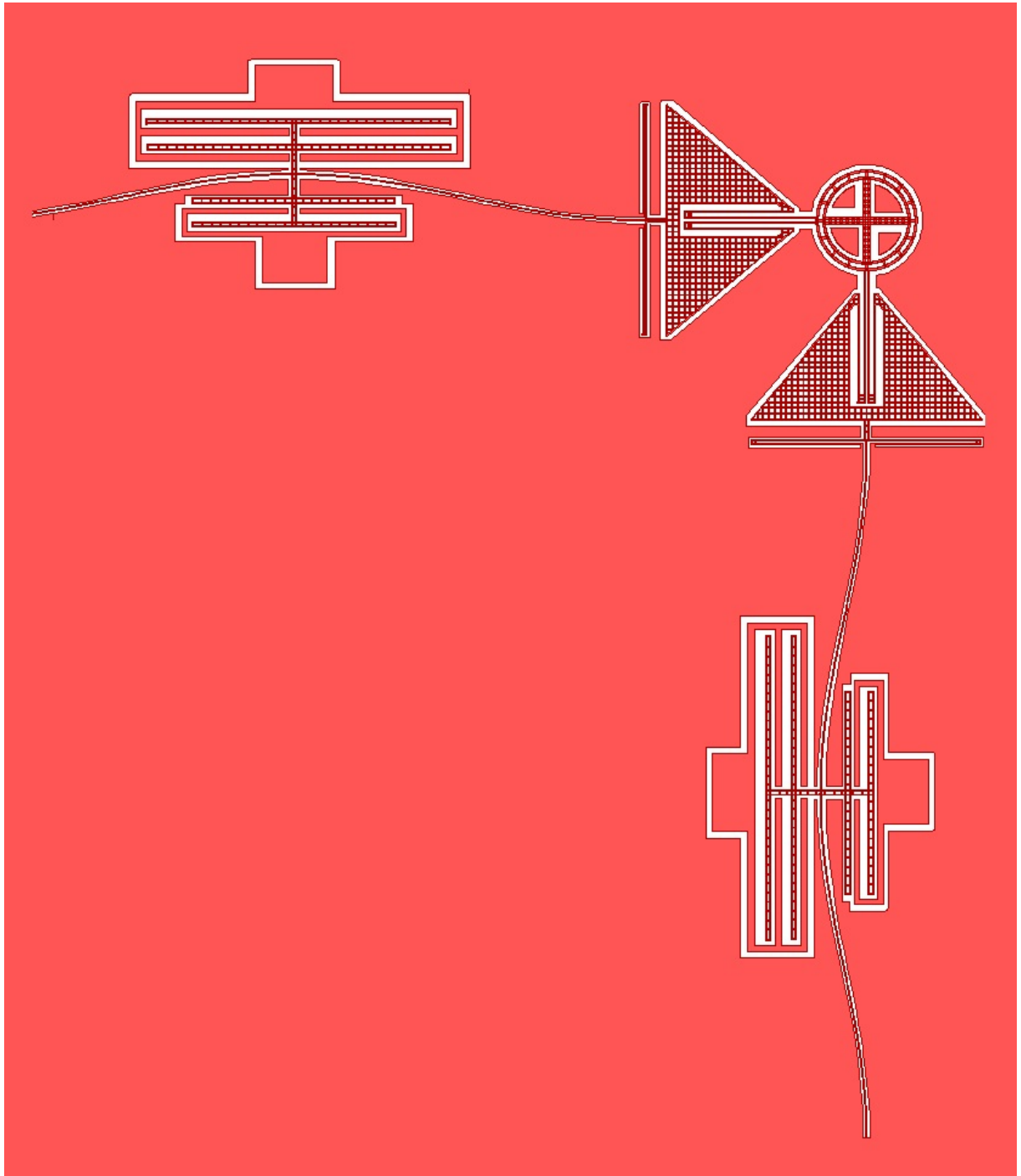Figure 12.12: 1 DOF compressive load design with comb-drive configuration

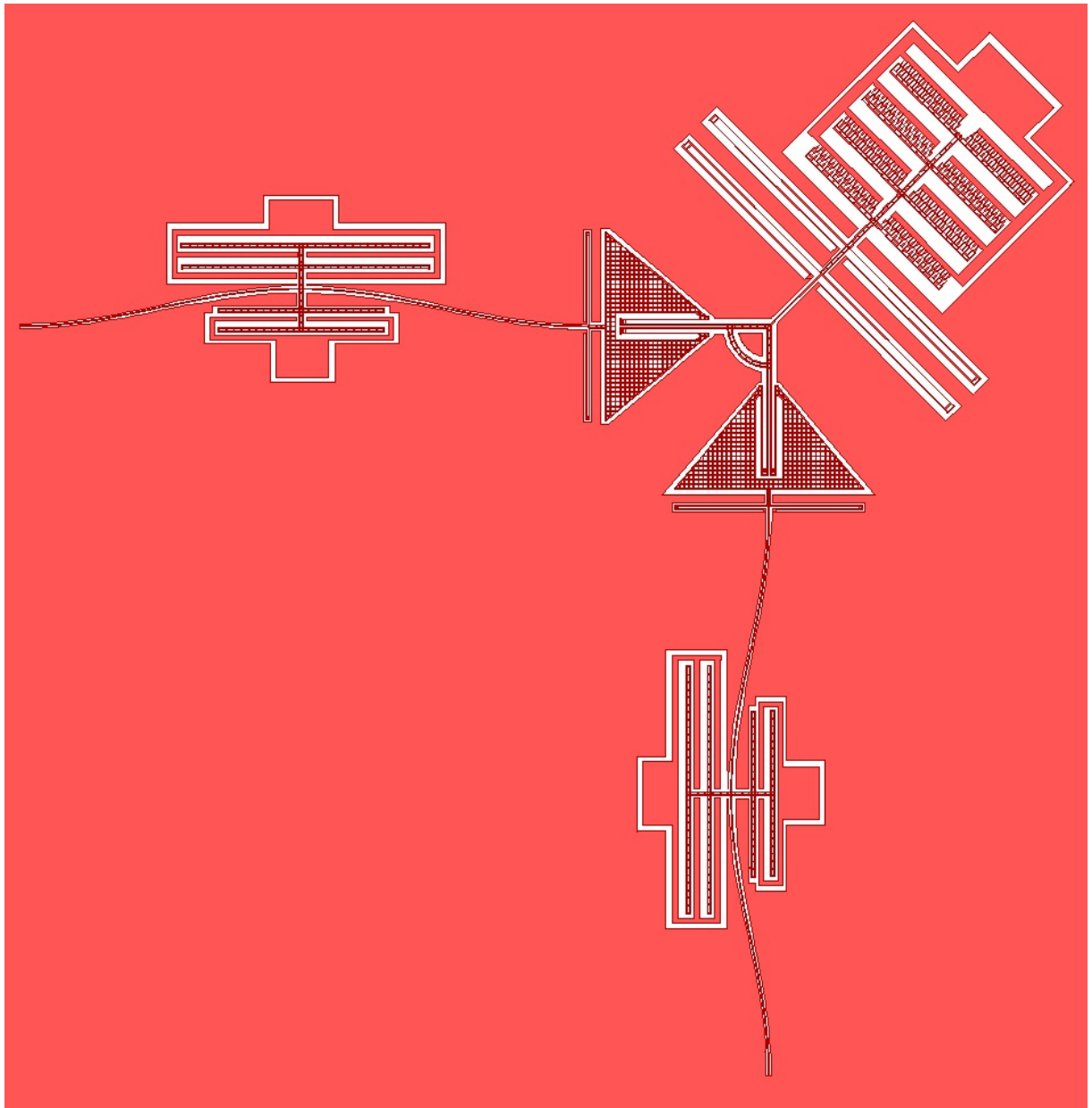Figure 12.13: 2 DOF Prebuckled beam design

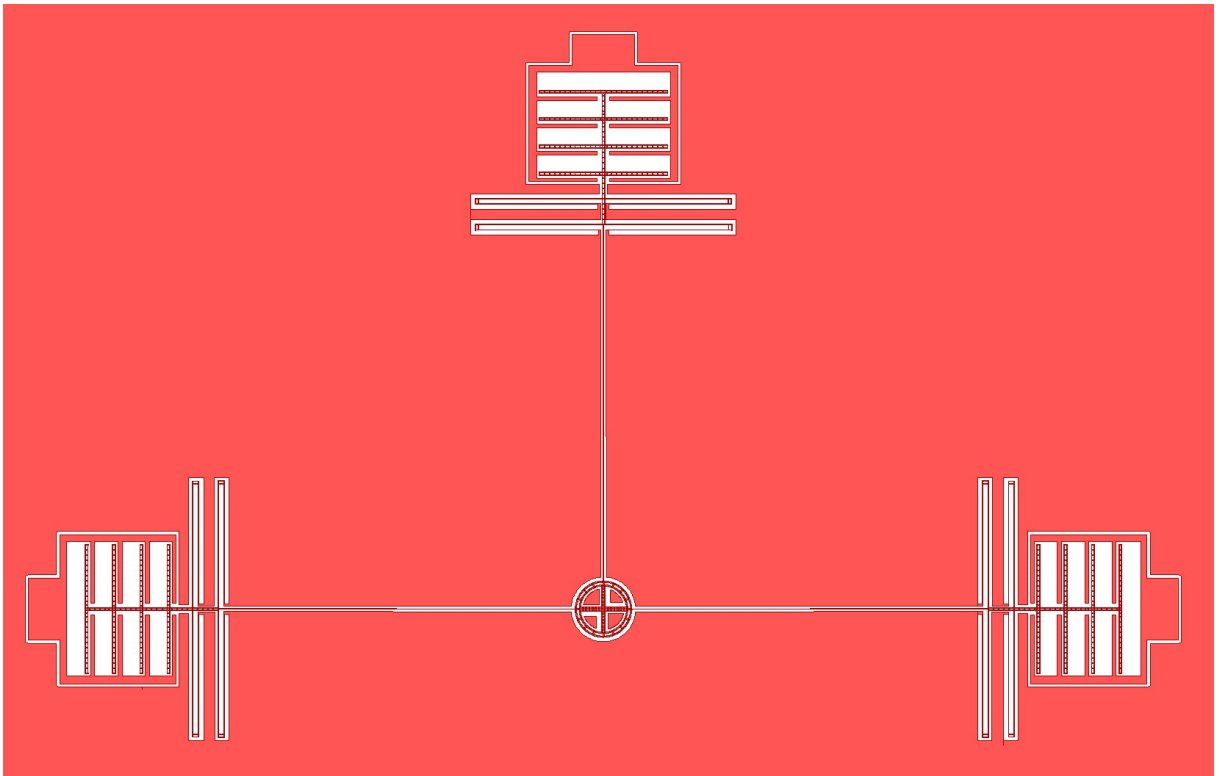Figure 12.14: 2 DOF Prebuckled beam test design

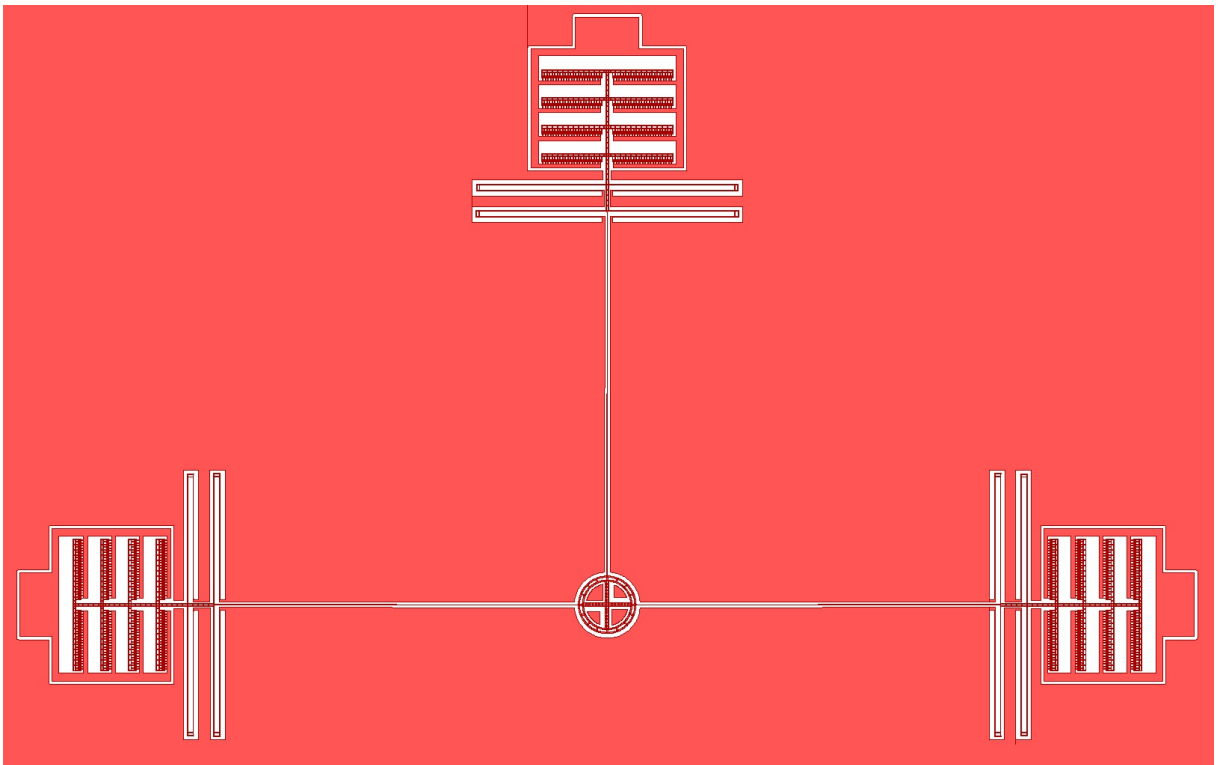Figure 12.15: 2 DOF Straight beam design with parallel plates configuration

Figure 12.16: 2 DOF Straight beam design with comb-drive configuration
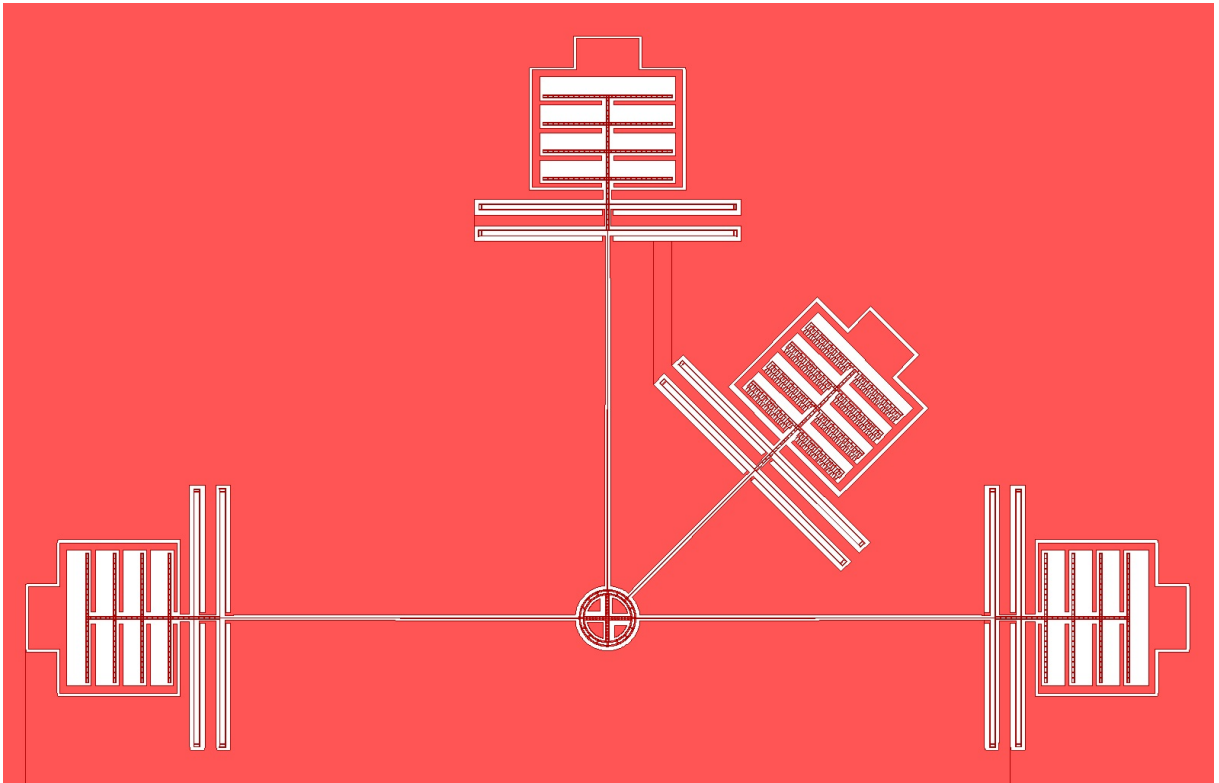
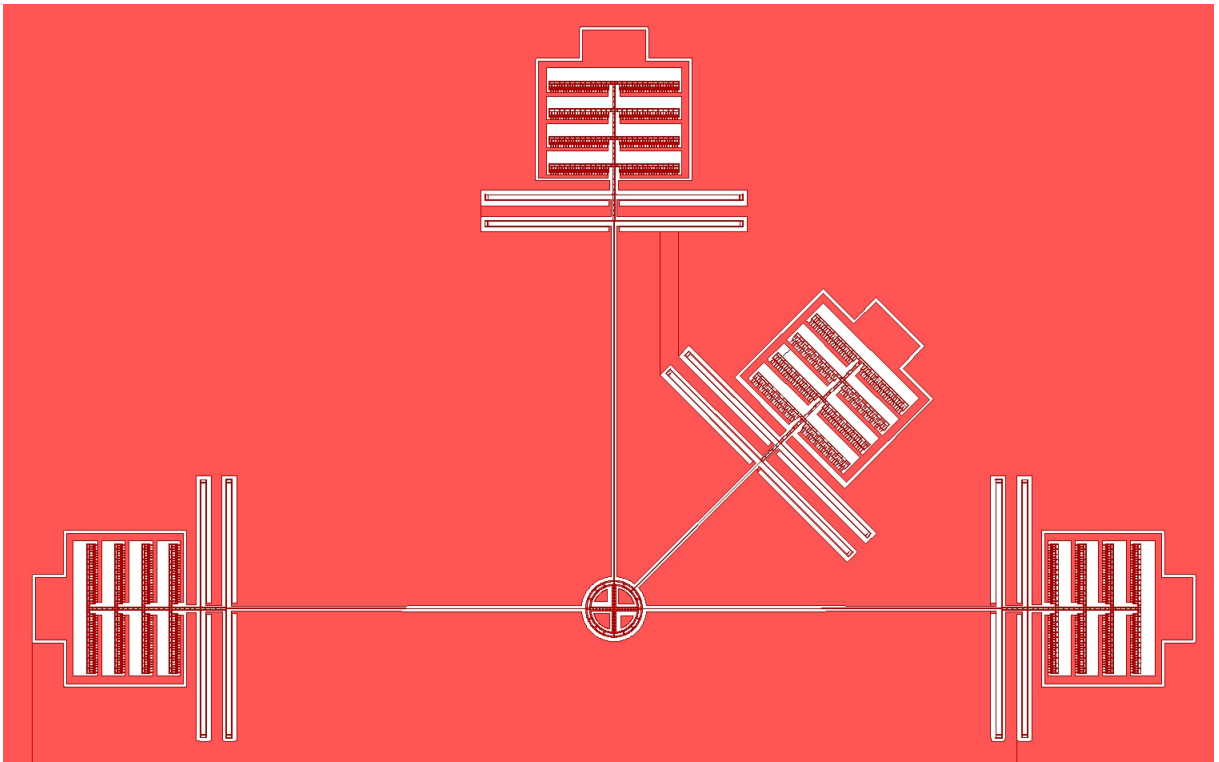Figure 12.17: 2 DOF Straight beam test design with parallel plates configuration

Figure 12.18: 2 DOF Straight beam test design with comb-drive configuration

Bibliography

[1] Jasmina Casals Terre, *MEMS Slides*. Producció Aeroespacial UPC, 2008.

[2] Miquel Sureda Anfres, *High field Electrokinetic effect: Theoretical analysis and capabilities for space propulsion*. UPC, November 2010.

[3] Robert L. Bayt, *Analysis, Fabrication and Testing of a MEMS-based Micropropulsion System*. Fluid Dynamics Research Laboratory Department of Aeronautics and Astronautics, Massachusetts Institue of Technology Cambridge, MA 02139, June 1999.

[4] Ignacio Romero Sanz, *Regimenes ionicos de emision via electrospray. Aplicacion a propulsion ionica* UNIVERSIDAD CARLOS III DE MADRID, Leganés, 2010.

[5] Manuel Gamero-Castaño and Vladimir Hruby, *Characterization of a Colloid Thruster Performing in the micro-Newton Thrust Range.* Natick, Massachusetts 01760.

[6] M.Tacher A.Saif, *On Tunable Bistable MEMS-Theory and Experiment.* JOURNAL OF MICROELECTROMECHANICAL SYSTEMS, VOL 9, NO.2, IEEE JUNE 2000.

[7] Cenk Acar, *Robust Micromachined Vibratory Gyroscopes.* UNIVERSITY OF CALIFORNIA IRVINE, 2004.

[8] Keith Miller, *SOIMUMPs Design Handbook.* MEMScAP Revision 4.0, 2004.

[9] J.Guo, H.Kuo, D.J.Young, W.H.Ko, *BUCKLED BEAM LINEAR OUTPUT CAPACITIVE STRAIN SENSOR* EECS Department, Case Western Reserve University Cleveland, OH, 44106.

[10] A.Ziolkowski.Imielowski, *Buckling and Post-buckling Behaviour of Prismatic Aluminium Columns Submitted to a Series of Compressive Loads.* Experimental Mechanics DOI 10.1007/s11340-010-9455-y, 6 December 2010.

[11] A.Torrents, *MEMS resonant load cells for micro-mechanical test frames: feasibility study and optimal design.* IOP PUBLISHING, 2010.

[12] ANALOG DEVICES, *www.analog.com\static\imported-files\data_sheets\AD7745_7746.pdf*

[13] Capacitive sensor interfaces, *http:\\www.eecs.berkeley.edu\boser\pdf\capacitor.pdf*

[14] MEMSNET, *http:\\www.memsnet.org*

[15] Yole-dev, *http:\\www.yole-dev.com\pagesAn\products\pdf\status_ of_ mems_ industry_2008_ flyer.pdf*

[16] Sensors theory, *http:\\www.lionprecision.com\tech-library\technotes\cap-0020-sensor-theory.html#capmeas*

[17] Sensors theory II, *http:\\www.spaceweather.ac.cn\chinese\Lectures\Lect20.pdf*

[18] ASTRIUM *www.astrium.eads.net*

[19] Wikipedia *www.wikipedia.org*

[20] FEEP microthrusters experimental developments, *http:\\eotvos.dm.unipi.it\TASI%20GG%20Presentation%20June09\FEEP.pdf*

[21] Fotoelectrosprayspray, *http:\\www.biounalm.com\2008\01\electrospray-nuevo-mtodo-para.html*

[22] MIT Opencourseware Capacitance and Dielectrics, *web.mit.edu\8.02t\www\802TEAL3D\visualizations\...\guide05.pdf*